Studies on Bacterial Transport Systems Responsible for the Import of Glycosaminoglycans from Host Extracellular Matrices

Sayoko OIKI

2018

Studies on Bacterial Transport Systems Responsible for the Import of Glycosaminoglycans from Host Extracellular Matrices

Sayoko OIKI

2018

CONTENTS

INTRODUCTION

Extracellular matrices, localized in all animal tissues and organs, serve as physical scaffolds for cellular constituents, cell differentiation and proliferation, homeostasis, and tissue formation (1). Glycosaminoglycans (GAGs) are ubiquitously secreted to the cell surface and are constituents of the matrices (2). GAGs are acidic polysaccharides consisting of repeating disaccharide units of a uronate and an amino sugar residues. They are classified as hyaluronan, chondroitin sulfate, heparin, and heparan sulfate based on the constituent monosaccharides, glycoside linkages, and sulfation patterns (3, 4) (Fig. 1). Hyaluronan consists of D-glucuronate (GlcUA) and *N*-acetyl-D-glucosamine (GlcNAc), chondroitin sulfate of GlcUA and *N*-acetyl-D-galactosamine (GalNAc). Heparin and heparan sulfate are constituted by GlcUA or L-iduronate (IdoUA) and D-glucosamine (GlcN) or GlcNAc (5). The uronate and amino sugar residues in hyaluronan and chondroitin sulfate are linked by 1,3-glycoside bonds, whereas residues in heparin and heparan sulfate are connected by 1,4-glycoside bonds. Except hyaluronan, these GAGs frequently contain sulfate groups in the uronate and/or amino sugar residues and function as protein-binding proteoglycans in extracellular matrices.

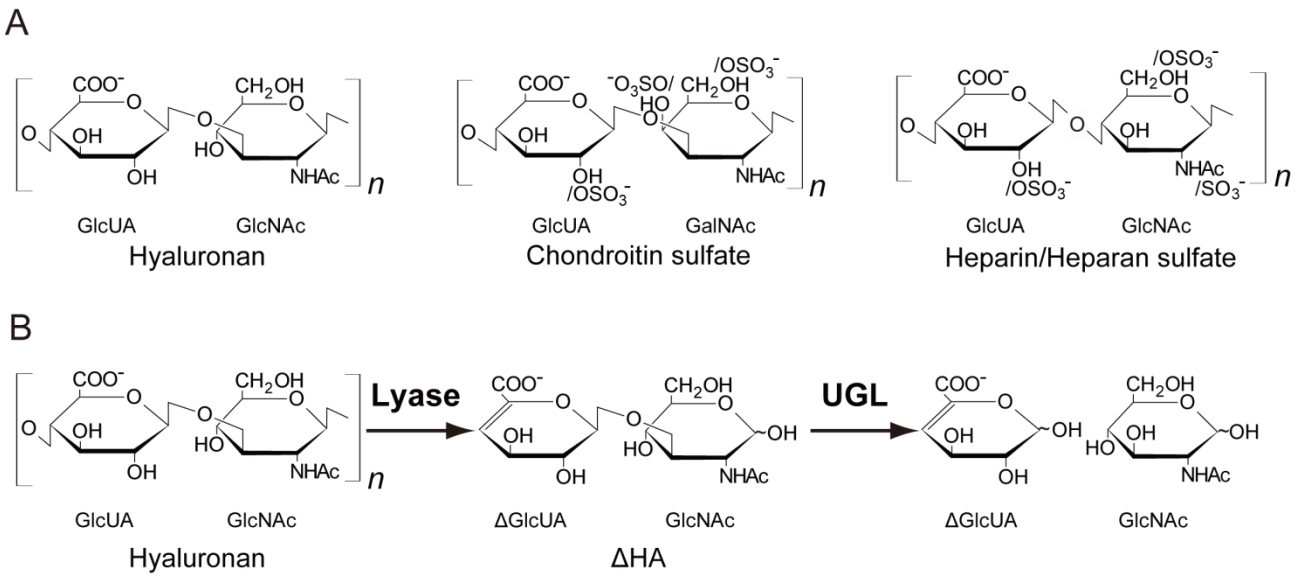

Figure 1. Structure of GAGs and GAG degradation by bacteria. (A) Structural formulas of GAGs. (B) Degradation of hyaluronan by streptococci. Streptococci depolymerize hyaluronan to unsaturated hyaluronan disaccharide (ΔHA) using hyaluronate lyase and the resultant disaccharides are degraded to unsaturated D-glucuronate (ΔGlcUA) and GlcNAc by UGL.

Some bacteria target animal GAGs for colonization and/or infection (6). Bacterial adhesion to host epithelial cells is an important step in both pathogenic infection and microbiota colonization of different mucosal surfaces (7). A large number of pathogenic bacteria such as *Helicobacter*, *Enterococcus*, *Listeria*, *Staphylococcus*, and *Streptococcus* bind to GAGs for adhesion to human epithelial cells (8). Most of these bacteria establish initial weak interaction with GAGs before making more stable contacts with host cell surface protein receptors, whereas some express cell-surface proteins that bind directly to GAGs or induce the release of GAGs from proteoglycan to prevent attack from host-derived antibacterial peptides (2). Moreover, GAGs are involved in adhesion of probiotic microbiota such as *Lactobacillus* and *Bifidobacterium* to human epithelial cells (9, 10). Recently, sugar-containing molecules, rather than proteins, have been suggested to mediate bacterial adhesion to the surface of host cells (11). Because of the variation in the negative charges resulting from different sulfation patterns, GAGs provide a unique opportunity for bacteria to target different molecules for cellular interaction (10).

After adhesion to GAGs, in some bacteria such as staphylococci and streptococci, extracellular or cell-surface polysaccharide lyases depolymerize GAGs to unsaturated disaccharides with C=C double bonds at the non-reducing terminus of the uronate through a β-elimination reaction (12–15) (Fig. 1). The resultant unsaturated GAG disaccharides are degraded in the cytoplasm by unsaturated glucuronyl hydrolase (UGL) into monosaccharides (an unsaturated uronate and an amino sugar) through the hydration of the C=C double bonds (16–18). On the other hand, little is known about the bacterial import of GAGs, although a few ATP-binding cassette (ABC) exporters of GAGs in bacteria (19, 20) and humans (21) have been identified. The metabolic fate of unsaturated uronate derived from GAGs also remains to be clarified. In the Carbohydrate-Active enZYmes Database (CAZy) (22), GAG lyases are categorized into families such as polysaccharide lyases (PLs) 6, 8, 12, 13, 15, 16, 21, and 23, whereas UGL is classified into a unique glycoside hydrolase (GH) 88 family. Among approximately 9,000 bacterial species contained in CAZy, over 1,000 species have genes encoding GAG lyases and/or UGL, suggesting that many bacteria target GAGs for depolymerization and/or degradation.

In the intestinal tract, the epithelial cell layer is covered by a dense layer of mucin, composed of core *O*-linked glycans containing galactose, GalNAc, and GlcNAc, over GAGs (23). The mucus is divided into an outer layer containing the microbiota and an inner layer, which keeps the epithelial cell surface free of bacteria (24). Although only 1% of intestinal microbiota has been estimated to enzymatically degrade host mucin (25), these species provide nutrients released from

mucin to other indigenous bacteria. For example, *Bacteroides*, *Ruminococcus*, *Bifidobacterium*, and *Clostridium* have been shown to degrade mucin (26). *Streptococcus pneumoniae* is also known to express mucin-degrading enzymes (27). *Akkermansia muciniphila* is specialized in degrading mucin, whereas *Bacteroides thetaiotaomicron* has the ability to degrade both dietary sugars and host mucosal sugars, and metabolizes host sugars when its diet is depleted (28). The intestinal microbiota co-operatively degrade the complex structure of mucin (29) to target GAGs for colonization.

Studies on bacterial GAG import systems provide further molecular insights into the physiology and pathogenicity of bacterial interaction with animals. For some bacteria among the indigenous microbiota, the GAG import system is required for assimilation of GAGs present on host cells. Generally, bacterial polysaccharide-degrading enzymes are expressed under the control of cytoplasmic transcriptional regulators sensing substrates (30, 31). Inhibition of the import system results in reduced expression of these degrading enzymes, thus leading to potential novel therapies for bacterial GAG-dependent infectious diseases. In this thesis, two bacterial GAG import systems were identified through molecular and structural biology approaches. CHAPTER I deals with the molecular identification of a *Streptococcus agalactiae* phosphotransferase system (PTS) that phosphorylates the imported sugar at the C-6 position, and with the characterization of streptococcal unsaturated uronate-metabolizing enzymes. CHAPTER II elucidates GAG-mediated interactions between host human cells and intestinal microbiota including streptococci and lactobacilli with PTS for GAG import. CHAPTER III describes the structure and function of the *Streptobacillus moniliformis* solute-binding protein-dependent ABC transporter responsible for the import of GAGs without any sugar modification.

References

1. Frantz, C., Stewart, K. M., and Weaver, V. M. (2010) The extracellular matrix at a glance. *J. Cell Sci.* **123**, 4195-4200
2. Kamhi, E., Joo, E. J., Dordick, J. S., and Linhardt, R. J. (2013) Glycosaminoglycans in infectious disease. *Biol. Rev.* **88**, 928-943
3. Gandhi, N. S., and Mancera, R. L. (2008) The structure of glycosaminoglycans and their interactions with proteins. *Chem. Biol. Drug Des.* **72**, 455-482
4. Scott, J. E. (1992) Supramolecular organization of extracellular matrix glycosaminoglycans, *in vitro* and in the tissues. *FASEB J.* **6**, 2639-2645

5. Prydz, K., and Dalen, K. T. (2000) Synthesis and sorting of proteoglycans. *J. Cell Sci.* **113**, 193-205
6. Sawitzky, D. (1996) Protein-glycosaminoglycan interactions: infectiological aspects. *Med. Microbiol. Immunol.* **184**, 155-161
7. Zarate, G., and Nader-Macias, M. (2006) Influence of probiotic vaginal lactobacilli on *in vitro* adhesion of urogenital pathogens to vaginal epithelial cells. *Lett. Appl. Microbiol.* **43**, 174-180
8. Garcia, B., Merayo-Lloves, J., Martin, C., Alcalde, I., Quiros, L. M., and Vazquez, F. (2016) Surface proteoglycans as mediators in bacterial pathogens infections. *Front. Microbiol.* **7**, 220
9. Martin, R., Martin, C., Escobedo, S., Suarez, J. E., and Quiros, L. M. (2013) Surface glycosaminoglycans mediate adherence between HeLa cells and *Lactobacillus salivarius* Lv72. *BMC Microbiol.* **13**, 210
10. Laparra, J., Lopez-Rubio, A., Lagaron, J., and Sanz, Y. (2010) Dietary glycosaminoglycans interfere in bacterial adhesion and gliadin-induced pro-inflammatory response in intestinal epithelial (Caco-2) cells. *Int. J. Biol. Macromol.* **47**, 458-464
11. Coppa, G. V., Facinelli, B., Magi, G., Marini, E., Zampini, L., Mantovani, V., Galeazzi, T., Padella, L., Marchesiello, R. L., and Santoro, L. (2016) Human milk glycosaminoglycans inhibit *in vitro* the adhesion of *Escherichia coli* and *Salmonella fyris* to human intestinal cells. *Pediatr. Res.* **79**, 603-607
12. Stern, R., and Jedrzejas, M. J. (2006) Hyaluronidases: their genomics, structures, and mechanisms of action. *Chem. Rev.* **106**, 818-839
13. Jedrzejas, M. (2007) Unveiling molecular mechanisms of bacterial surface proteins: *Streptococcus pneumoniae* as a model organism for structural studies. *Cell. Mol. Life Sci.* **64**, 2799-2822
14. Li, S., and Jedrzejas, M. J. (2001) Hyaluronan binding and degradation by *Streptococcus agalactiae* hyaluronate lyase. *J. Biol. Chem.* **276**, 41407-41416
15. Ibberson, C. B., Jones, C. L., Singh, S., Wise, M. C., Hart, M. E., Zurawski, D. V., and Horswill, A. R. (2014) *Staphylococcus aureus* hyaluronidase is a CodY-regulated virulence factor. *Infect. Immun.* **82**, 4253-4264
16. Hashimoto, W., Kobayashi, E., Nankai, H., Sato, N., Miya, T., Kawai, S., and Murata, K. (1999) Unsaturated glucuronyl hydrolase of *Bacillus* sp. GL1: novel enzyme prerequisite for

metabolism of unsaturated oligosaccharides produced by polysaccharide lyases. *Arch. Biochem. Biophys.* **368**, 367-374

17. Itoh, T., Hashimoto, W., Mikami, B., and Murata, K. (2006) Crystal structure of unsaturated glucuronyl hydrolase complexed with substrate molecular insights into its catalytic reaction mechanism. *J. Biol. Chem.* **281**, 29807-29816
18. Nakamichi, Y., Maruyama, Y., Mikami, B., Hashimoto, W., and Murata, K. (2011) Structural determinants in streptococcal unsaturated glucuronyl hydrolase for recognition of glycosaminoglycan sulfate groups. *J. Biol. Chem.* **286**, 6262-6271
19. Ouskova, G., Spellerberg, B., and Prehm, P. (2004) Hyaluronan release from *Streptococcus pyogenes*: export by an ABC transporter. *Glycobiology* **14**, 931-938
20. Cress, B. F., Englaender, J. A., He, W., Kasper, D., Linhardt, R. J., and Koffas, M. A. (2014) Masquerading microbial pathogens: capsular polysaccharides mimic host-tissue molecules. *FEMS Microbiol. Rev.* **38**, 660-697
21. Schulz, T., Schumacher, U., and Prehm, P. (2007) Hyaluronan export by the ABC transporter MRP5 and its modulation by intracellular cGMP. *J. Biol. Chem.* **282**, 20999-21004
22. Cantarel, B. L., Coutinho, P. M., Rancurel, C., Bernard, T., Lombard, V., and Henrissat, B. (2008) The Carbohydrate-Active EnZymes database (CAZy): an expert resource for glycogenomics. *Nucleic Acids Res.* **37**, D233-D238
23. Tailford, L. E., Crost, E. H., Kavanaugh, D., and Juge, N. (2015) Mucin glycan foraging in the human gut microbiome. *Front. Genetics* **6**, 81
24. Johansson, M. E., Larsson, J. M. H., and Hansson, G. C. (2011) The two mucus layers of colon are organized by the MUC2 mucin, whereas the outer layer is a legislator of host-microbial interactions. *Proc. Natl. Acad. Sci. U. S. A.* **108**, 4659-4665
25. Hoskins, L. C., and Boulding, E. T. (1981) Mucin degradation in human colon ecosystems: evidence for the existence and role of bacterial subpopulations producing glycosidases as extracellular enzymes. *J. Clin. Invest.* **67**, 163-172
26. Salyers, A., West, S., Vercellotti, J., and Wilkins, T. (1977) Fermentation of mucins and plant polysaccharides by anaerobic bacteria from the human colon. *Appl. Environ. Microbiol.* **34**, 529-533
27. King, S. (2009) Pneumococcal modification of host sugars: a major contributor to colonization of the human airway? *Mol. Oral Microbiol.* **25**, 15-24
28. Derrien, M., Vaughan, E. E., Plugge, C. M., and de Vos, W. M. (2004) *Akkermansia*

muciniphila gen. nov., sp. nov., a human intestinal mucin-degrading bacterium. *Int. J. Syst. Evol. Microbiol.* **54**, 1469-1476

29. Cockburn, D. W., and Koropatkin, N. M. (2016) Polysaccharide degradation by the intestinal microbiota and its influence on human health and disease. *J. Mol. Biol.* **428**, 3230-3252
30. Swint-Kruse, L., and Matthews, K. S. (2009) Allostery in the LacI/GalR family: variations on a theme. *Curr. Opin. Microbiol.* **12**, 129-137
31. Hayashi, C., Takase, R., Momma, K., Maruyama, Y., Murata, K., and Hashimoto, W. (2014) Alginate-dependent gene expression mechanism in *Sphingomonas* sp. strain A1. *J. Bacteriol.* **196**, 2691-2700

CHAPTER I

Streptococcus phosphotransferase system responsible for the import of non-sulfated glycosaminoglycan

Streptococci are classified into three groups on the basis of the hemolytic activity: α, incomplete lysis of red cells; β, complete lysis of red cells; and γ, no hemolysis (1). β-Streptococci are further classified into A–V based on antigenic differences in their cell-wall polysaccharides. For example, group α *S. pneumoniae* is a major causative bacterium of pneumonia and group β-A *Streptococcus pyogenes* causes pharyngitis and sepsis. Group β-B *S. agalactiae* is responsible for neonatal sepsis and meningitis and is indigenous to the gastrointestinal and urogenital tracts of 25%–40% of healthy women. However, *S. agalactiae* infects 50% of neonates from their mothers during the obstetrical delivery and becomes causative bacterium of neonatal invasive diseases (2). These three streptococci growing on hyaluronan as a sole carbon source (3–5) have been known to invade host cells upon depolymerization of hyaluronan in extracellular matrices (6).

In streptococcal genomes, enzymes for depolymerization and degradation of GAGs are encoded together with a putative PTS, a typical bacterial sugar import system (7). The genes encoding GAG lyase, UGL, and the PTS are assembled to form a GAG genetic cluster (Fig. 1-1). PTS is composed of Enzyme I (EI), histidine-containing phosphocarrier protein (HPr), and Enzyme II (EII), which has multiple hetero-subunits (IIA, IIB, IIC, and IID) (7). EI and HPr are located in the cytoplasm and non-specifically recognize sugar substrates, whereas EII is specific for substrates and consists of cell membrane and cytoplasmic domains. Mechanistically, PTS imports sugar by phosphorylating the substrate at the C-6 position, and successive phosphotransfer reactions from a phosphate donor, phosphoenolpyruvate, are mediated by EI, HPr, and EII (8). A large number of GAGs, except for hyaluronan, are frequently sulfated at the C-6 position (9) and unsaturated GAG disaccharides with a sulfate group at the C-6 position are unsuitable for substrates of PTS due to impossibility of phosphorylation. In fact, disruption of the EI gene in *Salmonella typhimurium* has been demonstrated to still grow on some sugars such as glucuronate and glucose-6-phosphate, indicating that these sugars with a carboxyl or phosphate group at the C-6 position are incorporated by other transport systems distinct from PTS (10). Although more than 20 sugars have been identified to be imported by PTS, no sugars with a modification at the C-6 position are included in these substrates (11).

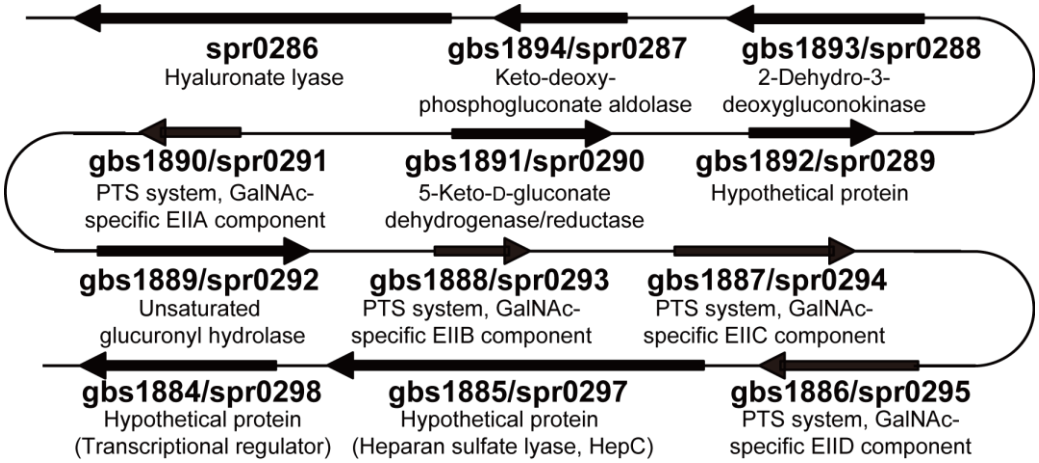

Figure 1-1. GAG genetic cluster in *S. agalactiae* and *S. pneumoniae*. "gbs" and "spr" refer to *S. agalactiae* and *S. pneumoniae*, respectively.

Because hyaluronan increases the expression level of the *S. agalactiae* GAG genetic cluster coding for the PTS (12), the PTS is suggested to incorporate depolymerized hyaluronan. Marion *et al*. have already shown that the PTS in conjunction with hyaluronate lyase and UGL in the *S. pneumoniae* genome is essential for growth on hyaluronan as a sole carbon source (3). The PTS mutation has been demonstrated to reduce its ability to colonize mouse upper respiratory tracts. While the PTS mutant has also been found to grow on monosaccharides constituting hyaluronan, at the same level of the parental wild-type strain, the substrate of the PTS remains to be identified.

In addition to genes coding for GAG lyase, UGL, and PTS, putative genes encoding 5-keto-D-gluconate dehydrogenase/reductase, a hypothetical protein, 2-dehydro-3-deoxygluconokinase (KdgK), and keto-deoxy-phosphogluconate aldolase (KdgA) are also arranged in the streptococcal GAG genetic cluster (Fig. 1-1). In the streptococcal cytoplasm, UGL acts on various unsaturated GAG disaccharides and produces unsaturated uronate and amino sugar (13). Although the metabolic pathway for amino sugars has been identified (14), the enzymatic route for metabolism of unsaturated uronates derived from GAGs remains to be clarified.

This CHAPTER deals with the *S. agalactiae* PTS encoded in the GAG genetic cluster as the importer of unsaturated hyaluronan disaccharides and with the metabolic pathway of unsaturated uronates produced from GAGs through bacterial degradation.

Materials and Methods

Materials. Hyaluronan sodium salt was purchased from Sigma Aldrich. Sodium salts of chondroitin sulfates A and C were from Wako Pure Chemical Industries. Heparin sodium salt was

from Nacalai Tesque.

Microorganisms and Culture Conditions. *S. agalactiae* NEM316 (ATCC 12403) was purchased from Institute Pasteur, and *S. agalactiae* JCM 5671 (ATCC 13813) was from Riken BioResource Center. *S. agalactiae* cells were statically grown at 37°C under 5% CO_2 in 3.7% brain heart infusion medium (BD Bacto) or 0.8% nutrient medium (0.3% beef extract and 0.5% peptone) (Difco) supplemented with 20% horse serum for 16–24 h. *Escherichia coli* strain DH5α cells harboring plasmids were cultured at 37°C in Luria-Bertani (LB) medium containing 100 μg/ml sodium ampicillin. For the expression of recombinant proteins, *E. coli* strain BL21(DE3) cells harboring plasmids were cultured at 30°C in LB medium containing 100 μg/ml sodium ampicillin to an optical density of 0.3–0.7 at 600 nm (OD_{600}), followed by addition of isopropyl-β-D-thiogalactopyranoside (IPTG) at a final concentration of 0.1 mM and growth at 16°C for 2 days.

Halo Detection for Degradation of GAGs. The halo detection method was adopted to investigate the GAG-degrading ability of *S. agalactiae*. The bacterial cells were grown on plates containing 0.2% dialyzed GAGs (hyaluronan, chondroitin sulfate A, C, or heparin), 0.8% nutrient medium, 20% horse serum, and 1% bovine serum albumin (BSA) solidified with 1% agar. After bacterial growth, addition of 2 M acetic acid (1 ml) to the plates resulted in the formation of a white precipitate due to interaction of GAGs with BSA, whereas areas containing degraded GAGs appeared as clear zones, or "halos."

Construction of Overexpression Systems. An overexpression system for *S. agalactiae* hyaluronate lyase was constructed in *E. coli* cells to provide enzyme for the preparation of unsaturated hyaluronan disaccharide for the PTS import assay. To clone the gbs1270 gene encoding hyaluronate lyase, polymerase chain reaction (PCR) was conducted in 10 μl of reaction mixture consisting of 0.2 U of KOD Plus Neo polymerase (Toyobo), *S. agalactiae* cells as a template, 0.3 pmol of each of forward and reverse primer, 2 nmol of dNTPs, 10 nmol of $MgCl_2$, 0.5 μl of dimethyl sulfoxide, and the commercial reaction buffer supplied with KOD Plus Neo polymerase. PCR conditions were as follows: 94°C for 2 min followed by 30 cycles of 98°C for 10 s, 35°C for 30 s, and 68°C for 2 min. The PCR product was ligated to *Hinc*II-digested pUC119 (Takara Bio) using Ligation High Ver. 2 (Toyobo), and the resultant plasmid was digested with *Nco*I and *Xho*I to isolate the gbs1270 gene. The gene fragment was confirmed to encode the correct gbs1270 by DNA sequencing (15). The *Nco*I and *Xho*I-digested gbs1270 gene was ligated into *Nco*I and *Xho*I-digested pET21d (Novagen) and *E. coli* BL21(DE3) host cells were transformed with the

resulting plasmid, pET21d-gbs1270. An overexpression system of *S. agalactiae* PTS EIIA was also constructed in *E. coli* cells for X-ray crystallography. To clone the gbs1890 gene encoding PTS EIIA, PCR was conducted as described above, but with different primers. The gene fragment was ligated into *Nde*I and *Xho*I-digested pET21b (Novagen) and *E. coli* BL21(DE3) host cells were transformed with the plasmid pET21b-gbs1890. The PCR primers used are shown in Table 1-1.

Table 1-1. Primers

gbs1270	forward	5’-GGCCATGGAAATCAAAAAGAAACATCGTATTATG-3’
gbs1270	reverse	5’-CCCTCGAGGATAGCTAATTGGTCTGTTTTTGTCATG-3’
gbs1890	forward	5’-GGCATATGATAAAAATTATTATTGTAGCACACGGC-3’
gbs1890	reverse	5’-GGCTCGAGAATGCCTCCCTCAAAAGTTGCTTCTGCAGT-3’

Underlines bases indicate the restriction sites.

Purification. Recombinant *E. coli* cells were harvested by centrifugation at 6,700 *g* and 4°C for 10 min and suspended in 20 mM Tris (hydroxymethyl) aminomethane-hydrochloride (Tris-HCl), pH 7.5. The cell suspension was ultrasonicated (Insonator Model 201M, Kubota) at 0°C and 9 kHz for 10 min, and the supernatant obtained after centrifugation at 20,000 *g* and 4°C for 20 min was used as the cell extract for further experimentation.

The [BL21(DE3)/pET21d-gbs1270 cell extract was used as the hyaluronate lyase source for the preparation of unsaturated hyaluronan disaccharide. PTS EIIA was purified from BL21(DE3)/pET21b-gbs1890 cell extract by metal affinity chromatography [TALON (Clontech)] and gel filtration chromatography [Sephacryl S-200 (GE Healthcare)]. After confirmation of protein purity by sodium dodecyl sulfate-polyacrylamide gel electrophoresis (SDS-PAGE), the purified protein was dialyzed against 20 mM Tris-HCl (pH 7.5). *S. agalactiae* UGL was purified from HMS174(DE3)pLysS/pET21b-SagUGL cell extract (12) by anion exchange chromatography [Toyopearl DEAE-650M (Tosoh Bioscience LLC)] and gel filtration chromatography [HiLoad 16/60 Superdex 75 pg (GE Healthcare)]. Two proteins (gbs1891 and gbs1892) were purified from the cell extract of BL21(DE3)pLysS/pET21b-gbs1891 (16) and BL21(DE3)pLysS/pET21b-gbs1892 (16), respectively, by affinity (TALON), anion exchange [Toyopearl SuperQ-650M (Tosoh Bioscience LLC)] and gel filtration chromatography (Sephacryl S-200).

Preparation of Unsaturated Hyaluronan Disaccharide. To investigate PTS import activity, unsaturated hyaluronan disaccharide was prepared using recombinant hyaluronate lyase. A reaction mixture containing BL21(DE3)/pET21d-gbs1270 cell extract, 0.2% hyaluronan, and 20 mM

Tris-HCl (pH 7.5) was incubated at 30°C for 2 days. The mixture was boiled to stop the reaction and centrifuged at 20,000 *g* for 20 min to remove aggregated proteins. The resultant supernatant was concentrated by freeze drying and subjected to gel filtration chromatography [Superdex Peptide 10/300 GL (GE Healthcare)]. The eluted fractions containing unsaturated hyaluronan disaccharide were identified by monitoring the absorbance at 235 nm derived from the C=C double bonds of the disaccharide. To confirm the presence of unsaturated hyaluronan disaccharide, pooled fractions were subjected to thin-layer chromatography (TLC) using a solvent system of 1-butanol:acetic acid:water (3:2:2, v:v:v). The depolymerization products from hyaluronan were visualized by heating the TLC plates [silica gel 60 F_{254} (Merck)] at 130°C for 5 min after spraying with 10% sulfuric acid in ethanol. The unsaturated hyaluronan disaccharide preparation was freeze dried and dissolved in sterilized water at a final concentration of 200 mM.

PTS Assay. To demonstrate the import of unsaturated hyaluronan disaccharides into *S. agalactiae* cells by PTS, pyruvate produced from phosphoenolpyruvate through import of the substrate by PTS was assayed. The reaction mixture containing toluene-treated cells permeable through cell-surface layer, phosphoenolpyruvate, sugars, NADH, and L-lactate dehydrogenase from rabbit muscle (Oriental Yeast) was measured in absorbance at 340 nm to determine NADH oxidation due to production of lactate from the pyruvate generated by the PTS reaction. This assay was based on previous reports with some modifications (17, 18). Briefly, *S. agalactiae* cells were grown at 37°C under 5% CO_2 for 16 h in 0.8% nutrient medium and 20% horse serum in the presence or absence of 0.2% dialyzed hyaluronan and then harvested by centrifugation at 2,610 *g* and 4°C for 5 min. Cells were washed twice with 5 mM $MgCl_2$ and 0.1 M potassium phosphate buffer (KPB), pH 7.2, and suspended in 1 ml of the same buffer and mixed with 50 µl of acetone:toluene (9:1, v:v) by vortexing twice for 2 min. The reaction mixture containing toluene-treated cells, 10 mM sugar, 0.1 mM NADH, 0.023 mg/ml L-lactate dehydrogenase, 10 mM NaF, 5 mM $MgCl_2$, and 0.1 M KPB (pH 7.5) was incubated at 37°C for 5 min, subsequently mixed with 5 mM phosphoenolpyruvate, and monitored by measuring the decrease in absorbance at 340 nm. The protein concentration of toluene-treated cells was determined using the bicinchoninic acid (BCA) assay (19). The PTS import activity value was calculated as the amount of pyruvate produced per minute per mg protein (nmol/min/mg).

X-ray Crystallography. To determine the three-dimensional structure of *S. agalactiae* PTS EIIA, the purified protein was concentrated to 9.24 mg/ml and crystallized by the sitting drop vapor diffusion method. The purified EIIA (1 µl) was mixed with an equal volume of a reservoir solution

consisting of 20% (w/v) polyethylene glycol (PEG) 3,350 and 0.2 M sodium thiocyanate (pH 6.9) and incubated at 20°C. The crystal was picked and instantaneously frozen in liquid nitrogen. X-ray diffraction data were collected at the BL38B1 station of SPring-8 (Harima, Japan). The data were indexed, integrated, and scaled using *HKL2000* software (20). The structure was determined through the molecular replacement method using *Molrep* in the *CCP4* software package and *E. coli* PTS EIIA (PDB ID, 1PDO) for mannose import (21). Structure refinement was conducted with *phenix refine* in *PHENIX* software (22). The model was refined manually with *winCoot* software (23). Figures for the protein structure were prepared using the *PyMOL* (24).

Assays for Cytoplasmic Enzymes. To analyze the inhibitory effects of compounds on *S. agalactiae* UGL, the purified enzyme was incubated at 30°C in a solution containing 0.2 mM unsaturated chondroitin disaccharide sulfated at the C-6 position of GalNAc (CΔ6S) as a substrate, 50 mM Tris-HCl (pH 7.5), and 5 mM polysaccharide or glycine. Gellan gum, xanthan gum, hyaluronan, chondroitin sulfate C, and heparin were used as polysaccharides containing GlcUA. UGL activity was measured by monitoring the decrease in absorbance at 235 nm due to the loss of the C=C double bond of CΔ6S.

To determine the enzymatic route for metabolism of unsaturated glucuronate (ΔGlcUA), CΔ6S was degraded by UGL to ΔGlcUA and GalNAc6S, and the resultant ΔGlcUA was non-enzymatically converted to 4-deoxy-L-*threo*-5-hexosulose uronate (DHU). DHU was reacted with two proteins, gbs1892 and gbs1891. To analyze the cofactor dependence of gbs1891, the enzyme activity was measured at 30°C in the presence of NADH or NADPH by monitoring the decrease in absorbance at 340 nm due to cofactor oxidation. The mimic substrate for purified gbs1891 and its mutants (S150A, Y163F, and K167A), 5-keto-D-gluconate (5-KG), was also used because the intrinsic substrate, 3-deoxy-D-*glycero*-2,5-hexodiulosonate (DK-II), is commercially unavailable.

Results

Degradation of GAGs by *S. agalactiae*

Because *S. agalactiae* is known to produce hyaluronate lyase depolymerizing not only hyaluronan but also chondroitin sulfate (25), the halo plate method was used to investigate the streptococcal GAG-degrading ability. Chondroitin sulfate is classified into chondroitin sulfates A, B, and C based on the position of the sulfate group (26). Chondroitin sulfate C is sulfated at the C-6 position of GalNAc, whereas chondroitin sulfates A and B are sulfated at the C-4 position of

GalNAc. The repeating units of chondroitin sulfates A, B, and C are GlcUA-GalNAc4S (GalNAc with a sulfate group at the C-4 position), IdoUA-GalNAc4S, and GlcUA-GalNAc6S (GalNAc with a sulfate group at the C-6 position), respectively (27). Because the plate containing the brain heart infusion suitable for streptococcal growth failed to produce the white precipitate resulting from the aggregation of GAGs and BSA in the presence of acetic acid, nutrient medium and horse serum were alternatively used for the halo plates. *S. agalactiae* NEM316 and *S. agalactiae* JCM 5671 containing GAG genetic cluster (Fig. 1-2) in their genomes were selected as typical strains of *S. agalactiae* to demonstrate GAG-degrading ability.

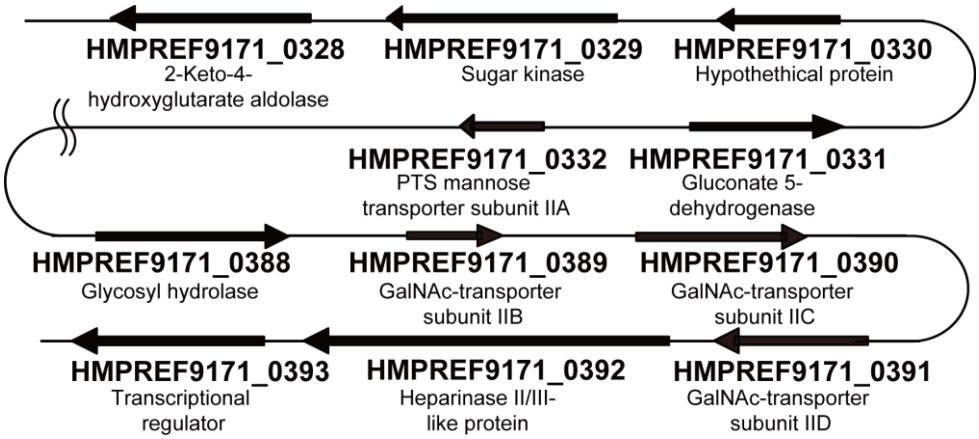

Figure 1-2. The GAG genetic cluster of *S. agalactiae* JCM 5671.

Although the GAG genetic cluster of *S. agalactiae* JCM 5671 is divided into two segments by the insertion of 55 genes between the HMPREF9171_0332 gene encoding the PTS EIIA and the HMPREF9171_0388 gene encoding UGL (Fig. 1-1 and 1-2), both *S. agalactiae* NEM316 and *S. agalactiae* JCM 5671 showed clear halos on plates containing hyaluronan, while no halos were observed on plates containing chondroitin sulfates A or C or heparin, indicating that *S. agalactiae* acted on hyaluronan, but not on chondroitin sulfates A and C, and heparin (Fig. 1-3). No degradation of chondroitin sulfates A and C by *S. agalactiae* was possibly due to low activity of the bacterial lyase toward chondroitin sulfates.

Because *S. agalactiae* was found to degrade hyaluronan, unsaturated hyaluronan disaccharide was prepared to investigate its PTS activity using recombinant bacterial hyaluronate lyase. An *E. coli* cell extract containing *S. agalactiae* hyaluronate lyase was reacted with hyaluronan, and the reaction product was purified by gel filtration chromatography (Fig. 1-4A). The eluted fractions

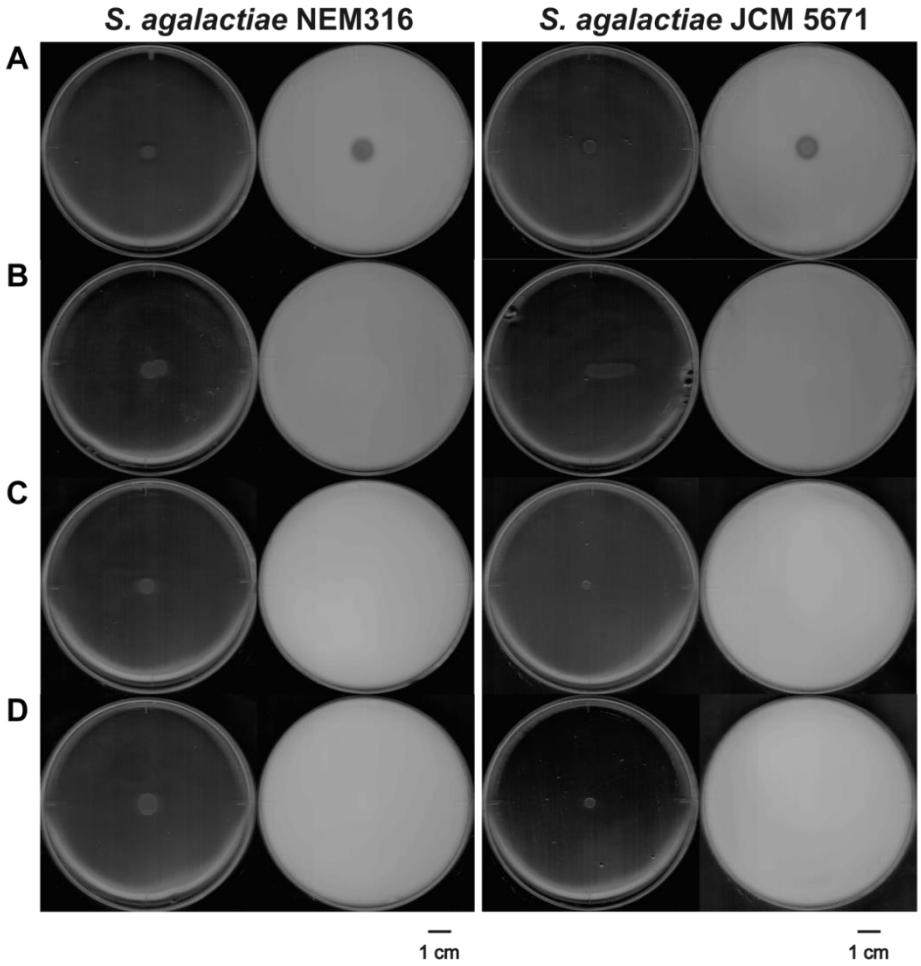

Figure 1-3. Degradation of GAGs by *S. agalactiae* NEM316 and *S. agalactiae* JCM 5671. The left and right plates in each panel are pictured before and after acetic acid addition, respectively. Plates contained hyaluronan (A), chondroitin sulfate A (B), chondroitin sulfate C (C), or heparin (D).

were subjected to TLC (Fig. 1-4B), and the fractions containing unsaturated hyaluronan disaccharide at elution volume of 21–23 ml were collected, concentrated, and used as a substrate for the PTS assay.

Import of Unsaturated Hyaluronan Disaccharide by *S. agalactiae* PTS

To demonstrate PTS-dependent import of unsaturated hyaluronan disaccharide by *S. agalactiae* NEM316, pyruvate production from phosphoenolpyruvate through PTS was measured using bacterial cells permeabilized by treatment with toluene (Fig. 1-5). Because *S. pneumoniae* has already been shown to incorporate cellobiose by PTS (28), cellobiose was used as a positive control. In contrast, D-glucosamine-6-phosphate (GlcN6P) was used as a negative control

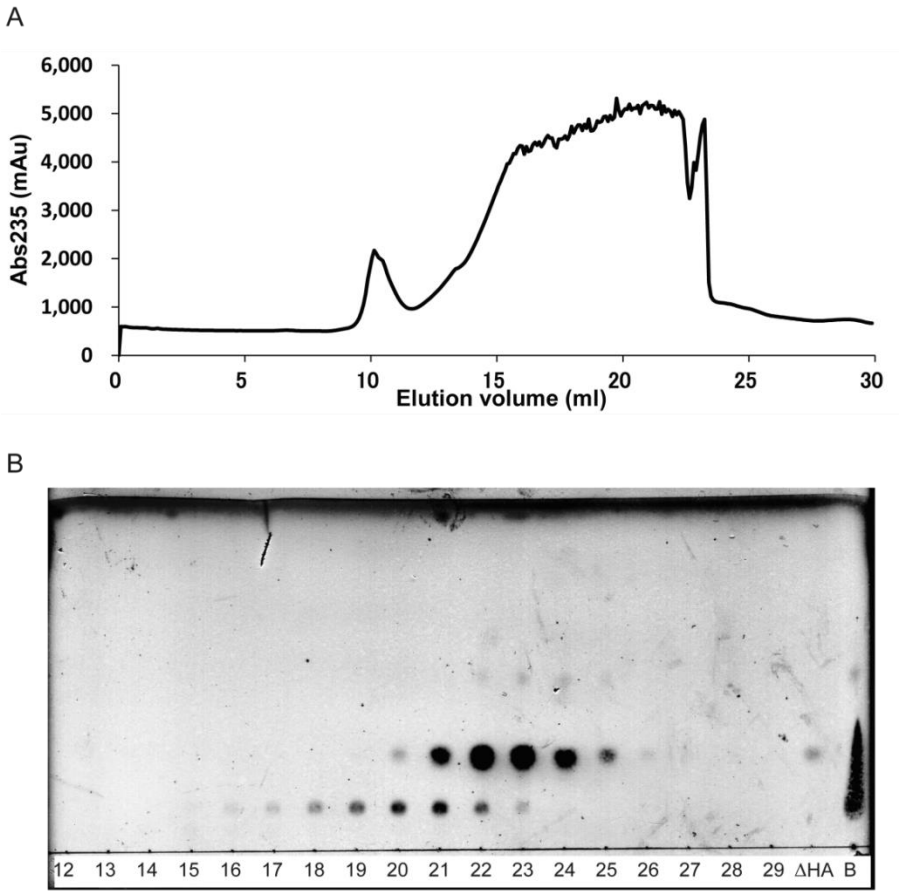

Figure 1-4. Preparation for unsaturated hyaluronan disaccharide. (A) Elution profile of unsaturated hyaluronan disaccharide (ΔHA) during gel filtration chromatography. (B) TLC fractions from gel filtration chromatography. Numbers denote elution volume (ml). B is a sample of the reaction mixture before chromatography.

because GlcN6P is unable to become a PTS substrate due to phosphorylation at the C-6 position. Gram-positive *Micrococcus luteus*, which has neither a GAG genetic cluster or cellobiose PTS genes in its genome, was also used as a negative control. Since DNA microarray results have shown that hyaluronan significantly increases the expression of the *S. agalactiae* GAG genetic cluster (12), PTS import activities were compared in the presence and absence of hyaluronan during bacterial growth.

As a result, *S. agalactiae* cells grown both in the presence and absence of hyaluronan increased the PTS activity for cellobiose import in comparison with the basal activity measured in the absence of sugar substrate, indicating that the bacterial PTS incorporated cellobiose. In contrast, *S. agalactiae* cells grown in the presence and absence of hyaluronan exhibited no enhanced PTS activity using GlcN6P as a substrate. These results indicated that permeabilized *S. agalactiae* cells

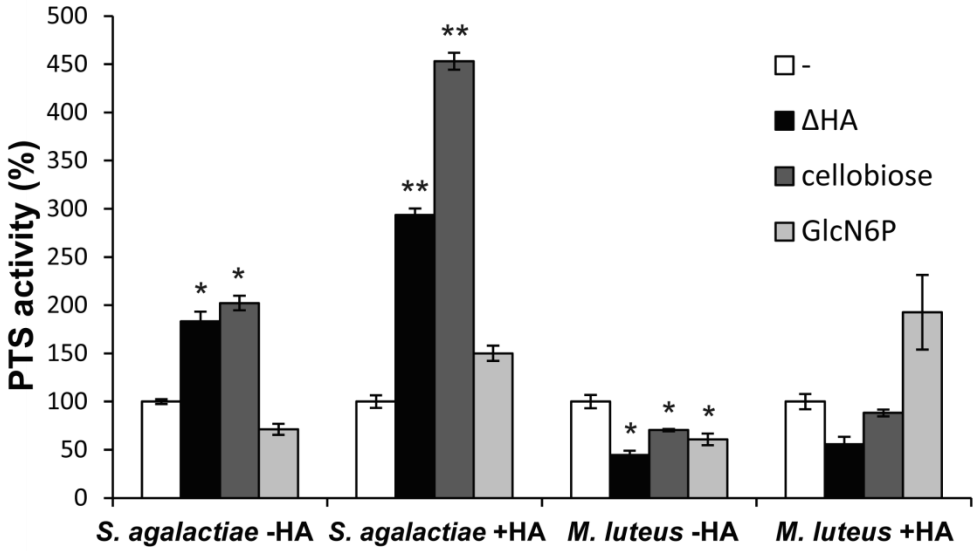

Figure 1-5. PTS activity for import of unsaturated hyaluronan disaccharide. Toluene-treated *S. agalactiae* or *M. luteus* cells in the presence or absence of hyaluronan were analyzed with the PTS assay. PTS activity was measured in the absence saccharide (basal activity; white) in the presence of unsaturated hyaluronan disaccharide (black), cellobiose (dark gray), or GlcN6P (gray) as substrates (**$p < 0.01$; *$p < 0.05$).

were functionally active and that this PTS assay was reliable. The bacterial cells grown in the presence of hyaluronan exhibited higher PTS activity for cellobiose import than those in the absence of hyaluronan, probably due to hyaluronan-dependent increases in the transcriptional level of PTS genes for cellobiose import (12). In contrast, *M. luteus* cells exhibited the same PTS activity level for cellobiose import as the basal controls, consistent with the lack of a cellobiose PTS in *M. luteus*. As with *S. agalactiae*, *M. luteus* cells exhibited little PTS activity for GlcN6P import.

The PTS import activity for unsaturated hyaluronan disaccharide of *S. agalactiae* cells grown in the absence and presence of hyaluronan was about 1.8 and 2.9 times higher than basal levels, respectively. These results directly demonstrate that *S. agalactiae* incorporates unsaturated hyaluronan disaccharide using a PTS.

Structure Determination of *S. agalactiae* EIIA

As a first step toward determining the overall structure of the *S. agalactiae* PTS complex (EIIABCD) for the import of unsaturated hyaluronan disaccharide, X-ray crystallography of $EIIA^{\Delta HA}$, EIIA for unsaturated hyaluronan disaccharide (ΔHA), was performed. Recombinant purified $EIIA^{\Delta HA}$ protein was crystallized and X-ray diffraction data were collected. Data collection and refinement statistics are shown in Table 1-2. The $EIIA^{\Delta HA}$ crystal belongs to the *P*1 group with

unit cell dimensions of a = 52.3, b = 53.8, and c = 94.9 Å, and α = 91.1, β = 90.0, and γ = 61.0°. The final model, containing six molecules in the asymmetric unit, was refined to an R_{work} of 20.8% up to a resolution of 1.8 Å. Ramachandran plot analysis indicated 99.0% of residues in the favored regions and 1.00% of residues in the additional allowed regions. The crystal structure of $EIIA^{\Delta HA}$ was determined by molecular replacement with *E. coli* PTS $EIIA^{man}$ (PDB ID, 1PDO) for mannose import as the initial model.

Table 1-2. Statistics of $EIIA^{\Delta HA}$ for data collection and structure refinement

	$EIIA^{\Delta HA}$
Data collection	
Space group	*P*1
Cell dimensions	
a, b, c (Å)	52.3, 53.8, 94.9
α, β, γ (°)	91.1, 90.0, 61.0
Resolution (Å)	50.0-1.80 (1.86-1.80) *
R_{merge}	7.4 (24.3)
$I / \sigma (I)$	26.6 (3.25)
Completeness (%)	96.1 (94.5)
Redundancy	2.1 (2.0)
Refinement	
Resolution (Å)	33.8-1.80 (1.82-1.80)
No. reflections	80171 (2274)
R_{work} / R_{free}	20.8 (26.4) / 24.2 (36.8)
No. atoms	
Protein	6038
Glycerol	66
Water	265
B-factor (Å^2)	
Protein	25.8
Glycerol	38.1
Water	29.2
Root Mean Square Deviations	
Bond lengths (Å)	0.006
Bond Angles (°)	1.06
Ramachandran plot (%)	
Favored region	99.0
Allowed region	1.00
Outlier region	0

*Data for the highest resolution shell is shown in parenthesis.

Crystal Structure of EIIA$^{\Delta HA}$

EIIA$^{\Delta HA}$ consists of 144 residues, although the C-terminal 14 residues (Leu131–Ile144) were unable to be assigned due to structural flexibility. With respect to the secondary structure of EIIA$^{\Delta HA}$, α-helices, β-sheets, and loops constitute 41.0%, 17.0%, and 42.0%, respectively. EIIA$^{\Delta HA}$ is composed of six α-helices (α1, Phe12–Ala24; α2, Ser41–Val52; α3, Thr68–Leu76; α4, Leu93–Met105; α5, Asp110–Glu122; α6, and Phe127–Thr129), five β-strands (β1, Lys3–His9; β2, Val30–Phe35; β3, Glu57–Thr62; β4, Lys84–Ser89; and β5, Val125–Asp126), and ten loops (L1, Met1–Ile2; L2, Gly10–Asn11; L3, Gly25–Tyr29; L4, Ile36–Ser40; Ile53–Lys56; L5, Asp63–Gly67; L6, Ser77–Lys83; L7, Gly90–Asn92; L8, Phe106–Val109; L9, Gly123–Ile124; and L10, Cys130). In the overall structure, a parallel β-sheet containing four β-strands (β1, β2, β3, and β4) is located at the center, and two (α2 and α3) and three α-helices (α1, α4, and α5) are located to pinch the β-sheet from both sides, resulting in formation of Rossman-fold frame (Fig. 1-6). β1–4 and α1–4 are alternately arranged and α4 is followed by α5 before β5. Gel filtration chromatography suggested that EIIA$^{\Delta HA}$ was smaller than a tetramer and likely to be dimer. In the dimer, the C-terminal β5 in adjacent monomers are arranged to align with mutual β4 and added to the parallel β-sheet located at the center of the monomer, forming an antiparallel β-sheet.

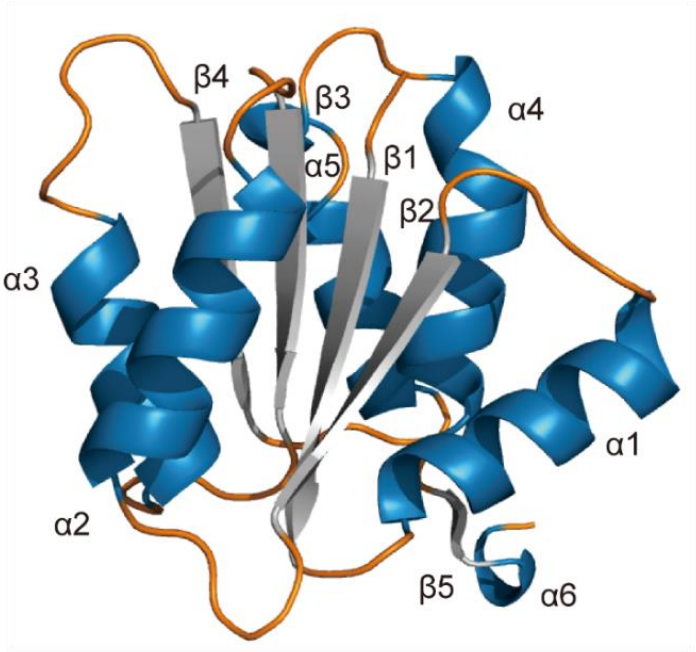

Figure 1-6. Overall structure of *S. agalactiae* PTS EIIA$^{\Delta HA}$. Blue, α-helices; gray, β-strands, and orange, loops.

Inhibition of *S. agalactiae* UGL by Glycine

After streptococcal PTS incorporates unsaturated hyaluronan disaccharide into the cytoplasm, UGL degrades the disaccharide to constituent monosaccharides. Streptococcal UGL is known to act on disaccharides derived from hyaluronan, chondroitin sulfate, heparin, and heparan sulfate (12, 13). An inhibitor of UGL is, therefore, expected to be a promising therapeutic agent for streptococcal infection. To identify such an inhibitor, the inhibitory potencies of several acidic polysaccharides, including GAGs, were assessed.

Hyaluronan and chondroitin sulfate C inhibited the enzyme activity only slightly, and no polysaccharide tested was a potent inhibitor (Table 1-3). On the other hand, glycine almost completely inhibited the enzyme activity at 5.0 mM. Glycine was found to be an antagonistic inhibitor for *S. agalactiae* UGL (K_i = 3.6 mM).

Table 1-3. Inhibitory potency of polysaccharides for *S. agalactiae* UGL

Inhibitor	Specific activity (U/mg)	Relative activity (%)
None	5.41 ± 0.22	100
Hyaluronan	4.13 ± 0.24	76.3
Chondroitin sulfate C	4.37 ± 0.37	80.7
Heparin	5.32 ± 0.06	98.4
Gellan	5.20 ± 0.39	96.2
Xanthan	5.36 ± 0.06	99.1
Glycine	0.24 ± 0.05	4.36

Each data represents the average of triplicate individual experiments (mean ± standard deviations).

Metabolic Pathway of Unsaturated Uronate Derived from GAG

ΔGlcUA, produced from unsaturated hyaluronan disaccharide by UGL is non-enzymatically converted to DHU. Interestingly, ΔGlcUA is structurally identical to unsaturated galacturonate due to the lack of a hydroxyl group at the C-4 position in both unsaturated uronates. Pectin-derived unsaturated galacturonate is known to be metabolized to 2-keto-3-deoxy-D-gluconate (KDG) by the successive reactions of 4-deoxy-L-*threo*-5-hexosulose uronate ketol-isomerase (KduI) and 2-keto-3-deoxy-D-gluconate dehydrogenase (KduD) (29). Therefore, ΔGlcUA-derived DHU is also considered to be converted to KDG by this isomerase and dehydrogenase. Thus, two *S. agalactiae* proteins with unknown functions encoded in the GAG genetic cluster, i.e., gbs1891, which is similar to 5-keto-D-gluconate dehydrogenase/reductase, and the hypothetical protein gbs1892, were focused on even though both of gbs1891 and gbs1892 exhibited little sequence identity with KduI and/or KduD. To investigate the function of gbs1891 and gbs1892, the proteins were expressed in

recombinant *E. coli* cells and purified to homogeneity. DHU was found to be converted to KDG in the presence of gbs1891 and gbs1892 in combination with cofactors (NADH or NADPH). Based on alternative replacement reaction using KduI and/or KduD, DHU was converted to DK-II by gbs1892 4-deoxy-L-*threo*-5-hexosulose uronate ketol-isomerase (DhuI) and subsequently to KDG by gbs1891 NADH-dependent 2-keto-3-deoxy-D-gluconate dehydrogenase (DhuD) (Fig. 1-7). KDG is suggested to be converted to pyruvate and glyceraldehyde 3-phosphate by KdgK and KdgA, also encoded in the GAG genetic cluster, on the basis of the KDG metabolic pathway established in the pectin-degrading *Erwinia chrysanthemi* (30).

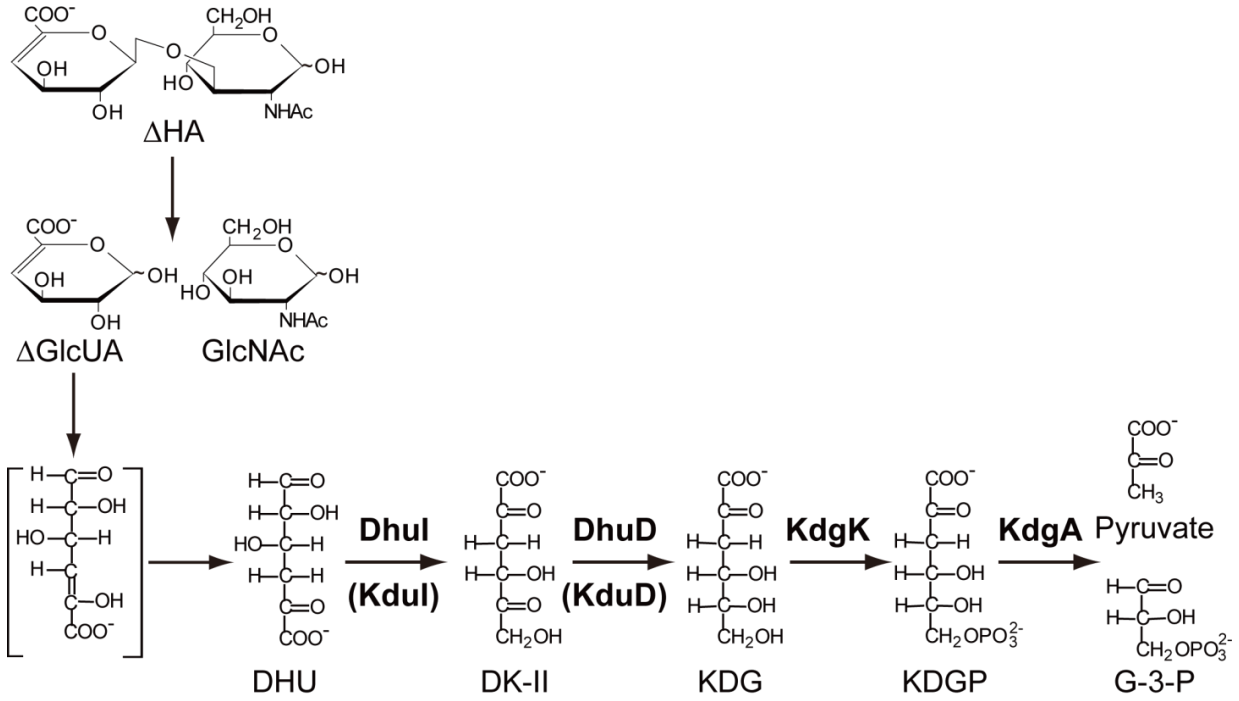

Figure 1-7. Bacterial metabolism of GAGs. After GAGs are degraded by lyase and UGL, the resultant unsaturated uronates are non-enzymatically converted to DHU. DHU is metabolized to KDG through successive reactions of DhuI and DhuD. KDG is suggested to be converted to pyruvate and glyceraldehyde-3-phosphate (G-3-P) by KdgK and KdgA.

The substrate specificity of DhuD was investigated using DK-II, 5-KG, 2-keto-D-gluconate, and gluconate. The enzyme was highly specific for DK-II and acted slightly on 5-KG. 2-Keto-D-gluconate and gluconate were inert as a substrate for DhuD. The kinetic parameters (K_m and k_{cat}) of DhuD for NADH using DK-II as the substrate were determined to be 9.62 ± 1.05 μM and 2.67 ± 0.07 /s, respectively. The K_m and k_{cat} of DhuD for NADH using 5-KG were 26.3 ± 16.2 μM and 1.57 ± 0.30 /s, respectively. The kinetic parameters of DhuD for NADPH failed to be

determined due to its low activity. Based on the primary structure, DhuD was found to belong to the short-chain dehydrogenase/reductase family (31). The active site of enzymes in this family is formed by a catalytic triad of Ser, Tyr, and Lys (32), and Ser150, Tyr163, and Lys167 are conserved in DhuD. Therefore, mutants in these residues (S150A, Y163F, and K167A) were also tested for enzymatic activity. DK-II was used as a substrate, the kinetic parameters for DK-II of the DhuD mutants failed to be determined due to its low concentration. Since DK-II is commercially unavailable and difficult to prepare on a large scale, 5-KG was used as a mimic substrate (Table 1-4). As a result, the K_m and k_{cat} of wild-type DhuD for 5-KG were determined to be 231 ± 51 mM and 0.521 ± 0.038 /s, respectively, whereas the three mutants exhibited significantly lower activities than wild-type, indicating that Ser150, Tyr163, and Lys167 function as a catalytic triad.

Table 1-4. Reductase activity of wild-type and mutant DhuD

	Specific activity (U/g)	Relative activity (%)
WT	484	100
S150A	0.323	0.0667
Y163F	2.14	0.443
K167A	0.246	0.0509

Discussion

Because of the ability of *S. agalactiae* to degrade hyaluronan, its PTS import activity was measured using unsaturated disaccharide derived from hyaluronan. As a result, the PTS activity using unsaturated hyaluronan disaccharide as a substrate was significantly enhanced compared with controls using no substrate or GlcN6P, indicating that *S. agalactiae* incorporates unsaturated hyaluronan disaccharide using a PTS. Furthermore, the PTS activity for import of unsaturated hyaluronan disaccharide in bacterial cells grown in the presence of hyaluronan was about two-fold higher than that in the absence of hyaluronan during the bacterial growth, suggesting an increase of PTS protein expression levels in the presence of hyaluronan. This result coincided with previous result of DNA microarray showing that hyaluronan significantly induces a two-fold increase in the expression of the GAG genetic cluster in the *S. agalactiae* genome. The *S. pneumoniae* PTS encoded in the GAG genetic cluster has already been demonstrated to be required for bacterial growth on hyaluronan as a sole carbon source and not to incorporate the monosaccharides (GlcUA and GlcNAc) constituting hyaluronan (3). On the basis of these *S. pneumoniae* data in combination with the present results regarding *S. agalactiae* PTS activity, the *Streptococcus* PTS encoded in the GAG genetic cluster was suggested to incorporate unsaturated hyaluronan disaccharide. This

molecular identification of the streptococcal PTS as the importer of unsaturated hyaluronan disaccharide is strongly supported by recent results showing that disruption of the *S. agalactiae* PTS encoded in the GAG cluster results in a strain with very little PTS activity using unsaturated hyaluronan disaccharide as a substrate (unpublished data).

While bacterial cells incorporate sugars by various mechanisms such as facilitated diffusion, primary and secondary active transport and group translocation, PTS is the major sugar import pathway in many bacteria (17, 33). PTS Enzyme II is classified into four families based on primary structure: (i) the glucose-fructose-lactose family; (ii) the ascorbate-galactitol family; (iii) the mannose family; and (iv) the dihydroxyacetone family (34). Characteristic features of the mannose family are as follows: EIIC is not a homo-membrane domain but a hetero-membrane domain in combination with EIID; EIIB receives a phosphate group from a histidine residue rather than a cysteine residue, and various sugars are used as substrates. *S. agalactiae* $EIIA^{\Delta HA}$ was most similar to *E. coli* mannose EIIA (PDB ID, 1PDO), *Thermoanaerobacter tengcongensis* mannose EIIA (PDB ID, 3LFH) and *Enterococcus faecalis* gluconate EIIA (PDB ID, 3IPR), which all belong to the mannose family, and the similarity scores by the jFATCAT-rigid algorithm were 319.4, 324.2, and 299.8, respectively (35, 36). Based on the well-conserved characteristic features of the mannose family, the *S. agalactiae* PTS for import of unsaturated hyaluronan disaccharide was revealed to be a member of the mannose family. Although these three-dimensional structures were well superimposed, the loops between α2 and β3, α3 and β4, and α4 and α5, present in the same area around the N-terminus, differed from each other (Fig. 1-8A). Based on the primary structure, homology modeling of *S. agalactiae* $EIIB^{\Delta HA}$ by SWISS-MODEL showed that $EIIB^{\Delta HA}$ is composed of an antiparallel β-sheet composed of eight β-strands and eight α-helices (Fig. 1-8C). The three-dimensional structures of *E. coli* HPr-$EIIA^{Man}$ and $EIIA^{Man}$-$EIIB^{Man}$ complexes have already been determined by NMR, and $EIIA^{Man}$ has also been found to form a dimer (37, 38). In the complex of HPr-$EIIA^{Man}$ and $EIIA^{Man}$-$EIIB^{Man}$, His10 of $EIIA^{Man}$ is an important residue for transferring a phosphate group from HPr to $EIIB^{Man}$ through $EIIA^{Man}$ (39). Because the interaction site of $EIIA^{Man}$ with HPr is similar to that of $EIIA^{Man}$ with $EIIB^{Man}$, HPr or $EIIB^{Man}$ must be separated while the other is bound to $EIIA^{Man}$. His10 of $EIIA^{Man}$ is also conserved in $EIIA^{\Delta HA}$ as His9 (Fig. 1-8B). Superimposition of the $EIIA^{\Delta HA}$ dimer and $EIIB^{\Delta HA}$ monomer with $EIIA^{Man}$-$EIIB^{Man}$ complex provided the structural insight that His9 of $EIIA^{\Delta HA}$ transfers a phosphate group from HPr to $EIIB^{\Delta HA}$ (Fig. 1-8D). While the arrangements of His10 of $EIIA^{\Delta HA}$ and His9 of $EIIA^{Man}$ almost corresponded with each other, the sidechains of His18 of $EIIB^{\Delta HA}$ and His175 of

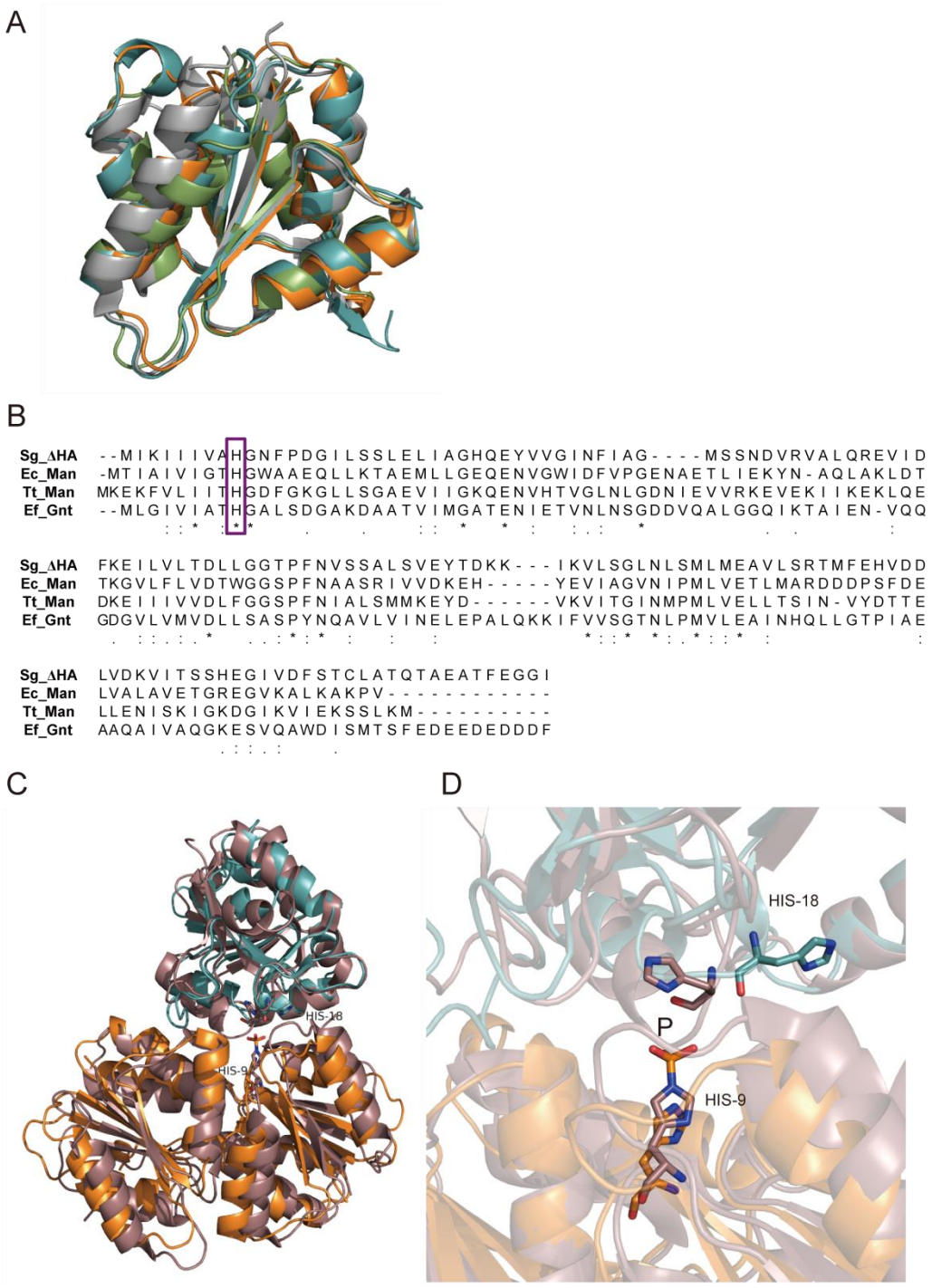

Figure 1-8. Features of *S. agalactiae* PTS EIIA$^{\Delta HA}$. (A) Homologous proteins of *S. agalactiae* PTS EIIA$^{\Delta HA}$. Orange, *S. agalactiae* PTS EIIA$^{\Delta HA}$ (Sg_ΔHA); light green, *E. coli* mannose PTS EIIA^{Man} (Ec_Man); gray, *T. tengcongensis* mannose PTS EIIA^{Man} (Tt_Man); and cyan, *E. faecalis* gluconate PTS EIIA^{Gnt} (Ef_Gnt). (B) Primary structure alignment of these homologous PTS EIIAs. (C) Superimposing *S. agalactiae* PTS EIIA$^{\Delta HA}$-EIIB$^{\Delta HA}$ and *E. coli* EIIA^{Man}-EIIB^{Man} complexes. Orange, *S. agalactiae* PTS EIIA$^{\Delta HA}$; cyan, *S. agalactiae* PTS EIIB$^{\Delta HA}$ (modeling); dark pink, *E. coli* EIIA^{Man}-EIIB^{Man} complex. (D) Transfer of a phosphate group from *S. agalactiae* PTS EIIA$^{\Delta HA}$ to PTS EIIB$^{\Delta HA}$.

$EIIA^{Man}$ were oriented in opposite directions. His9 of $EIIA^{\Delta HA}$, crucial for transferring a phosphate group, was located at the end of β1 and interacted with Asp63 by hydrogen bonds and with Phe12, Gly67, Pro69, and Phe35 by van der Waals contacts.

Although several compounds have been investigated as potential UGL inhibitors to date, no effective inhibitors have been discovered. The *S. agalactiae* enzyme was slightly inhibited by hyaluronan and chondroitin sulfate C (Table 1-3). The *S. agalactiae* UGL preferentially degrades unsaturated hyaluronan and chondroitin sulfate disaccharides with 1,3-glycoside bonds (12, 13), suggesting that parts of these hyaluronan and chondroitin sulfate C polysaccharides also bind to the active site of the enzyme. Glycine inhibits the enzyme activity of *Bacillus* sp. strain GL1 UGL (40). To determine whether glycine is an inhibitor of *S. agalactiae* UGL, the effect of the amino acid on the enzyme activity was evaluated. Glycine inhibited *S. agalactiae* UGL in a dose-dependent manner, similar to that of the *Bacillus* enzyme. A double reciprocal plot showed that glycine has a K_i of 3.6 mM for *S. agalactiae* UGL. Given that the K_i of glycine for the *Bacillus* enzyme has been determined to be 6.5 mM (40), glycine appears to exhibit a stronger inhibitory effect on *S. agalactiae* UGL than on the *Bacillus* enzyme. The crystal structure of *Bacillus* UGL complexed with glycine indicates that the carboxyl group of glycine binds to the active site corresponds to that of the unsaturated glucuronate residue in the substrate (40). Gln211, Arg221, and Trp225 in the *Bacillus* UGL are involved in recognition of the carboxyl group of the substrate and are conserved in other streptococcal UGLs, indicating that UGLs commonly recognize glycine.

GAGs-derived unsaturated uronates were found to be metabolized in *S. agalactiae* cells by isomerase and dehydrogenase activities. DHU that was generated non-enzymatically from unsaturated uronates was converted to KDG via DK-II through successive reactions catalyzed by DhuI and DhuD. DhuI and DhuD enzymatic activities corresponded to KduI and KduD, respectively, involved in pectin metabolism, although either no or low sequence identity was found between DhuI and KduI and between DhuD and KduD, respectively. The genes encoding DhuI and DhuD are also present in the GAG genetic cluster.

In this CHAPTER, *S. agalactiae* was found to incorporate unsaturated hyaluronan disaccharide by the PTS encoded in the GAG genetic cluster. Since, distinct from other sulfated GAGs, hyaluronan has no sulfate groups at the C-6 position of its constituent monosaccharides, unsaturated hyaluronan disaccharide is a suitable substrate for the PTS through transfer of a phosphate group to the C-6 position of the substrate. X-ray crystallography and docking simulations provided structural insights into the transfer of the phosphate group in the streptococcal PTS. The metabolic pathway of

unsaturated uronates from GAGs and its relevant enzymes/genes were elucidated for the first time in streptococci.

References

1. Patterson, M. J. (1996) Streptococcus. Chapter 13 *In*: Baron, S., editor. Medical Microbiology. 4 th edition. Galveston (TX): University of Texas Medical Branch at Galveston
2. Glaser, P., Rusniok, C., Buchrieser, C., Chevalier, F., Frangeul, L., Msadek, T., Zouine, M., Couve, E., Lalioui, L., and Poyart, C. (2002) Genome sequence of *Streptococcus agalactiae*, a pathogen causing invasive neonatal disease. *Mol. Microbiol.* **45**, 1499-1513
3. Marion, C., Stewart, J. M., Tazi, M. F., Burnaugh, A. M., Linke, C. M., Woodiga, S. A., and King, S. J. (2012) *Streptococcus pneumoniae* can utilize multiple sources of hyaluronic acid for growth. *Infect. Immun.* **80**, 1390-1398
4. Starr, C. R., and Engleberg, N. C. (2006) Role of hyaluronidase in subcutaneous spread and growth of group A streptococcus. *Infect. Immun.* **74**, 40-48
5. Wang, Z., Guo, C., Xu, Y., Liu, G., Lu, C., and Liu, Y. (2014) Two novel functions of hyaluronidase from *Streptococcus agalactiae* are enhanced intracellular survival and inhibition of proinflammatory cytokine expression. *Infect. Immun.* **82**, 2615-2625
6. Jedrzejas, M. J. (2001) Pneumococcal virulence factors: structure and function. *Microbiol. Mol. Biol. Rev.* **65**, 187-207
7. Postma, P., and Lengeler, J. (1985) Phosphoenolpyruvate: carbohydrate phosphotransferase system of bacteria. *Microbiol. Rev.* **49**, 232-269
8. Deutscher, J., Ake, F. M. D., Derkaoui, M., Zebre, A. C., Cao, T. N., Bouraoui, H., Kentache, T., Mokhtari, A., Milohanic, E., and Joyet, P. (2014) The bacterial phosphoenolpyruvate: carbohydrate phosphotransferase system: regulation by protein phosphorylation and phosphorylation-dependent protein-protein interactions. *Microbiol. Mol. Biol. Rev.* **78**, 231-256
9. Habuchi, O. (2000) Diversity and functions of glycosaminoglycan sulfotransferases. *Biochim. Biophys. Acta* **1474**, 115-127
10. Simoni, R. D., Levinthal, M., Kundig, F. D., Kundig, W., Anderson, B., Hartman, P. E., and Roseman, S. (1967) Genetic evidence for the role of a bacterial phosphotransferase system in sugar transport. *Proc. Natl. Acad. Sci. U. S. A.* **58**, 1963-1970

11. Barabote, R. D., and Saier, M. H. (2005) Comparative genomic analyses of the bacterial phosphotransferase system. *Microbiol. Mol. Biol. Rev.* **69**, 608-634
12. Maruyama, Y., Nakamichi, Y., Itoh, T., Mikami, B., Hashimoto, W., and Murata, K. (2009) Substrate specificity of streptococcal unsaturated glucuronyl hydrolases for sulfated glycosaminoglycan. *J. Biol. Chem.* **284**, 18059-18069
13. Nakamichi, Y., Maruyama, Y., Mikami, B., Hashimoto, W., and Murata, K. (2011) Structural determinants in streptococcal unsaturated glucuronyl hydrolase for recognition of glycosaminoglycan sulfate groups. *J. Biol. Chem.* **286**, 6262-6271
14. Kawada-Matsuo, M., Mazda, Y., Oogai, Y., Kajiya, M., Kawai, T., Yamada, S., Miyawaki, S., Oho, T., and Komatsuzawa, H. (2012) GlmS and NagB regulate amino sugar metabolism in opposing directions and affect *Streptococcus mutans* virulence. *PloS one* **7**, e33382
15. Sanger, F., Nicklen, S., and Coulson, A. R. (1977) DNA sequencing with chain-terminating inhibitors. *Proc. Natl. Acad. Sci. U. S. A.* **74**, 5463-5467
16. Maruyama, Y., Oiki, S., Takase, R., Mikami, B., Murata, K., and Hashimoto, W. (2015) Metabolic fate of unsaturated glucuronic/iduronic acids from glycosaminoglycans: Molecular identification and structure determination of streptococcal isomerase and dehydrogenase. *J. Biol. Chem.* **290**, 6281-6292
17. Kornberg, H. L., and Reeves, R. E. (1972) Inducible phosphoenolpyruvate-dependent hexose phosphotransferase activities in *Escherichia coli*. *Biochem. J.* **128**, 1339-1344
18. Moye, Z. D., Burne, R. A., and Zeng, L. (2014) Uptake and metabolism of *N*-acetylglucosamine and glucosamine by *Streptococcus mutans*. *Appl. Environ. Microbiol.* **80**, 5053-5067
19. Smith, P. K., Krohn, R. I., Hermanson, G., Mallia, A., Gartner, F., Provenzano, M., Fujimoto, E., Goeke, N., Olson, B., and Klenk, D. (1985) Measurement of protein using bicinchoninic acid. *Anal. Biochem.* **150**, 76-85
20. Otwinowski, Z., and Minor, W. (1997) Processing of X-ray diffraction data collected in oscillation mode. *Meth. Enzymol.* **276**, 307-326
21. Vagin, A., and Teplyakov, A. (1997) MOLREP: an automated program for molecular replacement. *J. App. Crystallog.* **30**, 1022-1025
22. Adams, P. D., Afonine, P. V., Bunkoczi, G., Chen, V. B., Davis, I. W., Echols, N., Headd, J. J., Hung, L.-W., Kapral, G. J., and Grosse-Kunstleve, R. W. (2010) PHENIX: a comprehensive Python-based system for macromolecular structure solution. *Acta*

Crystallogr. Sect. D: Cryst. Struct. Commun. **66**, 213-221

23. Emsley, P., Lohkamp, B., Scott, W. G., and Cowtan, K. (2010) Features and development of Coot. *Acta Crystallogr. Sect. D: Cryst. Struct. Commun.* **66**, 486-501
24. DeLano, W. L. (2002) The PyMOL molecular graphics system.
25. Baker, J. R., Hao, Y., Morrison, K., Averett, W. F., and Pritchard, D. G. (1997) Specificity of the hyaluronate lyase of group-B streptococcus toward unsulphated regions of chondroitin sulphate. *Biochem. J.* **327**, 65-71
26. Foot, M., and Mulholland, M. (2005) Classification of chondroitin sulfate A, chondroitin sulfate C, glucosamine hydrochloride and glucosamine 6 sulfate using chemometric techniques. *J. Pharm. Biomed. Anal.* **38**, 397-407
27. Mathews, M. B., and Inouye, M. (1961) The determination of chondroitin sulfate C-type polysaccharides in mixture with other acid mucopolysaccharides. *Biochim. Biophys. Acta* **53**, 509-513
28. Shafeeq, S., Kloosterman, T. G., and Kuipers, O. P. (2011) CelR-mediated activation of the cellobiose-utilization gene cluster in *Streptococcus pneumoniae*. *Microbiology* **157**, 2854-2861
29. Preiss, J., and Ashwell, G. (1963) Polygalacturonic acid metabolism in bacteria II. Formation and metabolism of 3-deoxy-D-*glycero*-2, 5-hexodiulosonic acid. *J. Biol. Chem.* **238**, 1577-1583
30. Hugouvieux-Cotte-Pattat, N., and Robert-Baudouy, J. (1994) Molecular analysis of the *Erwinia chrysanthemi* region containing the *kdgA* and *zwf* genes. *Mol. Microbiol.* **11**, 67-75
31. Persson, B., and Kallberg, Y. (2013) Classification and nomenclature of the superfamily of short-chain dehydrogenases/reductases (SDRs). *Chem. Biol. Interact.* **202**, 111-115
32. Filling, C., Nordling, E., Benach, J., Berndt, K. D., Ladenstein, R., Jornvall, H., and Oppermann, U. (2001) Structural role of conserved Asn179 in the short-chain dehydrogenase/reductase scaffold. *Biochem. Biophys. Res. Commun.* **289**, 712-717
33. Saier Jr, M. H. (1977) Bacterial phosphoenolpyruvate: sugar phosphotransferase systems: structural, functional, and evolutionary interrelationships. *Bacteriol. Rev.* **41**, 856-871
34. Saier, M., Hvorup, R., and Barabote, R. (2005) Evolution of the bacterial phosphotransferase system: from carriers and enzymes to group translocators. *Biochem. Soc. Trans.* **33**, 220-224
35. Andreas, P., Bliven, S., Rose, P. W., Bluhm, W. F., Bizon, C., Godzik, A., and Bourne, P. E.

(2010) Pre-calculated protein structure alignments at the RCSB PDB website. *Bioinformatics* **26**, 2983-2985

36. Ye, Y., and Godzik, A. (2003) Flexible structure alignment by chaining aligned fragment pairs allowing twists. *Bioinformatics* **19**, ii246-ii255
37. Williams, D. C., Cai, M., Suh, J., Peterkofsky, A., and Clore, G. M. (2005) Solution NMR structure of the 48-kDa $IIA^{Mannose}$-HPr complex of the *Escherichia coli* mannose phosphotransferase system. *J. Biol. Chem.* **280**, 20775-20784
38. Hu, J., Hu, K., Williams, D. C., Komlosh, M. E., Cai, M., and Clore, G. M. (2008) Solution NMR structures of productive and non-productive complexes between the A and B domains of the cytoplasmic subunit of the mannose transporter of the *Escherichia coli* phosphotransferase system. *J. Biol. Chem.* **283**, 11024-11037
39. Nunn, R. S., Markovic-Housley, Z., Genovesio-Taverne, J.-C., Flukiger, K., Rizkallah, P. J., Jansonius, J. N., Schirmer, T., and Erni, B. (1996) Structure of the IIA domain of the mannose transporter from *Escherichia coli* at 1.7 Å resolution. *J. Mol. Biol.* **259**, 502-511
40. Itoh, T., Hashimoto, W., Mikami, B., and Murata, K. (2006) Substrate recognition by unsaturated glucuronyl hydrolase from *Bacillus* sp. GL1. *Biochem. Biophys. Res. Commun.* **344**, 253-262

CHAPTER II

Interactions between intestinal microbiota and host cells through glycosaminoglycans

Human intestine is most densely populated with 10^{13}–10^{14} bacteria, belonging to approximately 500–1000 species (1), among any other organs and genomes of the microbiota in the intestine include at least 100 times as many genes as host human genome (2). Human intestinal microbiota provide strong influences on host human biology such as stimulation of intestinal cell maturation and proliferation, enhancement of proper immune development, and protection against pathogens (3). Therefore, the intestinal microbiota could be viewed as 'microbial organ' (4) and the composition of the intestinal microbiota varies among individuals. Members of bacterial phyla of *Bacteroides* and *Firmicutes* are most abundant in the human intestine, followed by *Proteobacteria*, *Verrumicrobia*, *Actinobacteria*, *Fusobacteria*, and *Cyanobacteria* (1). *Bacteroides* occupies more than 10% of total human intestinal microbiota (5) and assimilates various sugars. *Bacteroides thetaiotaomicron* and *Bacteroides ovatus* degrade GAGs such as hyaluronan, chondroitin sulfate, and heparin (6, 7). *Bacteroides fragilis* and *Bacteroides stercoris* assimilate chondroitin sulfate (8). Recently, investigation of GAG-degrading ability of intestinal microbiota from six Chinese using feces has shown that the intestinal microbiota degraded chondroitin sulfate to disaccharides (9). However, little is known about degradation of heparin by intestinal microbiota. Considering the high frequency of genes coding for UGL and polysaccharide lyase in indigenous bacteria, some intestinal bacteria seem to exhibit GAG-degrading activity in addition to *Bacteroides*. *Lactobacillus* is known as probiotics, giving beneficial health effects to host (10), although degradation of GAGs by *Lactobacillus* remains unclear.

S. agalactiae, one of intestinal and vaginal microbiota, is an opportunistic pathogen having PTS for import of unsaturated hyaluronan disaccharide as described in CHAPTER I. Colonization of *S. agalactiae* to pregnant intestinal and vaginal tract causes infection to pregnant amniotic cavity and subsequently infection to neonates by the aspiration of contaminated amniotic fluid (11). *S. agalactiae* is also known to invade the bloodstream of the neonatal lung. Therefore, the adhesion of *S. agalactiae* to pregnant intestinal and vaginal epithelial cells essential for virulence has been well studied (11, 12). However, the involvement of host GAGs in the streptococcal adhesion to host epithelial cells remains to be clarified, although α-C protein, prototype for long tandem repeat family of surface proteins in streptococci, has previously been shown to function as an adhesion

factor to heparan sulfate in epithelium cells (13, 14).

This CHAPTER deals with degradation of GAGs by intestinal microbiota from Japanese as well as probiotics such as *Lactobacillus*, and with interaction between intestinal/vaginal bacteria and host human cells through GAGs.

Materials and Methods

Materials. Hyaluronan sodium salt was purchased from Sigma Aldrich. Chondroitin sulfates A and C sodium salts were from Wako Pure Chemical Industries. Heparin sodium salt was from Nacalai Tesque.

Microorganisms, Human Cells, and Culture Conditions. As described in CHAPTER I, *S. agalactiae* NEM316 (ATCC 12403) and *S. agalactiae* JCM 5671 (ATCC 13813) were statically grown at 37°C under 5% CO_2 in 3.7% brain heart infusion medium (BD Bacto). *Lactobacillus rhamnosus* NBRC 3425 and *Lactobacillus pantheris* NBRC 106106 were purchased from the National Institute of Technology and Evaluation, Japan. *B. thetaiotaomicron* JCM 5827 and *Bacteroides clarus* JCM 16067 were from the Japan Collection of Microorganisms. *Lactobacillus* and *Bacteroides* cells were anaerobically grown at 37°C in Man Rogosa Sharpe (MRS) (Wako Pure Chemical Industries) and Gifu Anaerobic Medium (GAM) (Nissui Pharmaceutical), respectively. Human colon cancer Caco-2 cells (RCB0988), human vaginal melanoma HMV-II cells (RCB3685), and human vaginal fibroblast HOUFXXX cells (RCB1171) were purchased from Riken Bio Resource Center. Caco-2 cells were cultured in Dulbecco's modified eagle medium (DMEM) (Nacalai Tesque) containing 20% fetal bovine serum (FBS) (Biological Industries) and 1% non-essential amino acids (Wako Pure Chemical Industries). HMV-II and HOUFXXX cells were cultured in Ham's F-12 (Nacalai Tesque) containing 15% FBS. These human cells were seeded in 12-well plates at a density of 4.0 x 10^5 cells/well and cultured at 37°C under 5% CO_2 for 21 days to be differentiated. The medium was changed every 2–3 days.

Co-culture of Human Intestinal Microbiota. A medium containing 0.4% (w/v) GAG (chondroitin sulfate C or heparin), 0.45% yeast extract, 0.3% tryptone, 0.3% peptone, 0.08% L-cysteine hydrochloride, 0.45% NaCl, 0.25% KCl, 0.045% $MgCl_2 \cdot 6H_2O$, 0.02% $CaCl_2 \cdot 2H_2O$, and 0.04% KH_2PO_4 was prepared for the co-culture of human intestinal microbiota according to the previous report with a slight modification (15). The human fecal suspension (10 μl) in saline (0.15 M NaCl) was added to 10 ml of the co-culture medium. Intestinal microbiota from a Japanese man in his 50's or a Japanese woman in her 20's were anaerobically grown at 37°C in the medium. A

portion (50 μl) was periodically sampled from the culture broth and centrifuged at 9,700 *g* and room temperature for 5 min. The supernatant was stored at –20°C until ready for use.

GAG Assay. The 1,9-dimethylmethylene blue (DMMB) assay was adopted to measure GAG concentration (16). The assay is based on spectrophotometric detection of metachromatic changes in DMMB due to combination with sulfate groups of sulfated GAGs such as chondroitin sulfate C and heparin (17). To prepare DMMB reagent, 0.304 g of glycine and 0.16 g of NaCl were dissolved in 80 ml of pure water. After 9.5 ml of 0.1 M acetic acid and 0.016 mg of DMMB were added, the solution was adjusted to 100 ml with pure water. The DMMB reagent (800 μl) was mixed with the culture supernatant (80 μl) and its GAG concentration was measured in absorbance at 525 nm. The culture medium containing chondroitin sulfate C or heparin was used for calibration curve (10, 20, 30, 40, and 50 μg/ml). The experiments were performed in triplicate.

TLC. To investigate degradation of GAGs, the culture supernatant was subjected to TLC. The culture supernatant (1 μl) was spotted on the TLC plate. Developing solvent contained 1-butanol/acetic acid/water (3/2/2, v/v). The TLC plate was sprayed with 10% (v/v) sulfuric acid in ethanol, followed by heating at 130°C for 5 min. GAGs were detected at the original spot point without a migration on the TLC plate, while depolymerized GAG oligosaccharides migrated from the original point on the plate.

Halo Detection for Degradation of GAGs by Bacteria. Halo detection method was adopted to investigate the GAG-degrading ability of some intestinal bacteria. As described in CHAPTER I, GAGs form white precipitates due to complex with BSA in the presence of acetic acid, while no precipitation of degraded GAGs with BSA caused clear a zone, halo. Intestinal bacterial cells such as *Lactobacillus* and *Bacteroides* species were precultured in nutrient-rich medium for a day. The cultured cells were harvested by centrifugation at 9,700 *g* and room temperature for 5 min and washed twice with saline. The cells were suspended in the saline to OD_{600} = 1 and the bacterial suspension (10 μl) was spotted in the plate. The plate for halo detection contained 0.2% dialyzed GAG (hyaluronan, chondroitin sulfate C, or heparin), 0.1% yeast extract, 0.1% KH_2PO_4, 0.1% Na_2HPO_4, 0.01% $MgSO_4 \cdot 7H_2O$, 1% BSA, and 1% agar. After growth, 2 M acetic acid (1 ml) was poured on the plates to form white precipitates by aggregation of GAG and BSA.

Adhesion Assay. To examine the GAG-mediated interactions between human cells and bacterial cells, adhesion assay was conducted using Caco-2, HMV-II, and HOUFXXX cells with streptococci according to previous reports (18–20) with some modifications. *S. agalactiae* NEM316 cells grown in the absence or presence of 0.2% hyaluronan/chondroitin sulfate C/heparin were

washed three times with calcium and magnesium-free phosphate buffered saline [PBS (-)] and resuspended in DMEM to OD_{600} = 0.25. Caco-2 cells were washed twice with PBS (-) and incubated at 37°C under 5% CO_2 for 1 h after addition of DMEM (0.5 ml) with or without 30 μg/ml of hyaluronan/chondroitin sulfate C/heparin and the bacterial resuspension (0.5 ml). The ratio of bacterial cells to human cells was about 100:1. Human cells in the presence of bacterial cells in each well were washed three times with PBS (-) to remove non-specifically bound bacterial cells, and lysed with nonionic detergent [0.25% (w/v) Triton X-100 (1 ml)] at 37°C under 5% CO_2 for 1 h. Because HMV-II and HOUFXXX cells were sensitive to PBS (-), the cells were alternatively washed with Ham's F-12. After lysis of human cells, *S. agalactiae* cells were spread on brain heart infusion plate and incubated at 37°C under 5% CO_2 overnight to count the colony–forming units (cfu) of the bacterial cells adhered to human cells. In addition to streptococci, lactobacilli were also subjected to the adhesion assay to Caco-2 cells.

Results

Degradation of GAGs by Human Intestinal Microbiota

Because a large number of human intestinal bacteria have genes essential for depolymerization and degradation of GAGs according to the CAZy database, GAG-degrading ability of human intestinal microbiota was investigated. Each of the intestinal microbiota from two Japanese was anaerobically co-cultured in the nutrient medium containing chondroitin sulfate C or heparin. Hyaluronan was unavailable because only sulfated GAGs are detected by DMMB assay for measuring GAG concentrations. The culture broth was periodically sampled and the resultant supernatant after centrifugation was subjected to TLC and GAG assay (Fig. 2-1). In TLC, GAGs such as chondroitin sulfate C and heparin in the absence of the microbiota were detected at the original spot due to polysaccharide without degradation. No degradation products from GAGs were detected in the co-cultured supernatant for the first few days. As days passed, both the spots of chondroitin sulfate C and heparin at the origin disappeared, indicating that intestinal microbiota began to degrade GAGs. In combination with degradation of GAGs, oligosaccharides derived from chondroitin sulfate C and heparin were detected for several days, and these resultant oligosaccharides were also completely degraded after co-culture for 13 days. The complete degradation of GAGs demonstrated import of GAG oligosaccharides into bacterial cells in Japanese intestinal microbiota. Concentration of GAGs in the culture supernatant decreased in accordance with the result of TLC. Because DMMB reacts GAG chain including over tetrasaccharide (21),

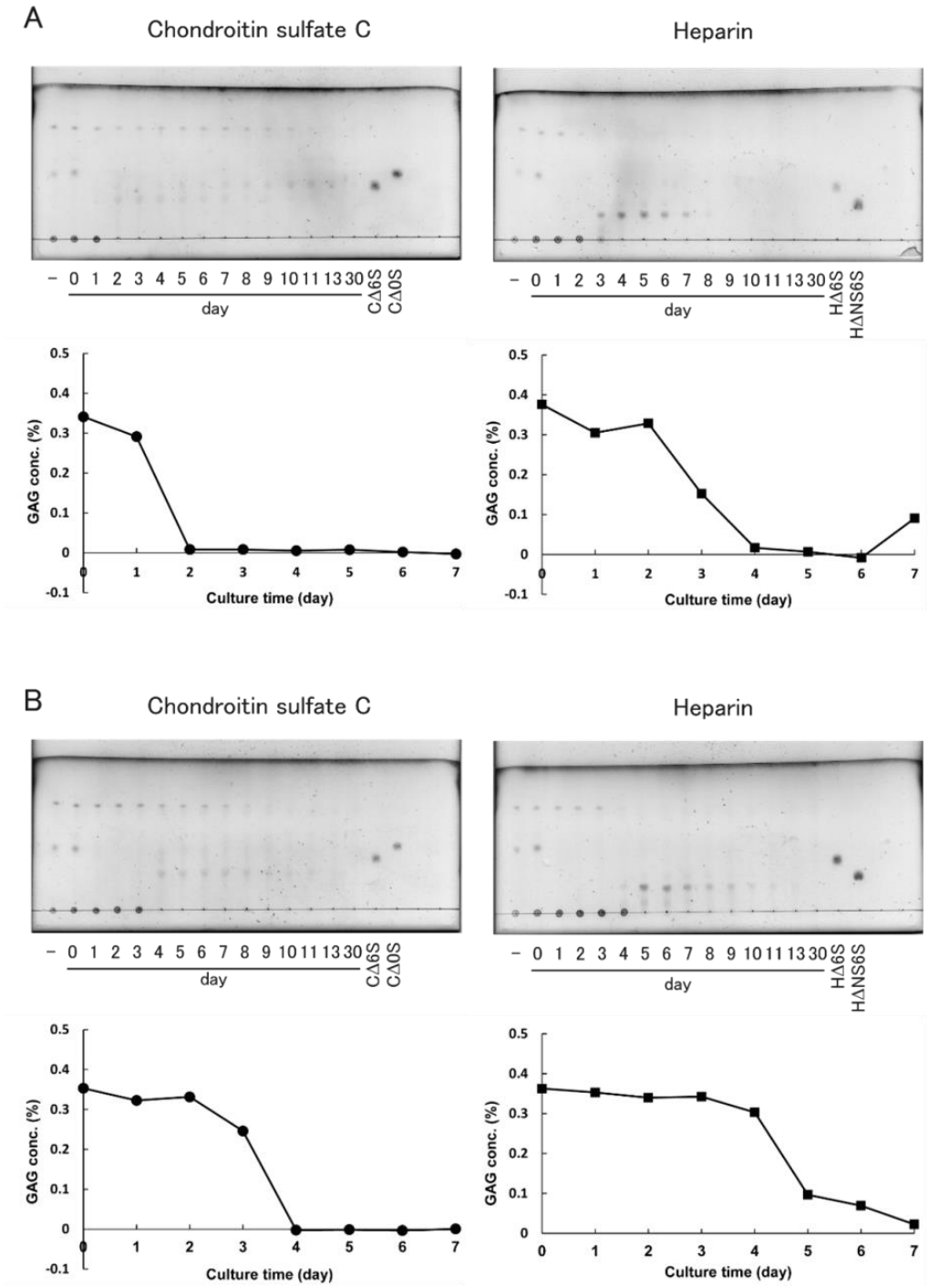

Figure 2-1. Degradation of GAGs by human intestinal microbiota. Intestinal microbiota from two Japanese were co-cultured for 30 d in the nutrient medium containing chondroitin sulfate C (left) or heparin (right). (A) The microbiota from Japanese man in his 50's. (B) The microbiota from Japanese woman in her 20's. TLC (upper) and GAG assay (lower) of the co-cultured supernatant. –, nutrient medium containing GAGs without microbiota; CΔ0S, sulfate group-free unsaturated chondroitin disaccharide; CΔ6S, unsaturated chondroitin disaccharide with a sulfate group at the C-6 position of GalNAc; HΔ0S, sulfate group-free unsaturated heparin disaccharide; and HΔNS6S, unsaturated heparin disaccharide with two sulfate groups at the N and C-6 positions of GlcNAc.

GAG disaccharides were undetected by the GAG assay. Intestinal microbiota from Japanese man in his 50's degraded chondroitin sulfate C by day 2 and heparin by day 3. On the other hand, intestinal microbiota from Japanese woman in her 20's degraded chondroitin sulfate C by day 4 and heparin by day 5. Both microbiota degraded chondroitin sulfate C faster than heparin, probably indicating the availability of chondroitin sulfate C by human intestinal microbiota.

GAG-Degrading Ability of Probiotics

Human intestinal microbiota from two Japanese were demonstrated to degrade both of chondroitin sulfate C and heparin. Hereafter, each bacterium constituting the intestinal microbiota including probiotics was investigated to degrade GAGs by halo plate detection method. *Lactobacillus* is known as a typical member of probiotics among the intestinal microbiota, though the bacterial GAG-degrading ability remains to be clarified. Bacterial cells were grown on the plate containing each of GAGs, BSA, and a small amount of yeast extract, followed by addition of acetic acid. *L. rhamnosus* and *L. pantheris* were used as representatives of the species. As a result, both lactobacilli cells showed a clear halo on the plate in the presence of heparin but not in the presence of hyaluronan and chondroitin sulfate C, indicating that these lactobacilli degrade heparin (Fig. 2-2). In addition to *L. rhamnosus* and *L. pantheris*, *Lactobacillus animalis*, *Lactobacillus casei*, *L. casei* subsp. *casei*, *L. casei* subsp. *rhamnosus*, and *Lactobacillus paracasei* subsp. *paracasei*, and *Enterococcus faecalis* have recently been demonstrated to degrade heparin (22), while no GAGs were degraded by *Lactobacillus acidophilus*, *Lactobacillus aviarius* subsp. *aviarius*, *Lactobacillus brevis*, *Lactobacillus parabuchneri*, *L. paracasei* subsp. *torelans*, *Lactobacillus reuteri*, and *Lactobacillus saerimneri*, and *Bifidobacterium bifidum*.

Recently, some *Bacteroides* species are regarded as next generation probiotics beneficial to human health (23, 24), although the genus has long been treated as an opportunistic pathogen. *Bacteroides* species are dominant in the intestinal microbiota and some of them are known to degrade GAGs. As described previously (25), *B. thetaiotaomicron* degraded hyaluronan and chondoroitin sulfate C. *B. clarus* was also found to show a halo on the plate in the presence of hyaluronan or chondroitin sulfate C (Fig. 2-3). In addition to *B. thetaiotaomicron* and *B. clarus*, *Bacteroides intestinalis*, *Bacteroides ovatus*, *Bacteroides paurosaccharoliticus*, and *Bacteroides stercoris* have recently been shown to degrade hyaluronan and chondroitin sulfate C (22), while *Bacteroides dorei*, *Bacteroides helcogenes*, *Bacteroides salanitronis*, *Bacteroides uniformis*, and *Bacteroides vulgatus* exhibited no GAG-degrading ability. These results indicate that *Bacteroides*

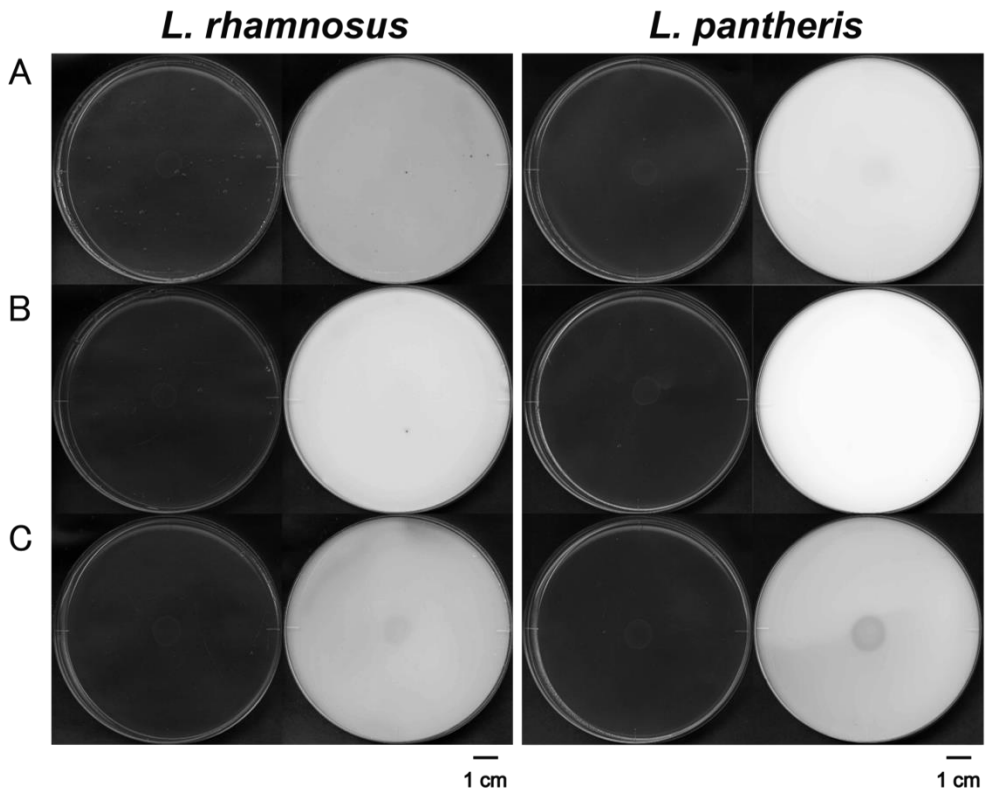

Figure 2-2. Degradation of GAGs by *L. rhamnosus* and *L. pantheris*. The left and right plates represent before and after addition of acetic acid, respectively. Plates contained hyaluronan (A), chondroitin sulfate C (B), and heparin (C).

species show a preference for 1,3-glycoside bond-typed hyaluronan and chondroitin sulfate C, distinct from *Lactobacillus*.

Adhesion of *S. agalactiae* to Human Cells

To study the involvement of GAGs in adhesion of *S. agalactiae* to intestinal and vaginal cells such as intestinal colon carcinoma Caco-2, vaginal melanoma HMV-II (26), and vaginal fibroblast HOUFXXX cells, competitive adhesion assay was conducted. *S. agalactiae* cells were incubated with the confluent human cells in the presence or absence of GAGs, followed by lysis of human cells, plating and counting for the number of bacterial cells attached to human cells (Fig. 2-4). Inhibition of adhesion by addition of GAGs suggests that bacterial cells target host extracellular GAGs for their adhesion to human cells (27). Because *S. agalactiae* cells grown in the presence of hyaluronan have been demonstrated to significantly increase the expression level of the GAG genetic cluster (28), the effect of GAGs in the bacterial culture on adhesion to host epithelial cells was also investigated.

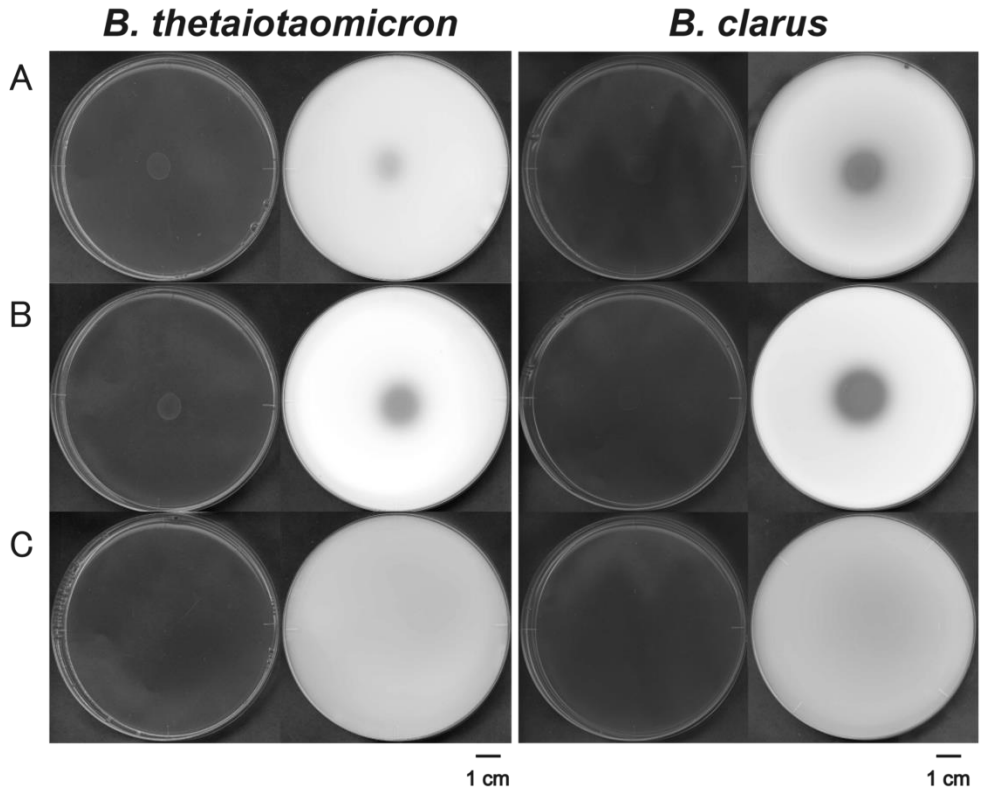

Figure 2-3. Degradation of GAGs by *B. thetaiotaomicron and B. clarus*. The left and right plates represent before and after addition of acetic acid, respectively. Plates contained hyaluronan (A), chondroitin sulfate C (B), and heparin (C).

In the adhesion assay with Caco-2 cells (Fig. 2-4A), *S. agalactiae* cells showed an adherence ability to Caco-2 cells. The adhesion of *S. agalactiae* cells grown in the absence of GAGs to Caco-2 cells was slightly inhibited by addition of hyaluronan and chondroitin sulfate C, while no significant difference in the bacterial attachment was observed between co-cultures in the absence and presence of GAGs. On the other hand, heparin exhibited no inhibitory effect on the adhesion of *S. agalactiae* cells grown in the absence of GAGs. Furthermore, chondroitin sulfate C and heparin competitively inhibited the adhesion of *S. agalactiae* cells grown in the presence of chondroitin sulfate C and heparin, respectively, while hyaluronan showed no inhibitory effect on adhesion of the bacterial cells grown in the presence of hyaluronan.

In the case of adhesion assay with HMV-II cells (Fig. 2-4B), *S. agalactiae* cells were confirmed to adhere to HMV-II cells. Hyaluronan and heparin slightly inhibited the adhesion of both *S. agalactiae* cells grown in the absence and presence of hyaluronan or heparin to HMV-II cells. While chondroitin sulfate C showed an inhibitory effect on the adhesion of the bacterial cells grown in the presence of chondroitin sulfate C, the GAG promoted the adhesion of the bacterial

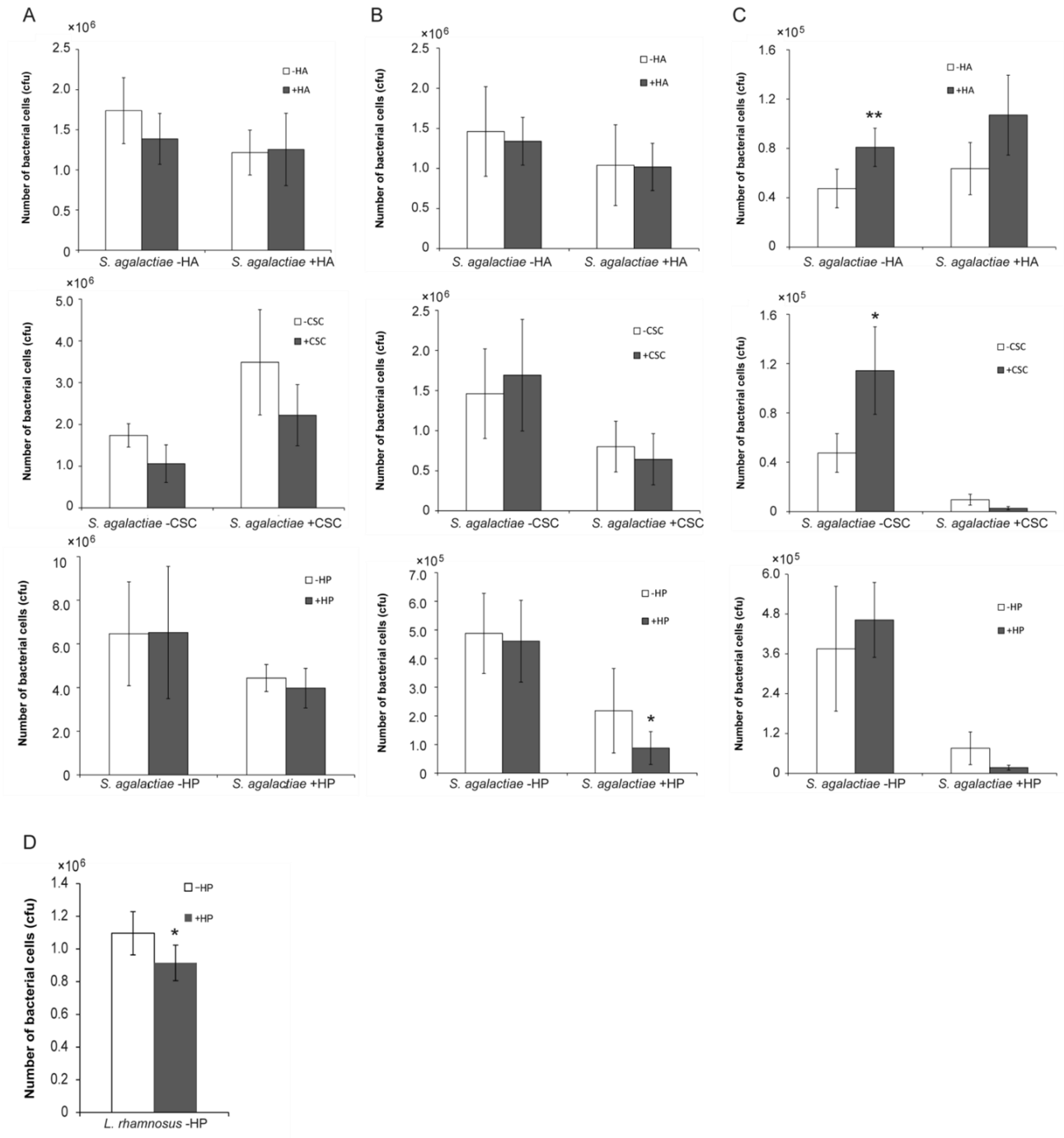

Figure 2-4. Adhesion of bacteria to human intestinal and vaginal cells. The number of *S. agalactiae* cells adhered to Caco-2 (A), HMV-II (B), and HOUFXXX (C) human cells. (D) The number of *L. rhamnosus* cells adhered to Caco-2. Upper, hyaluronan; middle, chondroitin sulfate C; and lower, heparin. *S. agalactiae* cells were grown in the absence and presence of GAGs. (**$p < 0.01$; *$p < 0.05$)

cells grown in the absence of chondroitin sulfate C.

In the bacterial attachment to HOUFXXX cells (Fig. 2-4C), hyaluronan showed a promotive

effect on the adhesion of both *S. agalactiae* cells grown in the absence and presence of hyaluronan to HOUFXXX cells. Chondroitin sulfate C also promoted the adhesion of the bacterial cells grown in the absence of chondroitin sulfate C, although the GAG inhibited the adhesion of the bacterial cells grown in the presence of chondroitin sulfate C. Additionally, heparin significantly inhibited the adhesion of *L. rhamnosus* cells to Caco-2 cells (Fig. 2-4D).

Discussion

The intestinal microbiota from two Japanese were demonstrated to exhibit an ability to degrade chondroitin sulfate C and heparin, while disaccharides derived from chondroitin sulfate remain after extensive reaction of GAG with Chinese intestinal microbiota (9). Degradation of chondroitin sulfate C and heparin was observed after a few-days culture, indicating that other nutrient factors such as yeast extract and tryptone in the medium were assimilated before degradation of GAGs. Therefore, in the intestinal tract, intestinal microbiota are considered to utilize food-derived nutrient factors followed by GAGs, which are constitutively secreted from host cells. On the other hand, there is another possibility that GAG-degrading bacteria are rare in the microbiota, while most *Bacteroides* abundant in the microbiota can degrade GAGs as described in previous reports and this CHAPTER. In fact, the intestinal microbiota from two Japanese degraded chondroitin sulfate C quickly compared to heparin. This result suggests that the microbiota abundantly contained *Bacteroides* with a high chondroitin sulfate C-degrading ability.

There is no report on degradation of GAGs by probiotics. Probiotic lactobacilli in human intestinal microbiota were found to degrade heparin for the first time. Moreover, half (7/14 species) of lactobacilli tested showed an ability to degrade heparin (22) and all of heparin-degrading lactobacilli are evolutionary close in the phylogenetic tree (29). Almost all of GAG-degrading *Lactobacillus* species such as *L. rhamnosus*, *L. casei*, and *L. paracasei* include GAG genetic cluster in the bacterial genome (Fig. 2-5). The proteins encoded in the GAG genetic cluster of *L. rhamnosus* are annotated as follows: LC705_02682, heparinase II/III like (HepC); LC705_02683, preprotein translocase subunit (YajC); LC705_02684, GalNAc-specific EIIA component of PTS; LC705_02685, GalNAc-specific EIID component of PTS; LC705_02686, GalNAc-specific EIIC component of PTS; LC705_02687, GalNAc-specific EIIB component of PTS; LC705_02688, UGL; LC705_02689, conserved protein; LC705_02690, transcriptional regulator IclR family; LC705_02691, KduI; LC705_02692, KduD; LC705_02693, KdgA; LC705_02694, KdgK; LC705_02695, ribose 5-phosphate isomerase A; and LC705_02696, hyaluronate lyase (HysA).

Lactobacillus species with a GAG-degrading ability shown here seem to inevitably have the GAG genetic cluster. On the basis of the GAG genetic cluster in the *L. rhamnosus* genome, the PTS was suggested to be involved in import of GAGs. Because PTS phosphorylates sugar substrates at the C-6 position during the import, unsaturated heparin disaccharides except for those with a sulfate group at the C-6 position were expected to become substrates for the *Lactobacillus* PTS. More recently, the *Lactobacillus* KduI and KduD have first been identified to metabolize unsaturated uronate derived from GAG (22).

In addition to lactobacilli, *B. clarus* was shown to degrade hyaluronan and chondroitin sulfate C for the first time, although some *Bacteroides* species have already been demonstrated to exhibit a GAG-degrading ability (6, 8, 30, 31). More than half (6/11 species) of *Bacteroides* species tested were found to degrade hyaluronan and chondroitin sulfate C (22). Because *Bacteroides* species are known to account for approximately 20% of the normal microbiota of the human intestine (32), GAG-degrading bacteria are considered to occupy a certain ratio in the intestinal microbiota.

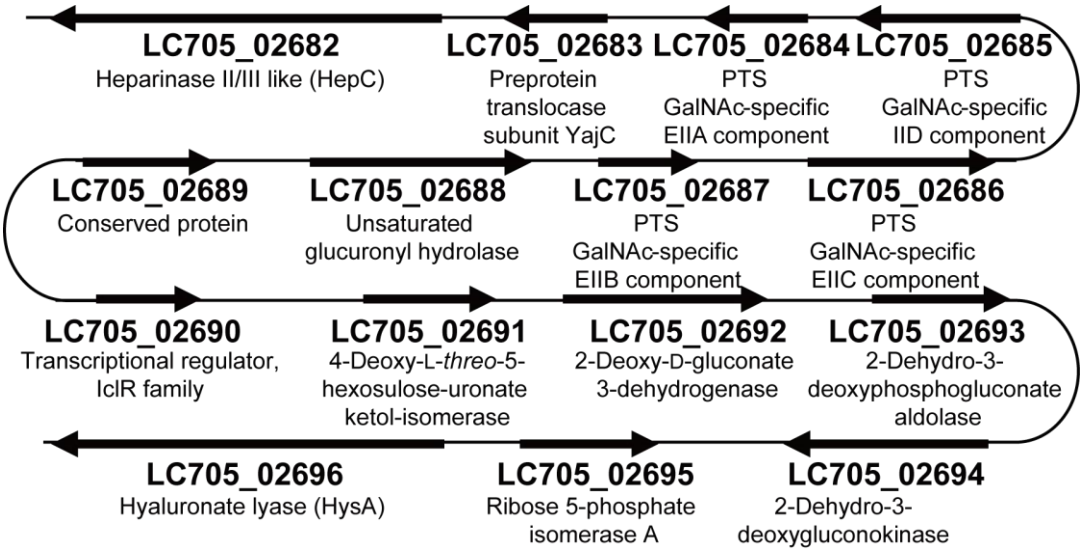

Figure 2-5. GAG genetic cluster of *L. rhamnosus*.

Human intestinal epithelial Caco-2 cells synthesize heparan sulfate as a predominant GAG, and hyaluronan and chondroitin sulfate as minor components of the cell surface (31). Competitive adhesion assay suggested that hyaluronan and chondroitin sulfate C, but not heparin, played significant roles in adhesion of *S. agalactiae* cells to Caco-2 cells. On the other hand, *L. rhamnosus* cells were inhibited to attach to Caco-2 cells by heparin, indicating that the *Lactobacillus* cells adhered to human intestinal epithelial cells through heparin. Marion *et al*. have demonstrated that

the gene disruptions of PTS, hyaluronate lyase, and UGL encoded in the GAG genetic cluster in *S. pneumoniae*, indigenous to human respiratory tract, reduced the ability to colonize the murine upper respiratory tract (34). In combination with this knowledge and present result that *S. agalactiae* and *L. rhamnosus* with the GAG genetic cluster containing PTS were considered to adhere to Caco-2 cells through hyaluronan and heparin, respectively, bacterial adhesion and colonization to human epithelial cells through GAGs was suggested to be involved in the bacterial depolymerization, import, degradation, and metabolism of GAGs. However, *S. agalactiae* cells have a possibility to adhere to GAGs non-specifically due to the high charge density. Therefore, further studies are required for understanding of the bacterial interaction with host human cells through GAGs. For example, the competitive adhesion assay will be carried out after treatment of human cells with GAG-degrading enzymes.

In addition to Caco-2, HMV-II and HOUFXXX cells were used as models for vaginal epithelial and fibroblast cells, respectively. Human vaginal epithelial and fibroblast cells are known to synthesize hyaluronan (35). Moreover, human melanoma cells have chondroitin sulfate at the cell surface and fibroblasts secrete dermatan sulfate (36). From the result of the competitive adhesion assay with HMV-II, *S. agalactiae* cells were suggested to adhere to vaginal epithelial cells through hyaluronan and heparin. In the human vagina, *Lactobacillus* plays a major role in maintenance for the vaginal health by preventing the growth and invasion of pathogenic bacteria through the mechanisms such as secretion of organic acids including lactic acid, production of antibacterial substances, competition for nutrient, steric exclusion for the adhesion to the epithelial cells, co-aggregation, and stimulation of the immune system of the host (37, 38). Although *Lactobacillus* has been shown to inhibit the adhesion and growth of *S. agalactiae* in vaginal epithelial cells (37, 39), the results obtained here suggested that *S. agalactiae* cells adhered to vaginal epithelial cells through hyaluronan and degraded the vaginal hyaluronan.

In this CHAPTER, human gut microbiota were found to degrade chondroitin sulfate C and heparin. Several probiotic *Lactobacillus* species degraded heparin, and included the GAG genetic cluster in their genome. *S. agalactiae* in human intestine and vagina was suggested to adhere to host epithelial cells through hyaluronan.

References

1. Sommer, F., and Backhed, F. (2013) The gut microbiota–masters of host development and physiology. *Nature Rev. Microbiol.* **11**, 227-238

2. Gill, S. R., Pop, M., DeBoy, R. T., Eckburg, P. B., Turnbaugh, P. J., Samuel, B. S., Gordon, J. I., Relman, D. A., Fraser-Liggett, C. M., and Nelson, K. E. (2006) Metagenomic analysis of the human distal gut microbiome. *Science* **312**, 1355-1359
3. Cockburn, D. W., and Koropatkin, N. M. (2016) Polysaccharide degradation by the intestinal microbiota and its influence on human health and disease. *J. Mol. Biol.* **428**, 3230-3252
4. Jia, W., Li, H., Zhao, L., and Nicholson, J. K. (2008) Gut microbiota: a potential new territory for drug targeting. *Nature Rev. Drug Discov.* **7**, 123-129
5. Diamant, M., Blaak, E., and De Vos, W. (2011) Do nutrient–gut–microbiota interactions play a role in human obesity, insulin resistance and type 2 diabetes? *Obesity Rev.* **12**, 272-281
6. Salyers, A., Vercellotti, J., West, S., and Wilkins, T. (1977) Fermentation of mucin and plant polysaccharides by strains of *Bacteroides* from the human colon. *Appl. Environ. Microbiol.* **33**, 319-322
7. Xu, J., Bjursell, M. K., Himrod, J., Deng, S., Carmichael, L. K., Chiang, H. C., Hooper, L. V., and Gordon, J. I. (2003) A genomic view of the human–*Bacteroides thetaiotaomicron* symbiosis. *Science* **299**, 2074-2076
8. Ahn, M. Y., Shin, K. H., Kim, D.-H., Jung, E.-A., Toida, T., Linhardt, R. J., and Kim, Y. S. (1998) Characterization of a *Bacteroides* species from human intestine that degrades glycosaminoglycans. *Can. J. Microbiol.* **44**, 423-429
9. Shang, Q., Yin, Y., Zhu, L., Li, G., Yu, G., and Wang, X. (2016) Degradation of chondroitin sulfate by the gut microbiota of Chinese individuals. *Int. J. Biol. Macromol.* **86**, 112-118
10. Schrezenmeir, J., and de Vrese, M. (2001) Probiotics, prebiotics, and synbiotics–approaching a definition. *Am. J. Clin. Nutr.* **73**, 361S-364S
11. Lalioui, L., Pellegrini, E., Dramsi, S., Baptista, M., Bourgeois, N., Doucet-Populaire, F., Rusniok, C., Zouine, M., Glaser, P., and Kunst, F. (2005) The SrtA Sortase of *Streptococcus agalactiae* is required for cell wall anchoring of proteins containing the LPXTG motif, for adhesion to epithelial cells, and for colonization of the mouse intestine. *Infect. Immun.* **73**, 3342-3350
12. Jelinkova, J., Grabovskaya, K. B., Ryc, M., Bulgakova, T. N., and Totolian, A. A. (1986) Adherence of vaginal and pharyngeal strains of group B streptococci to human vaginal and pharyngeal epithelial cells. *Zentralbl. Bakteriol.* **262**, 492-499
13. Bolduc, G., Baron, M., Gravekamp, C., Lachenauer, C., and Madoff, L. (2002) The alpha C

protein mediates internalization of group B *Streptococcus* within human cervical epithelial cells. *Cell. Microbiol.* **4**, 751-758

14. Kamhi, E., Joo, E. J., Dordick, J. S., and Linhardt, R. J. (2013) Glycosaminoglycans in infectious disease. *Biol. Rev.* **88**, 928-943
15. Li, M., Li, G., Zhu, L., Yin, Y., Zhao, X., Xiang, C., Yu, G., and Wang, X. (2014) Isolation and characterization of an agaro-oligosaccharide (AO)-hydrolyzing bacterium from the gut microflora of Chinese individuals. *PloS one* **9**, e91106
16. Farndale, R. W., Sayers, C. A., and Barrett, A. J. (1982) A direct spectrophotometric microassay for sulfated glycosaminoglycans in cartilage cultures. *Connect. Tissue Res.* **9**, 247-248
17. Enobakhare, B. O., Bader, D. L., and Lee, D. A. (1996) Quantification of sulfated glycosaminoglycans in chondrocyte/alginate cultures, by use of 1, 9-dimethylmethylene blue. *Anal. Biochem.* **243**, 189-191
18. Forestier, C., De Champs, C., Vatoux, C., and Joly, B. (2001) Probiotic activities of *Lactobacillus casei rhamnosus*: *in vitro* adherence to intestinal cells and antimicrobial properties. *Res. Microbiol.* **152**, 167-173
19. Abachin, E., Poyart, C., Pellegrini, E., Milohanic, E., Fiedler, F., Berche, P., and Trieu-Cuot, P. (2002) Formation of D-alanyl-lipoteichoic acid is required for adhesion and virulence of *Listeria monocytogenes*. *Mol. Microbiol.* **43**, 1-14
20. Sava, I. G., Zhang, F., Toma, I., Theilacker, C., Li, B., Baumert, T. F., Holst, O., Linhardt, R. J., and Huebner, J. (2009) Novel interactions of glycosaminoglycans and bacterial glycolipids mediate binding of enterococci to human cells. *J. Biol. Chem.* **284**, 18194-18201
21. Coulson-Thomas, V. J., and Gesteira, T. F. (2014) Dimethylmethylene blue assay (DMMB). *Bio Protoc.* **4**, e1236
22. Kawai, K., Kamochi, R., Oiki, S., Murata, K., and Hashimoto, W. (2018) Probiotics in human gut microbiota can degrade host glycosaminoglycans. *Sci. Rep.* Revised manuscript submitted (SREP-17-41781)
23. Mazmanian, S. K., Round, J. L., and Kasper, D. L. (2008) A microbial symbiosis factor prevents intestinal inflammatory disease. *Nature* **453**, 620-625
24. El Hage, R., Hernandez-Sanabria, E., and Van de Wiele, T. (2017) Emerging trends in "Smart probiotics": functional consideration for the development of novel health and industrial applications. *Front. Microbiol.* **8**, 1889

25. Linn, S., Chan, T., Lipeski, L., and Salyers, A. A. (1983) Isolation and characterization of two chondroitin lyases from *Bacteroides thetaiotaomicron*. *J. Bacteriol.* **156**, 859-866
26. Hasumi, K., Sakamoto, G., Sugano, H., Kasuga, T., and Masubuchi, K. (1978) Primary malignant melanoma of the vagina: study of four autopsy cases with ultrastructural findings. *Cancer* **42**, 2675-2686
27. Rostand, K. S., and Esko, J. D. (1997) Microbial adherence to and invasion through proteoglycans. *Infect. Immun.* **65**, 1-8
28. Maruyama, Y., Nakamichi, Y., Itoh, T., Mikami, B., Hashimoto, W., and Murata, K. (2009) Substrate specificity of streptococcal unsaturated glucuronyl hydrolases for sulfated glycosaminoglycan. *J. Biol. Chem.* **284**, 18059-18069
29. Zheng, J., Ruan, L., Sun, M., and Ganzle, M. (2015) A genomic view of lactobacilli and pediococci demonstrates that phylogeny matches ecology and physiology. *Appl. Environ. Microbiol.* **81**, 7233-7243
30. Hyun, Y. J., Jung, I. H., and Kim, D. H. (2012) Expression of heparinase I of *Bacteroides stercoris* HJ-15 and its degradation tendency toward heparin-like glycosaminoglycans. *Carbohydr. Res.* **359**, 37-43
31. Raghavan, V., and Groisman, E. A. (2015) Species-specific dynamic responses of gut bacteria to a mammalian glycan. *J. Bacteriol.* **197**, 1538-1548
32. Holdeman, L., Good, I., and Moore, W. (1976) Human fecal flora: variation in bacterial composition within individuals and a possible effect of emotional stress. *Appl. Environ. Microbiol.* **31**, 359-375
33. Levy, P., Robert, A., and Picard, J. (1988) Biosynthesis of glycosaminoglycans in the human colonic tumor cell line Caco-2: structural changes occurring with the morphological differentiation of the cells. *Biol. Cell* **62**, 255-264
34. Marion, C., Stewart, J. M., Tazi, M. F., Burnaugh, A. M., Linke, C. M., Woodiga, S. A., and King, S. J. (2012) *Streptococcus pneumoniae* can utilize multiple sources of hyaluronic acid for growth. *Infect. Immun.* **80**, 1390-1398
35. Akgul, Y., Word, R. A., Ensign, L. M., Yamaguchi, Y., Lydon, J., Hanes, J., and Mahendroo, M. (2014) Hyaluronan in cervical epithelia protects against infection-mediated preterm birth. *J. Clin. Invest.* **124**, 5481-5489
36. Poole, A. R. (1986) Proteoglycans in health and disease: structures and functions. *Biochem. J.* **236**, 1-14

37. Zarate, G., and Nader-Macias, M. (2006) Influence of probiotic vaginal lactobacilli on *in vitro* adhesion of urogenital pathogens to vaginal epithelial cells. *Lett. Appl. Microbiol.* **43**, 174-180

38. Rousseau, V., Lepargneur, J., Roques, C., Remaud-Simeon, M., and Paul, F. (2005) Prebiotic effects of oligosaccharides on selected vaginal lactobacilli and pathogenic microorganisms. *Anaerobe* **11**, 145-153

39. Tomas, M. S. J., Ocana, V. S., Wiese, B., and Nader-Macias, M. E. (2003) Growth and lactic acid production by vaginal *Lactobacillus acidophilus* CRL 1259, and inhibition of uropathogenic *Escherichia coli*. *J. Med. Microbiol.* **52**, 1117-1124

CHAPTER III

Streptobacillus ABC transporter involved in the import of sulfated glycosaminoglycans

In addition to streptococci, a pathogenic Gram-negative bacterium *Streptobacillus moniliformis* has a similar GAG genetic cluster. *S. moniliformis* usually colonizes the rodent oral cavity and causes Rat-bite fever in humans either directly or indirectly exposed to rodents (1). Rat-bite fever is characterized by polyarthralgia, high fever, and headache, and its fatality rate reaches to 10% among untreated patients (2). In the *S. moniliformis* GAG genetic cluster, a periplasmic solute-binding protein (Smon0123)-dependent ABC transporter (Smon0121-Smon0122/Smon0120-Smon0120) is encoded in place of PTS. A typical bacterial ABC transporter is constituted by four protein subunits: two membrane-spanning subunits forming transport pathway across the membrane and ATP-binding subunits interacting with membrane-spanning subunits at the cytoplasmic surface to supply the energy generated by hydrolysis of ATP (3). Gram-negative and Gram-positive bacterial ABC transporters generally receive substrates from solute-binding proteins (4–6). Substrate-bound protein interacts with inward-facing transporter to trigger ATP hydrolysis and conformational change to outward-facing transporter (7). The substrate is consequently released from the protein into the translocation pathway of outward-facing transporter. Therefore, ABC transporter incorporates substrates into the cytoplasm without any substrate modifications (4). GAGs sulfated at the C-6 position are considered to become substrates for ABC transporters distinct from PTS, which incorporates substrates through phosphorylation at the C-6 position. This CHAPTER deals with molecular identification of *S. moniliformis* GAG import system, structural determination of the solute-binding protein in complex with sulfated and non-sulfated GAG disaccharides by X-ray crystallography, and functional characterization of the ABC transporter.

Materials and Methods

Materials. Sufate group-free unsaturated chondroitin disaccharide (CΔ0S), unsaturated chondroitin disaccharide with a sulfate group at the C-4 position of GalNAc (CΔ4S), and unsaturated chondroitin disaccharide with a sulfate group at the C-6 position of GalNAc (CΔ6S) were purchased from Seikagaku Biobusiness. Unsaturated hyaluronan disaccharide (ΔHA), unsaturated heparin disaccharide with a sulfate group at the C-6 position of GlcNAc (HΔ6S), and

unsaturated heparin disaccharide with two sulfate groups at the N and C-6 positions of GlcNAc (HΔNS6S) were from Sigma-Aldrich. Sulfate-group free unsaturated heparin disaccharide (HΔ0S), and unsaturated chondroitin disaccharide with two sulfate groups at the C-4 and C-6 positions of GalNAc (CΔ4S6S) were from Dextra Laboratories (Fig. 3-1). SYPRO Orange (Invitrogen), n-dodecyl-β-D-maltoside (DDM) (Nacalai Tesque), and n-octyl-β-D-glucoside (n-OG) (Dojindo) were commercially available. Oligonucleotides were synthesized by Hokkaido System Science. Restriction endonucleases and DNA-modifying enzymes were purchased from Toyobo.

Microorganisms and Culture Conditions. *S. moniliformis* DSM 12112 and its genome were purchased from Deutsche Sammlung von Mikroorganismen und Zellkulturen. Its complete genome sequence is available in GenBank under accession number, CP001779. *S. moniliformis* cells were statically grown at 37°C under 5% CO_2 in 0.8% nutrient medium (Difco) containing 20% horse serum (Thermo Fisher Scientific) for 24–48 h. For expression of *S. moniliformis* UGL encoded by Smon0127 gene and solute-binding protein encoded by Smon0123 gene, *E. coli* cells were cultured as described in CHAPTER I. For expression of *S. moniliformis* ABC transporter [Smon0121-Smon0122(10xHis)/Smon0120-Smon0120], the *E. coli* cells harboring the plasmid were cultured at 30°C in Terrific broth (8) (1.2% tryptone, 2.4% yeast extract, 0.4% glycerol, 0.05% $MgSO_4 \cdot H_2O$, 1.4% K_2HPO_4, and 0.26% KH_2PO_4) containing 1% glucose, 2 mM $MgCl_2$, and 33 μg/ml sodium ampicillin. At OD_{600} = 0.3–0.7, IPTG was added to the culture at a final concentration of 0.4 mM, and the cells were further cultured at 25°C for 16 h.

Halo Detection for GAG Degradation. To investigate the GAG-degrading ability of *S. moniliformis*, a plate method (9) was adopted in the similar way as described in CHAPTER I. The bacterial cells were cultured on plates containing 1% BSA (Wako), 1% agar, 0.2% dialyzed GAG (hyaluronan, chondroitin sulfate A, C, or heparin), 0.8% nutrient medium, and 20% horse serum. Addition of 2 M acetic acid (1 ml) to the cultured plates caused white precipitates due to interaction between GAG and BSA, while GAG-degraded regions remained to be clear zones as a halo.

Construction of the Overexpression System. Overexpression systems for Smon0127 and Smon0123 were constructed in the similar way as described in CHAPTER I. Briefly, Smon0127 and Smon0123 genes were amplified by PCR and the PCR products were ligated with *Hinc*II-digested pUC119. The resultant plasmids were digested with *Nco*I and *Xho*I, and the Smon0127 and Smon0123 gene fragments were ligated with *Nco*I and *Xho*I-digested pET21d. The resultant plasmids were designated as pET21d-Smon0127 and pET21d-Smon0123. For crystallization of Smon0123, N- and/or C-terminal residues-truncated Smon0123 mutants were

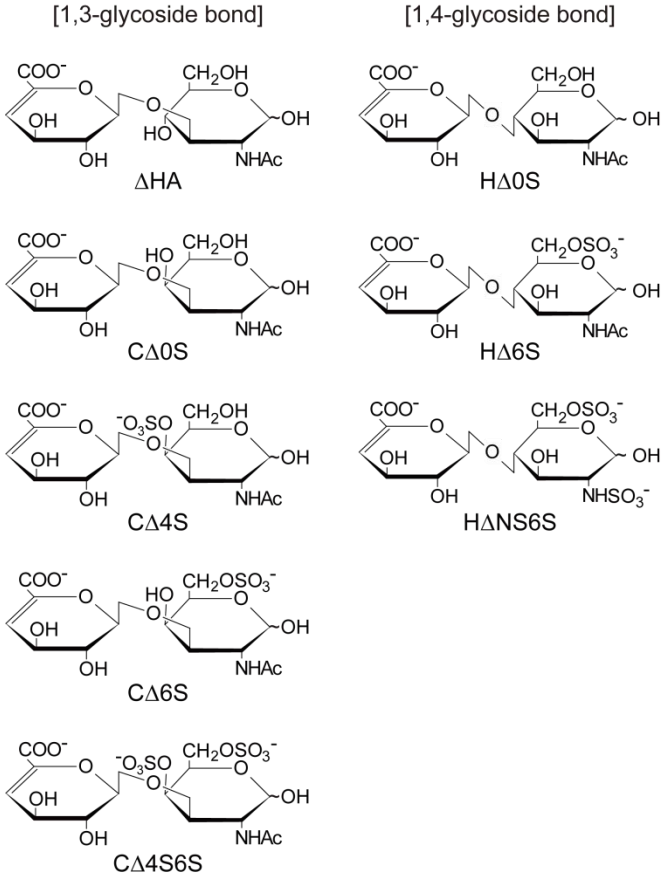

Figure 3-1. Structural formulas of unsaturated GAG disaccharides.

constructed by using forward and reverse primers for PCR. The plasmid pET21d-Smon0123 was used as a template. The reaction mixtures for PCR except for the template were prepared as described in CHAPTER I. The PCR conditions were as follows: 94°C for 2 min followed by 30 cycles of 98°C for 10 s, 61°C for 30 s, and 68°C for 45 s. The PCR products were inserted into *Nco*I and *Xho*I-digested pET21d by using In-Fusion kit (Clontech). The resultant plasmids for truncated Smon0123 mutants were designated as pET21d-Smon0123 [(N-0/C-0), (N-0/C-5), (N-0/C-20), (N-18/C-0), (N-18/C-5), (N-18/C-20), (N-28/C-0), (N-28/C-5), and (N-28/C-20)]. Truncated mutant proteins contained no his-tag sequence.

The overexpression system for the ABC transporter [Smon0121-Smon0122(10xHis)/Smon0120-Smon0120] was constructed by using the *S. moniliformis* operon gene. The Smon0120-0121-0122 gene fragment with additional sequence coding for four histidine residues at C-terminus of Smon0122 was amplified by PCR using the bacterial genome as a template. After subcloning in the similar way, the resultant plasmid was designed as pET21d-Smon0121-Smon0122(10xHis)/Smon0120-Smon0120.

For expression of each protein, *E. coli* host cells were transformed with each of the constructed plasmids. *E. coli* BL21(DE3)Gold, BL21(DE3)-CodonPlus-RIL (Novagen), and BL21(DE3)Gold-pLysS (Novagen) were used for expression of Smon0127, Smon0123, and Smon0121-Smon0122(10xHis)/Smon0120-Smon0120, respectively. DNA manipulations were conducted as described previously (8). The sequences of primers are shown in Table 3-1.

Table 3-1. Primers for PCR

Smon0127	forward	5′-GGCCATGGAATTATTTAAGGAAGTAATAGAAAAAT-3'
	reverse	5′-GGCTCGAGCCAATAAATATTCCACTCTGGTTTTAA-3'
Smon0123	forward	5′-GGCCATGGAAAAATTATTAGCATTAGGACTTTTAG-3'
	reverse	5′-GGCTCGAGTTTATTAAAATTCTTGAATGCTTCATT-3'
Smon0123 (N-0)	forward	5′-AGGAGATATACCATGAAAAAATTATTAGC-3′
Smon0123 (N-18)	forward	5′-AGGAGATATACCATGAAAAAAGAAGAAACTACAACAGGAC-3′
Smon0123 (N-28)	forward	5′-AGGAGATATACCATGGAAACAACAATATTTGCAATGC-3′
Smon0123 (C-0)	reverse	5′-GGTGGTGGTGCTCGATTATTTATTAAAATTCTTGAAT-3′
Smon0123 (C-5)	reverse	5′-GGTGGTGGTGCTCGATTAGAATGCTTCATTTTGAATTTGTT-3′
Smon0123 (C-20)	reverse	5′-GGTGGTGGTGCTCGATTATTCTAATCTCTTAATATATGCATCCCA-3′
Smon0121-Smon0122(10xHis) /Smon0120-Smon0120	forward	5′-AGGAGATATACCATGGCAGAAGTAATATTAAAGAAAGTTG-3′
Smon0121-Smon0122(10xHis) /Smon0120-Smon0120	reverse	5′-GTGGTGGTGGTGGTGATGATGATGATGTCCTTTTACTGCTCCTAGTGTT-3′

Underlines in primers indicate the restriction sites for molecular cloning.

Purification. For purification of Smon127 and Smon123, the recombinant *E. coli* grown cells [BL21(DE3)Gold/pET21d-Smon0127, BL21(DE3)-CodonPlus-RIL/pET21d-Smon0123, and BL21(DE3)-CodonPlus-RIL/pET21d-Smon0123(mutants)] were harvested by centrifugation at 6,700 *g* and 4°C for 10 min and suspended in 20 mM Tris-HCl (pH 7.5). The *E. coli* cell extracts were obtained by ultrasonication (Insonator Model 201M, Kubota) at 0°C and 9 kHz for 10 min and the following centrifugation at 20,000 *g* and 4°C for 20 min. Smon0127 or Smon0123 was purified from the cell extracts by metal affinity chromatography [TALON (Clontech)], anion exchange

chromatography [Resource Q (GE Healthcare)], and gel filtration chromatography [HiLoad 16/60 Superdex 200 pg (GE Healthcare)]. Histidine-tagged sequence-free Smon0123 mutants were purified from the cell extracts by anion exchange chromatography [Toyopearl DEAE-650M (Tosoh Bioscience LLC)] and gel filtration chromatography (HiLoad 16/60 Superdex 200 pg).

For purification of Smon0121-Smon0122/Smon0120-Smon0120, the recombinant *E. coli* cells [BL21(DE3)Gold-pLysS/pET21d-Smon0121-Smon0122(10xHis)/Smon0120-Smon0120] were harvested in a same way and suspended in a standard buffer [20 mM Tris-HCl (pH 8.0), 0.1 M NaCl, 2 mM $MgCl_2$, 10% glycerol, 1 mM phenylmethylsulfonyl fluoride, and 2 mM ethylenediaminetetraacetic acid]. After disruption of *E. coli* cells by ultrasonication as described above, the cell extract was ultracentrifuged at 100,000 *g* and 4°C for 60 min. The precipitant membrane was solubilized at 6°C in the standard buffer containing 1% DDM [critical micelle concentration (CMC), 0.0087%] by gentle rotation for 16 h, and subsequently ultracentrifuged at 100,000 *g* and 4°C for 60 min. The resultant supernatant solution was applied to metal affinity chromatography [Ni-NTA (Qiagen)]. After being washed with the standard buffer containing 20 mM imidazole (pH 8.0) and 0.0087% DDM, the protein was eluted using linear gradient of imidazole (20–200 mM) in the standard buffer. The collected fractions were subjected to SDS-PAGE and the fractions containing the ABC transporter were concentrated by ultrafiltration [Vivaspin 15R (Sartorius), molecular mass cut-off, 30 kDa]. The concentrated protein solution was applied to gel filtration chromatography (HiLoad 16/60 Superdex 200 pg) with the standard buffer containing 0.018% DDM, followed by SDS-PAGE. The purified ABC transporter was concentrated by ultrafiltration and the concentration of the protein was measured using BCA Protein Assay Kit (Thermo Fisher Scientific).

Immunoblotting. Antibodies to the purified Smon0123(N-18/C-0) were raised in a rabbit by Kitayama Labes and the serum was used as polyclonal antibodies against Smon0123. To investigate expression of Smon0123 in *S. moniliformis*, the bacterial cells grown in the presence or absence of 0.2% dialyzed GAG (hyaluronan, chondroitin sulfate A, C, or heparin) were subjected to SDS-PAGE followed by immunoblotting using anti-Smon0123 antibodies. Anti-IgG conjugated with horseradish peroxidase (HRP) (GE Healthcare) and Immobilon Western Chemiluminescent HRP substrate (Millipore) were used to detect the target protein. Anti-*S. pyogenes* UGL (SpyUGL) antibodies (10) were used as a primary antibody for detection of Smon0127. Furthermore, the purified Smon0121-Smon0122(10xHis)/Smon0120-Smon0120 was subjected to SDS-PAGE followed by immunoblotting using anti-histidine tag antibodies (GE Healthcare).

Enzyme Assay. The activity of *S. moniliformis* UGL (Smon0127) was measured by monitoring the decrease in absorbance at 235 nm derived from the C=C double bond in unsaturated GAG disaccharides. The assay was conducted at 30°C in reaction mixture of 20 mM Tris-HCl (pH 7.5), 0.2 mM substrate, and the enzyme. Various unsaturated GAG disaccharides such as ΔHA, CΔ0S, CΔ4S, CΔ6S, HΔ0S, and HΔ6S were used as substrates. One unit of the enzyme activity was defined as the amount of enzyme required to degrade 1 μmol of substrate per minute as described previously (10, 11). The enzyme was also assayed using various concentrations (0–1 mM) of CΔ0S, and kinetic parameters (K_m and k_{cat}) were determined according the Michaelis-Menten equation (Synergy Software). To investigate sulfatase activity both in the culture supernatant and toluene-treated *S. moniliformis* cells, the enzyme was assayed by TLC using CΔ4S as a substrate. For further examination of the sulfatase activity by Smon0123, the reaction mixture containing 70 μM Smon0123, 4 mM CΔ4S, CΔ6S, or CΔ4S6S, and 50 mM Tris-HCl (pH 7.5) was incubated at 30°C for 8 h. The mixture was boiled to stop reaction and centrifuged at 8,000 *g* for 3 min. The resultant supernatants were subjected to TLC for 5 μl.

Differential Scanning Fluorimetry (DSF). To investigate interactions between Smon0123 and unsaturated GAG disaccharides, DSF (12) was adopted using the MyiQ2 real-time PCR instrument (Bio-Rad). The reaction mixture contained 0–1 mM each of disaccharides (CΔ0S and *N*,*N*'-diacetylchitobiose), 50 mM Tris-HCl (pH 7.5), 0.1% SYPRO Orange, and 8.58 μM Smon0123. The temperature increased from 25–95°C by 0.5°C per cycle (141 cycles). The relative fluorescent unit (RFU) values derived from SYPRO Orange hydrophobically bound to unfolded proteins were measured during the heating. The inflection point of the increase in the RFU was determined as melting temperature (T_m). Various disaccharides such as CΔ0S, CΔ4S, CΔ6S, CΔ4S6S, ΔHA, HΔ0S, HΔ6S, and HΔNS6S were used at 50 μM as a ligand.

Fluorescence Spectrum Analysis. The fluorescence intensity of Smon0123 with escalated concentration of ligands was measured by spectrofluorometer [FP-6500 (JASCO)] to examine the binding affinity of Smon0123 with unsaturated GAG disaccharides. Parameters under reaction conditions were determined as follows: excitation band width, 1 nm; emission band width, 10 nm; response, 2 s; sensitivity, high; excitation wavelength, 280 nm, start to end emission wavelength, 300–500 nm; data pitch, 1 nm; and scan speed, 100 nm/min. The reaction mixture contained 0.1 μM Smon0123, 50 mM Tris-HCl (pH 7.5), and 0–20 μM ligands. Various disaccharides such as CΔ0S, CΔ4S, CΔ6S, ΔHA, HΔ0S, HΔ6S, HΔNS6S, *N*,*N*'-diacetylchitobiose, and cellobiose were used as a ligand. The interaction between Smon0123 and GAG polysaccharides such as hyaluronan,

chondroitin sulfate C, and heparin was also investigated using BSA as a negative control. The ratio of decreasing fluorescence intensity by addition of increasing ligands in comparison with the intensity in the absence of ligands was plotted and the dissociation constant (K_d) was determined using the least-squares method (13).

X-ray Crystallography. To determine the three-dimensional structure of Smon0123, the purified Smon0123 mutants were concentrated and crystallized by sitting drop vapor diffusion method. In 96-well sitting drop plates, 1 μl of Smon0123 mutants was mixed with equal volume of the reservoir solution for crystallization and incubated at 20°C for 2 weeks. The compositions of reservoir solutions were as follows: ligand-free Smon0123 (N-28/C-5) (21.2 mg/ml), 0.2 M potassium sodium tartrate tetrahydrate, 0.1 M tri-sodium citrate dehydrate (pH 5.6), and 2 M ammonium sulfate; CΔ0S-bound Smon0123 (N-18/C-5) (12.5 mg/ml), 1 mM CΔ0S, 0.2 M ammonium chloride, 0.1 M sodium 2-(*N*-morpholino)ethanesulfonate (MES) (pH 6.0), and 20% (w/v) PEG 6,000; CΔ4S-bound Smon0123 (N-18/C-5) (12.5 mg/ml), 1 mM CΔ4S, 0.2 M ammonium chloride, 0.1 M sodium 2-[4-(2-hydroxyethyl)-1-piperazinyl]ethanesulfonate (HEPES) (pH 7.0), and 20% (w/v) PEG 6,000; CΔ6S-bound Smon0123 (N-18/C-5) (12.5 mg/ml), 1 mM CΔ6S, 0.2 M potassium thiocyanate, and 20% (w/v) PEG 3,350; CΔ4S6S-bound Smon0123 (N-18/C-5) (10.8 mg/ml), 1 mM CΔ4S6S, 18% (w/v) PEG 4,000, 20% (w/v) isopropanol, and 0.1 M HEPES (pH 7.5). Each single crystal was picked up with a nylon loop, soaked in the reservoir solution that contained 20% ethylene glycol as a cryoprotectant, and instantly frozen in a cold nitrogen gas stream. X-ray diffraction images were collected with synchrotron radiation on the beamlines BL26B1 and BL38B1 of SPring-8 (Harima, Japan). The data were indexed, integrated, and scaled using the *HKL2000* program (14). The structure was determined through molecular replacement method with the *Molrep* program in the *CCP4* program package (15). Structure refinement was conducted with *phenix refine* in the *PHENIX* program (16). The model was refined manually with the *winCoot* program (17). Figures for the protein structure were prepared using the *PyMOL* program (18).

Preparation of Proteoliposomes. A soybean L-α-phosphatidylcholine type IV-S (Sigma) was dissolved at 50 mg/ml in 1.5 ml chloroform. Chloroform was removed by rotary evaporation (N-1000-WD, Eyela), and residual solvent was removed under vacuum for 3 h. The resultant dried lipid films were suspended in 20 mM Tris-HCl (pH 8.0) containing 1 mM dithiothreitol (DTT). After sonication 3–5 times by probe-type sonicator (Sonics & Materials) on ice, the suspension was frozen in liquid nitrogen and thawed at 37°C. After 3 repeats of freezing and thawing, this liposome

solution was stored at –80°C. The liposome was thawed at 37°C and extruded 11 times through a 100 nm polycarbonate membrane by a Mini-Extruder (Avanti Polar Lipids). The 20% n-OG (3.5 µl) was added to the filtered liposome (45 µl) and the mixture was kept at room temperature for 5 min. The 4 mg/ml purified Smon0121-Smon0122(10xHis)/Smon0120-Smon0120 was added to the mixture and kept at room temperature for 10 min. The resultant mixture was diluted to 0.047% of n-OG with 20 mM Tris-HCl (pH 8.0) and placed on ice for 30 min. This solution was used as proteoliposome.

ATPase Assay. The reaction mixture (200 µl) for ATPase assay contained proteoliposome (0.1 µM Smon0121-Smon0122(10xHis)/Smon0120-Smon0120), 10 mM $MgCl_2$, 2 mM ATP, 20 mM Tris-HCl (pH 8.0), 1.5 µM Smon0123(N-18/C-0), and 0.1 mM each of various disaccharides. The reaction mixture without Smon0123 was pre-incubated at 37°C and reaction was started when Smon0123 was added. A portion of the reaction mixture (30 µl) was removed every 20 min during 0–80 min and added to 30 µl of 12% SDS to stop the reaction. After stopping reaction at 80 min, a mixture of 6% ascorbic acid in 1 M HCl and 1% ammonium molybdate (60 µl) was added to the reaction solution (60 µl) and incubated at room temperature for 5 min. Subsequently, a mixture of 2% sodium citrate, 2% sodium metaarsenite, and 2% acetic acid (90 µl) was added to the solution and incubated at 37°C for 10 min (19). This reaction mixture was measured in absorbance at 850 nm to determine phosphate ion concentration generated through ATP hydrolysis. ATPase activity was represented as phosphate ion (nmol) produced by 1 mg Smon0121-Smon0122(10xHis)/Smon0120-Smon0120 per 1 min. The value measured using proteoliposome and disaccharides was subtracted from that using liposomes without any proteins and ligands.

Magnitude of Hinge-Bending Motion. To calculate the magnitude of the hinge-bending motion, N domains of substrate-free and substrate-bound Smon0123 were superimposed. Rotation matrix, translation vectors, rotation angles, and screwing distances of C domains of substrate-free and substrate-bound Smon0123 were calculated from centers of gravity by *FIT* program (20, 21).

Results

S. moniliformis GAG genetic cluster

The Gram-negative bacterium *S. moniliformis* (22) was found to possess a similar GAG genetic cluster with genes encoding a solute-binding protein-dependent ABC transporter (Fig. 3-2). Based on the primary structure, the proteins encoded in the genetic cluster were annotated as

follows: Smon0115, 2-dehydro-3-deoxygluconokinase (KdgK); Smon0116, 2-dehydro-3-deoxyphosphogluconate aldolase (KdgA); Smon0117, Polysaccharide Lyase (PL) family 8 hyaluronate lyase (HysA); Smon0118, 2-deoxy-D-gluconate 3-dehydrogenase (KduD); Smon0119, 4-deoxy-L-*threo*-5-hexosulose-uronate ketol-isomerase (KduI); Smon0120, multiple sugar transport system (ATP-binding protein); Smon0121, putative aldouronate transport system (permease protein); Smon0122, putative aldouronate transport system (permease protein); Smon0123, putative aldouronate transport system (substrate-binding protein); Smon0124, PL family 12 heparinase II/III family protein (HepC); Smon0125, PL family 8 hyaluronate lyase (HysA); Smon0126, sulfatase; Smon0127, Glycoside Hydrolase (GH) family 88 unsaturated chondroitin disaccharide hydrolase (UGL); Smon0128, hypothetical protein. In the case of streptococci, the importer (phosphotransferase system) of fragmented hyaluronan was found to be encoded in the GAG genetic cluster as described in CHAPTER I. The ABC transporter encoded in the *Streptobacillus* GAG genetic cluster was, therefore, expected to be responsible for import of GAGs.

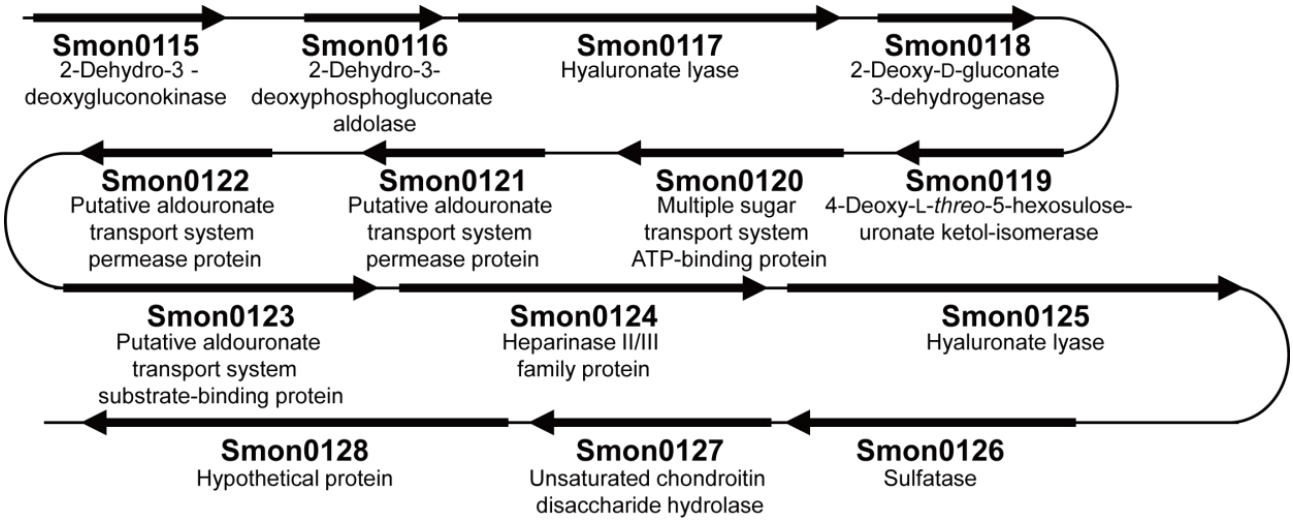

Figure 3-2. GAG genetic cluster of *S. moniliformis*.

GAG Degradation by *S. moniliformis*

To investigate degradation of GAGs by *S. moniliformis*, a plate method for halo detection (9) was adopted (Fig. 3-3). *S. moniliformis* cells were grown on nutrient plates containing BSA and each of GAGs (hyaluronan, chondroitin sulfate A, C, or heparin), and acetic acid was poured onto the plates after the bacterial growth. While GAGs formed white precipitates due to interaction with BSA in the presence of acetic acid, degraded GAGs caused clear zones, halos. In the case of *S.*

moniliformis, halos were observed on plates containing hyaluronan, chondroitin sulfate A, or C (Fig. 3-3A–C right), indicating that *S. moniliformis* degraded hyaluronan and chondroitin sulfates A and C. Surprisingly, the bacterium showed no growth in the presence of heparin (Fig. 3-3D, left and Fig. 3-4A).

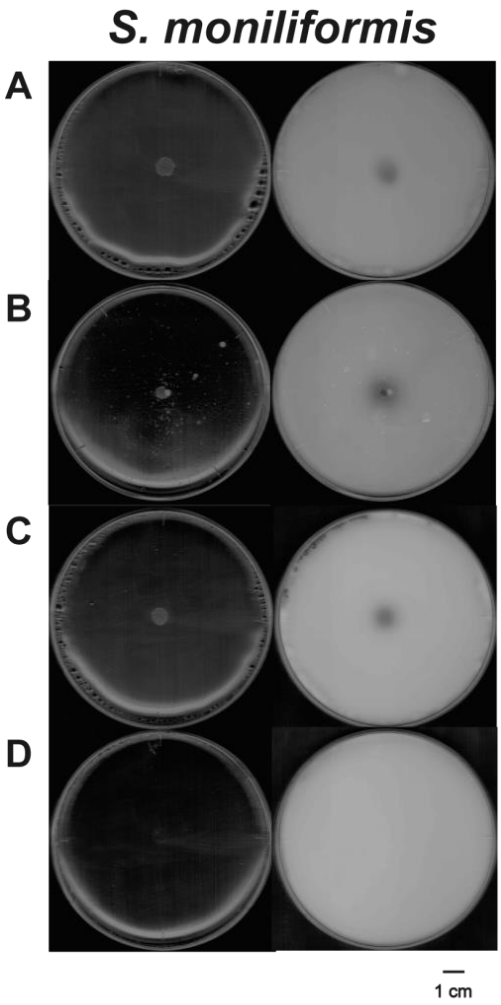

Figure 3-3. Degradation of GAGs by *S. moniliformis*. Left and right plates represent before and after addition of acetic acid, respectively. Plates contained hyaluronan (A), chondroitin sulfate A (B), chondroitin sulfate C (C), and heparin (D).

Expression of the GAG Genetic Cluster in *S. moniliformis*

S. moniliformis cells in the presence of hyaluronan and chondroitin sulfate C grew better than those in the absence of GAG (Fig. 3-4). Based on the result that *S. moniliformis* degraded hyaluronan and chondroitin sulfate C, the expression of the bacterial GAG genetic cluster was examined by immunoblot analysis. Although Smon0123 was predicted to contain a signal peptide

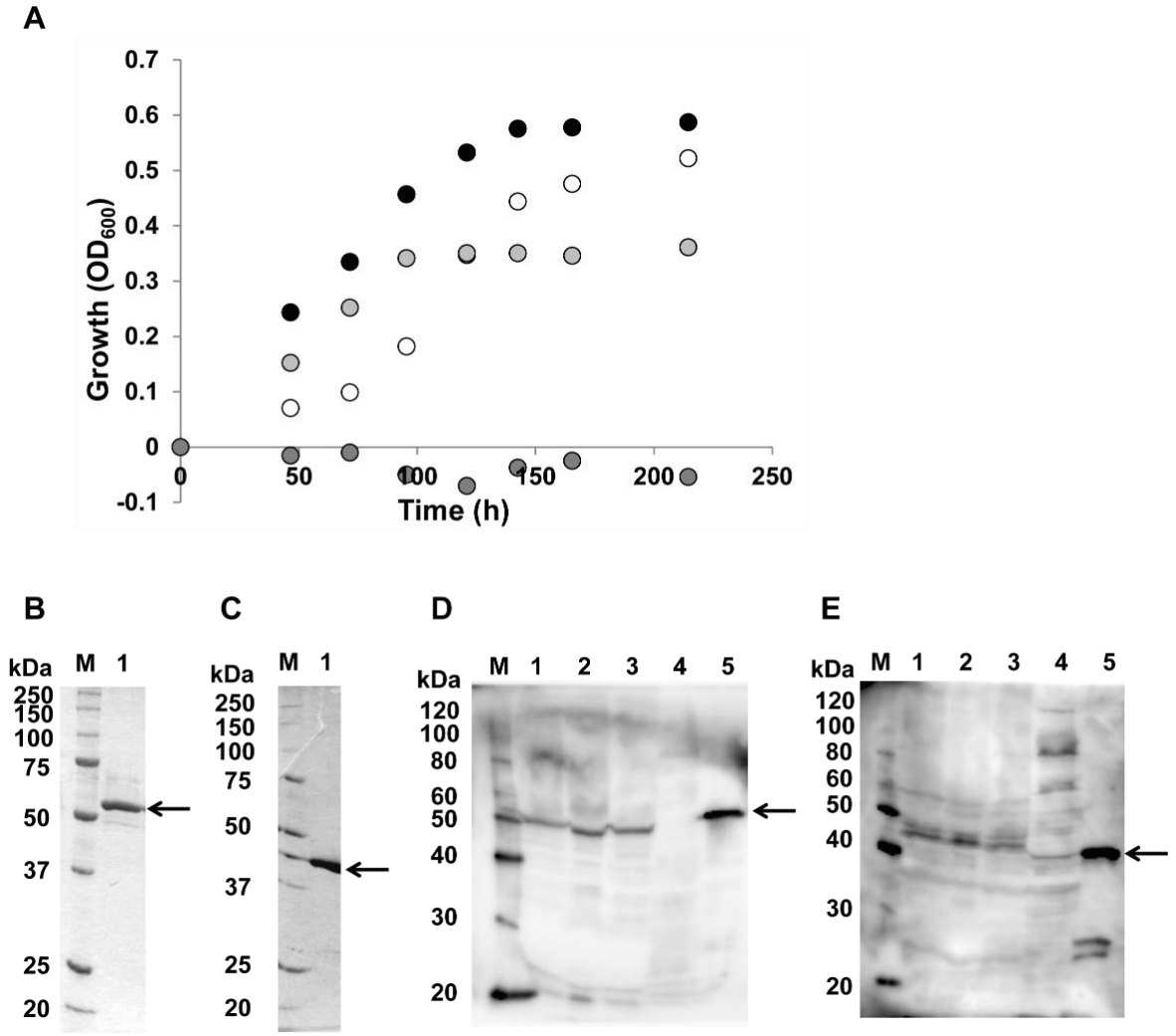

Figure 3-4. Expression of the *Streptobacillus* GAG genetic cluster. (A) Growth curve of *S. moniliformis* in the presence or absence of GAGs. White, in the absence of GAG; gray, in the presence of hyaluronan; black, in the presence of chondroitin sulfate C; and dark gray, in the presence of heparin. (B) and (C) SDS-PAGE followed by staining with Coomassie Brilliant Blue (CBB). Lane M, protein standards with molecular masses of 250, 150, 100, 75, 50, 37, 25, and 20 kDa for CBB staining; lane 1, purified Smon0123 (B) and Smon0127 (C). SDS-PAGE followed by immunoblotting using anti-Smon0123 antibodies (D) and anti-SpyUGL antibodies (E). Lane M, protein standards with molecular masses of 120, 100, 80, 60, 50, 40, 30, and 20 kDa used for immunoblotting; lane 1, *S. moniliformis* cells in the absence of GAG; lane 2, *S. moniliformis* cells in the presence of hyaluronan; lane 3, *S. moniliformis* cells in the presence of chondroitin sulfate C; lane 4, *E. coli* cells in the absence of GAG; lane 5, positive control [purified Smon0123 (D) and SagUGL (E)].

with a molecular mass of 2 kDa by a LipoP program (23), the molecular masses of Smon0123 and Smon0127 were estimated to be 57 and 46 kDa, respectively. Anti-Smon0123 antibodies were prepared using recombinant Smon0123 as antigens. Because Smon0127 exhibits a significant sequence identity (48%) with SpyUGL, anti-SpyUGL antibodies (10) were used to detect Smon0127. The purified recombinant Smon0123 and *S. agalactiae* UGL (SagUGL) (24) were

subjected to immunoblotting as the positive control (Fig. 3-4D and E, lane 5). Both Smon0123 and Smon0127 were constitutively expressed in bacterial cells grown in the GAG-free medium (Fig. 3-4D and E, lane 1). The intensity of both protein bands increased in the presence of GAG, particularly hyaluronan (Fig. 3-4D and E, lane 2). These results indicated that the GAG genetic cluster was constitutively expressed in *S. moniliformis* cells and that its expression was enhanced in the presence of GAG.

Enzymatic Properties of UGL and Sulfatase

To investigate enzymatic properties of Smon0127 (UGL) expressed in bacterial cells, the overexpression system of Smon0127 was constructed in *E. coli* cells, and the recombinant Smon0127 was expressed and purified to homogeneity (Fig. 3-4C). Absorbance at 235 nm derived from the C=C double bond in unsaturated GAG disaccharide decreased by the addition of Smon0127 to the substrate, indicating that Smon0127 functions as UGL. Various unsaturated GAG disaccharides such as ΔHA, CΔ0S, CΔ4S, CΔ6S, HΔ0S, and HΔ6S were used as substrates. Smon0127 was the most active on CΔ0S (specific activity, 4.46 units/mg). Specific activities of the enzyme toward each substrate were as follows: ΔHA, 2.26 units/mg; CΔ4S, 0.342 units/mg; CΔ6S, 0.272 units/mg; HΔ0S, 0.0441 units/mg; and HΔ6S, 0.0436 units/mg. The substrate specificity of

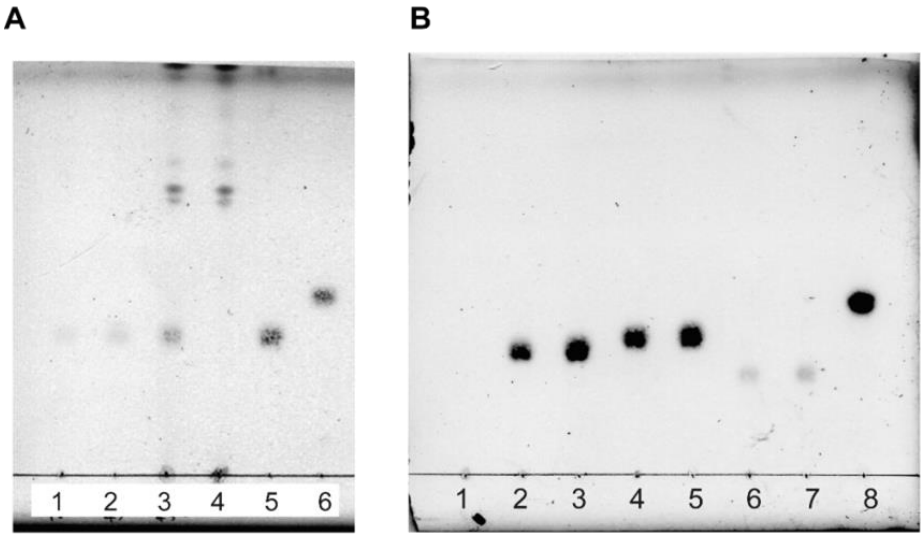

Figure 3-5. Sulfatase activity of *S. moniliformis*. (A) Sulfatase activity of toluene-treated *S. moniliformis* cells. Lane 1, toluene-treated cells and CΔ4S; 2, native cells and CΔ4S; 3, culture supernatant and CΔ4S; 4, culture supernatant; 5, CΔ4S; and 6, CΔ0S. (B) Sulfatase activity of Smon0123. Lanes 1, Smon0123; 2, Smon0123 and CΔ4S; 3, CΔ4S; 4, Smon0123 and CΔ6S; 5, CΔ6S; 6, Smon0123 and CΔ4S6S; 7, CΔ4S6S; and 8, CΔ0S.

Smon0127 demonstrated that the enzyme preferred sulfate group-free unsaturated GAG disaccharides with the 1,3- rather than 1,4-glycoside bond, although sulfated substrates (CΔ4S and CΔ6S) also became substrates for Smon0127. Kinetic parameters toward CΔ0S were determined to be K_m = 0.162 mM and k_{cat} = 4.27 /s. These values are comparable with streptococcal UGL values (24), indicating that Smon0127 physiologically functions in *S. moniliformis* cells. Regarding sulfatase assay, the spot of CΔ4S on the TLC plate in the presence of the extracellular fraction was unchanged, suggesting that sulfatase activity was undetected extracellularly (Fig. 3-5). On the other hand, the substrate was considered to be degraded by intracellular enzymes such as UGL and/or sulfatase, because the spot of CΔ4S attenuated on the TLC plate.

Interactions between Smon0123 and Unsaturated GAG Disaccharides

The putative solute-binding protein Smon0123 was expressed in *E. coli* cells, purified to homogeneity (Fig. 3-4B), and subjected to DSF (12) to examine the interactions between Smon0123 and unsaturated GAG disaccharides (Fig. 3-6). This method is feasible for analyzing the interaction between the solute-binding protein and the substrate (25). The reaction mixture containing a solute-binding protein, ligand, and fluorescent chemical (SYPRO Orange) was gradually raised in temperature by DSF. The RFU was changed due to the formation of hydrophobic interaction between unfolded protein and SYPRO Orange. The inflection point of the increase on the RFU is defined as the melting temperature (T_m) (12). As the ligand-bound protein is thermally more stable than the ligand-free form due to the conversion of the rigid form, T_m in the presence of a ligand was higher than that in the absence of a ligand. Generally, the solute-binding protein adopts two conformations during substrate binding, substrate-free open form and substrate-bound closed form (26), indicating that there is a transitional state (substrate-bound open form) in the conformational change. This conformational change due to the interaction between the protein and the ligand is represented as two T_m values, T_{open} and T_{closed}, corresponding to the substrate-bound open form and substrate-bound closed form, respectively. Smon0123 in the presence of CΔ0S at 1 mM showed two T_m values (44.4 and 66.0°C), while Smon0123 in the absence of a ligand gave a single T_m value (46.7°C). T_{closed} (66.0°C) was significantly higher than T_m (46.7°C) (Fig. 3-6A, middle), suggesting that Smon0123 had a significant affinity with CΔ0S through the conformational change. On the other hand, the fluorescence profile of Smon0123 in the presence of the non-GAG disaccharide, *N*,*N*'-diacetylchitobiose (single T_m, 45.6°C) at 1 mM was comparable with that in the absence of ligand. Various unsaturated GAG disaccharides were used at 50 μM in a similar manner

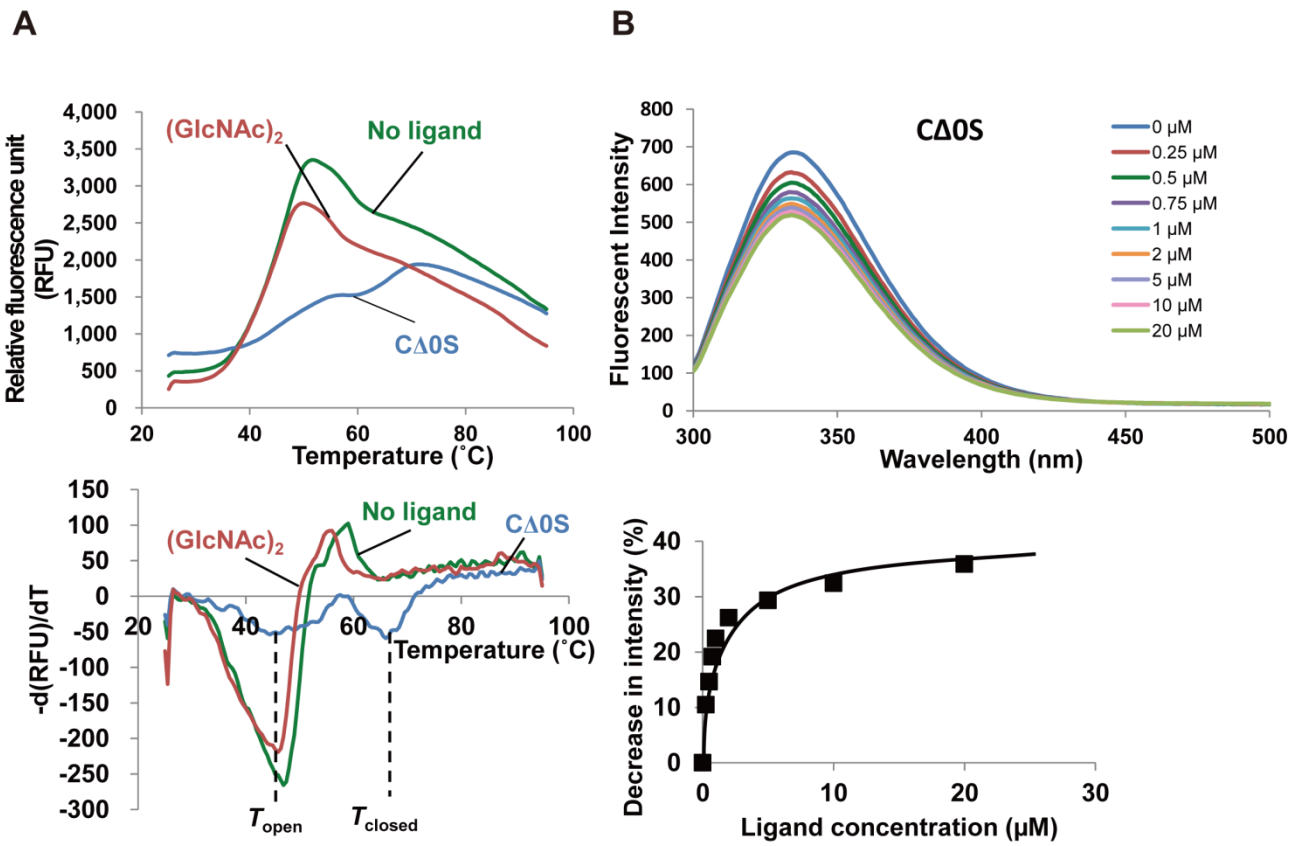

Ligand	T_{open} / T_{closed} (˚C)
CΔ0S	47.0 / 59.2
CΔ4S	44.3 / 59.5
CΔ6S	48.3 / 58.6
ΔHA	44.5 / 56.2
HΔ0S	46.3
HΔ6S	44.5
HΔNS6S	44.8
No ligand	44.8

Ligand	K_d (μM)
CΔ0S	0.635 ± 0.122
CΔ4S	1.60 ± 0.231
CΔ6S	2.76 ± 0.195
CΔ4S6S	3.86 ± 0.243
ΔHA	1.60 ± 0.393
HΔ0S	3.56 ± 0.790
HΔ6S	3.57 ± 0.669
HΔNS6S	3.90 ± 1.02
chitobiose	7.50 ± 1.26
cellobiose	5.41 ± 0.606

Figure 3-6. Affinity of Smon0123 with unsaturated GAG disaccharides. (A) DSF analysis. Upper, fluorescence profile of Smon0123 with CΔ0S (green, 0 mM; and cyan, 1 mM) or 1 mM *N*,*N*'-diacetylchitobiose (red). Middle, negative derivative curve plot derived from the fluorescence profile. Lower, the values of T_{open} and T_{closed} in the presence or absence of various unsaturated GAG disaccharides. (B) Fluorescence spectrum analysis. Upper, wavelength-scanned fluorescence intensity of Smon0123 with CΔ0S (blue, 0 μM; red, 0.25 μM; green, 0.50 μM; purple, 0.75 μM; cyan, 1.0 μM; orange, 2.0 μM; lilac, 5.0 μM; pink, 10 μM; and olive, 20 μM). Middle, the relative fluorescence intensity by addition of increasing ligand concentrations was plotted after modification based on volume change in the cuvette. K_d was determined using the least-squares method. Lower, dissociation constants of Smon0123 with various unsaturated GAG disaccharides. Chitobiose, *N*,*N*'-diacetylchitobiose.

(Fig. 3-6A, lower). Two T_m values (T_{open} and T_{closed}) of Smon0123 in the presence of CΔ0S, CΔ4S, CΔ6S, or ΔHA were detected, while each single T_m value of Smon0123 in the presence of HΔ0S, HΔ6S, or HΔNS6S kept low at around 45°C. These data suggest that Smon0123 binds to unsaturated GAG disaccharides with the 1,3-glycoside bond (CΔ0S, CΔ4S, CΔ6S, and ΔHA) rather than the 1,4 bond (HΔ0S, HΔ6S, and HΔNS6S).

Due to the difficulty in determining the affinity level by DSF, interactions between Smon0123 and unsaturated GAG disaccharides were further analyzed by measuring the fluorescence intensity of Smon0123 in the presence or absence of ligands (Fig. 3-6B). The fluorescence intensity derived from tryptophan residues of Smon0123 proportionally decreased to increasing ligand concentrations (Fig. 3-6B, upper). The ratio of decreasing fluorescence intensity was plotted with respect to ligand concentration, and the dissociation constants were determined from the saturation curve (Fig. 3-6B, middle). Smon0123 showed the highest affinity with CΔ0S (K_d, 0.635 ± 0.122 μM), followed by ΔHA, CΔ4S, CΔ6S, and CΔ4S6S (Fig. 3-6B, lower). The affinity level of Smon0123 with unsaturated heparin disaccharides was low comparable with that with CΔ4S6S. Although K_d values for *N*,*N*'-diacetylchitobiose (7.50 ± 1.26 μM) or cellobiose (5.41 ± 0.606 μM) were also calculated, these were estimated to basal levels in this assay. The binding ability of Smon0123 to GAG polysaccharides (hyaluronan, chondroitin sulfate C, and heparin) was also investigated and no specific interaction between Smon0123 and these GAG polysaccharides was observed.

Structure Determination of Smon0123

Because Smon0123 exhibited an affinity with sulfate-free and -bound unsaturated chondroitin disaccharides (CΔ0S, CΔ4S, CΔ6S, and CΔ4S6S), the binding mode of Smon0123 to these substrates was analyzed by X-ray crystallography. Although Smon0123 with the full-length protein containing a signal peptide was crystallized under some conditions, these crystals were unsuitable for X-ray analysis due to the low-resolution data. Thus, N- and/or C-terminal truncated mutants were crystallized. Among mutants, N-terminal 28 and C-terminal 5 residue-truncated Smon0123 (N-28/C-5) and N-terminal 28 and C-terminal 5 residue-truncated Smon0123 (N-18/C-5) formed crystals suitable for X-ray crystallography. Smon0123 (N-28/C-5) was crystallized in the absence of unsaturated GAG disaccharides and Smon0123 (N-18/C-5) was crystallized with each unsaturated chondroitin disaccharides (CΔ0S, CΔ4S, CΔ6S, and CΔ4S6S). X-ray diffraction data and refinement statistics are shown in Table 3-2. The crystal of ligand-free Smon0123 (N-28/C-5) belongs to the $P2_1$ group with unit cell dimensions of a = 73.7, b = 142, c = 73.7 Å, α = 90.0, β =

Table 3-2. Statistics of substrate-free and -bound Smon0123 for data collection and structure refinement

	Smon0123 (N-28/C-5)	**Smon0123 (N-18/C-5) /CΔ0S**	**Smon0123 (N-18/C-5) /CΔ4S**	**Smon0123 (N-18/C-5) /CΔ6S**	**Smon0123 (N-18/C-5) /CΔ4S6S**
Data collection					
Space group	$P2_1$	$P2_12_12_1$	$P2_12_12_1$	$P2_12_12_1$	$P1$
Cell dimensions					
a, b, c (Å)	73.7, 142, 73.7	79.7, 112, 166	80.0, 113, 166	80.3, 112, 167	49.7, 69.2, 166
α, β, γ (°)	90.0, 106, 90.0	90.0, 90.0, 90.0	90.0, 90.0, 90.0	90.0, 90.0, 90.0	89.9, 90.0, 90.0
Resolution (Å)	50.0-1.78	50.0-1.78	50.0-1.81	50.0-2.00	50.0-1.96
R_{merge}	4.3 (40.7)	5.8 (31.0)	11.6 (25.2)	9.4 (40.6)	7.3 (11.2)
I / σ (I)	29.2 (3.00)	30.3 (5.15)	37.5 (7.07)	36.3 (7.13)	28.1 (2.9)
Completeness (%)	98.6 (98.6)	99.2 (96.9)	98.6 (96.7)	98.3 (95.6)	97.4 (91.3)
Redundancy	2.0 (3.9)	3.9 (7.5)	3.7 (7.2)	3.2 (7.4)	2.1 (1.0)
Refinement					
Resolution (Å)	39.4-1.78	41.6-1.78	39.5-1.81	45.7-1.99	40.4-1.95
No. reflections	138900 (4099)	143057 (4328)	136214 (4159)	100999 (2530)	156219 (4217)
R_{work} / R_{free}	20.7 (26.1) / 23.6 (32.1)	17.4 (20.6) / 20.5 (28.7)	19.3(22.9) / 21.8 (27.6)	19.7(20.5) / 24.8 (25.9)	17.3 (22.0) / 21.6 (26.9)
No. atoms					
Protein	7701	11525	11573	11499	15332
Sugar	0	78	90	90	136
Ca^{2+}	2	3	3	3	4
Water	769	1153	940	757	1293
B-factor (Å^2)					
Protein	23.4	23.8	20.1	23.8	24.4
Sugar	0	10.5	12.6	20.7	21.8
Ca^{2+}	43.1	16.1	18.8	22.0	27.1
Water	29.3	24.4	24.1	23.5	26.6
R. m. s. deviations					
Bond lengths (Å)	0.003	0.007	0.009	0.02	0.02
Bond Angles (°)	0.635	1.07	1.11	1.54	1.80
Ramachandran plot (%)					
Favored region	98.2	98.5	97.9	97.5	97.9
Allowed region	1.79	1.48	1.89	1.89	2.12
Outlier region	0	0.07	0.21	0.61	0

*Data for the highest resolution shell is shown in parenthesis.

106, and γ = 90.0°. The crystals of Smon0123 (N-18/C-5) with CΔ0S, CΔ4S, and CΔ6S all belong to the $P2_12_12_1$ group, and unit cell dimensions are around a = 80, b = 112, c = 166 Å. By contrast, the crystal of Smon0123 (N-18/C-5) with CΔ4S6S belongs to $P1$ group with unit cell dimensions of a = 49.7, b = 69.2, c = 166 Å, α = 89.9, β = 90.0, and γ = 90.0°. The crystal structure of Smon0123 (N-18/C-5)/CΔ0S was determined by molecular replacement with alginate-binding protein (AlgQ1)

(PDB ID, 1Y3N) as the initial model. The crystal structures of ligand-free Smon0123 (N-28/C-5) and ligand (CΔ4S, CΔ6S, or CΔ4S6S)-bound Smon0123 (N-18/C-5) were also determined by molecular replacement with Smon0123 (N-18/C-5)/CΔ0S as the initial model.

Overall Structure of Smon0123

The overall structures of substrate-free and CΔ6S-bound Smon0123 (N-18/C-5) are shown in Fig. 3-7. Although Smon0123 (N-18/C-5) consists of 482 amino acid residues, N-terminal 9 amino acid residues (Met1Lys19–Gly26) showed no electron density, possibly due to disorder. Smon0123 is composed of two major domains (N- and C-domains), and each domain has two small subdomains. N-domain is constituted by residues Pro27–Ile151 (N1 subdomain) and residues Gly328–Ala418 (N2 subdomain), and C-domain contains residues Lys152–Gly327 (C1 subdomain) and Lys419–Phe500 (C2 subdomain). Each domain included a parallel and an antiparallel β-sheet surrounded by many α-helices and formed the α/β sandwich structure. Both N- and C-domains were connected through three loops: residues Tyr146–Ser154 (N1-C1), residues Arg319–Thr324 (C1-N2), and residues Ala414–Ser415 (N2-C2). In the complex crystal structures of Smon0123 with unsaturated chondroitin disaccharides (CΔ0S, CΔ4S, CΔ6S, and CΔ4S6S), the substrate was bound to a cleft between the two N- and C-domains (Fig. 3-7B). Far from the cleft, a calcium ion was bound to the C1 subdomain.

Binding Mode of Smon0123 to Unsaturated Chondroitin Disaccharides

Interactions between Smon0123 and each unsaturated chondroitin disaccharide (CΔ0S, CΔ4S, CΔ6S, or CΔ4S6S) are shown in Table 3-3–6 and Fig. 3-9B. Unsaturated GAG disaccharides were bound to Smon0123 by hydrogen bonds and van der Waals (C-C) contacts. The numbers of hydrogen bonds between Smon0123 and unsaturated chondroitin disaccharides are 9 for CΔ0S (ΔGlcUA, 4; GalNAc, 5), 14 for CΔ4S (ΔGlcUA, 4; GalNAc4S, 10), 8 for CΔ6S (ΔGlcUA, 4; GalNAc6S, 4), and 14 for CΔ4S6S (ΔGlcUA, 5; GalNAc4S6S, 9). The numbers of C-C contacts between Smon0123 and unsaturated chondroitin disaccharides are 50 for CΔ0S (ΔGlcUA, 27; GalNAc, 23), 48 for CΔ4S (ΔGlcUA, 26; GalNAc4S, 22), 53 for CΔ6S (ΔGlcUA, 28; GalNAc6S, 25), and 44 for CΔ4S6S (ΔGlcUA, 29; GalNAc4S6S, 15). Smon0123 strictly recognized both residues of unsaturated uronate (ΔGlcUA) and amino sugar (GalNAc/GalNAc4S/GalNAc6S/GalNAc4S6S). Especially, basic residues directly or indirectly binding to the sulfate groups of the substrates such as Arg204, Lys210, and Arg393 formed a

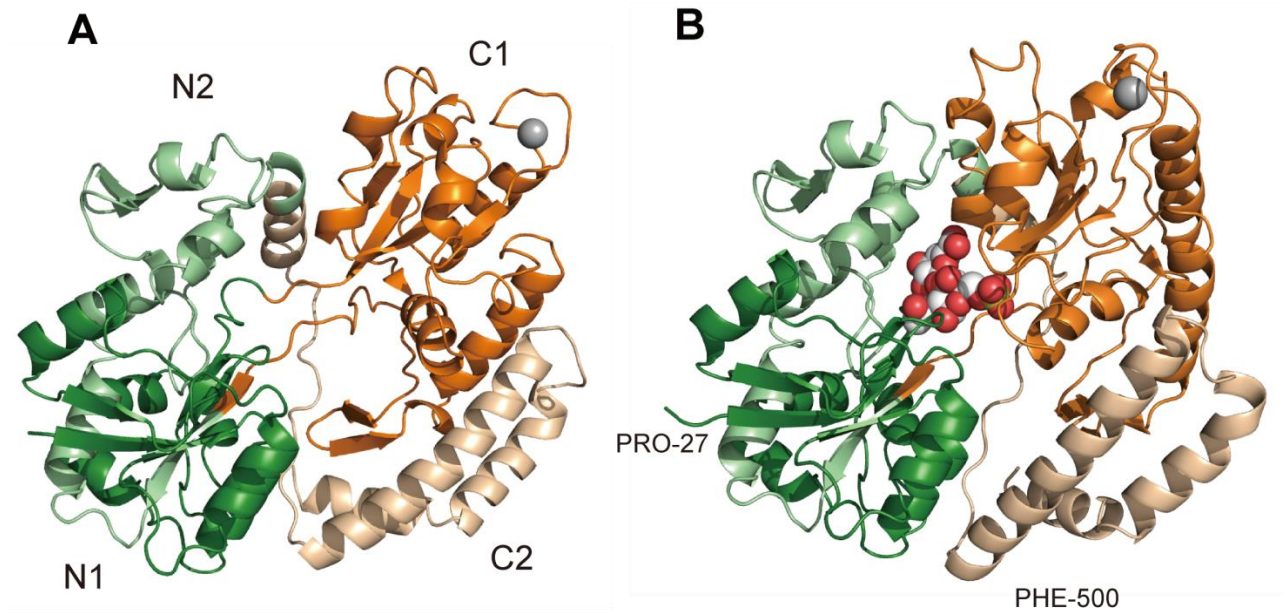

Figure 3-7. Overall structures of Smon0123. Substrate-free (A) and substrate-bound (B) Smon0123. Green, N1 subdomain; light green, N2 subdomain; orange, C1 subdomain; and light orange, C2 subdomain. The ball model shows CΔ6S (white, carbon atom; red, oxygen atom; blue, nitrogen atom; and yellow, sulfur atom). Gray ball shows the calcium ion.

positively charged space for accommodating the sulfate group. An aromatic residue, Trp284, showed stacking interactions with both ΔGlcUA and GalNAc/GalNAc4S/GalNAc6S. Numerous water molecules mediated indirect interactions between Smon0123 and unsaturated chondroitin disaccharides by the formation of hydrogen bonds.

Conformational Changes between Substrate-Free and -Bound Smon0123

The following differences between substrate-free and -bound Smon0123 were noted by investigating the interactions across four subdomains (N1-C1-N2-C2) (Fig. 3-8). i) In substrate-bound Smon0123, Asn97 (N1 subdomain) and Ser445 (C2 subdomain) formed hydrogen bonds, which are not observed in substrate-free Smon0123. This additional bond was formed because of the close contact of N1 and C2 subdomains. ii) Hydrogen bonds between Ser417 (N2 subdomain) and Arg293 (C1 subdomain)/Ser289 (C1 subdomain) in substrate-free Smon0123 disappeared, and alternative hydrogen bonds between Gly385 (N2 subdomain) and Asn294 (C1 subdomain), between Glu410 (N2 subdomain) and Tyr422 (C2 subdomain), and between Leu411 (N2 subdomain) and Lys419 (C2 subdomain) were formed in substrate (CΔ0S, CΔ4S, and CΔ6S)-bound Smon0123. iii) The hydrogen bond between Glu416 (N2 subdomain) and Lys419 (C2 subdomain) in substrate-free Smon0123 disappeared in substrate-bound Smon0123. While

Table 3-3. Interactions between Smon0123 (N-18/C-5) and CΔ0S

Hydrogen bonds (<3.3 Å)

Sugar	Atom	Protein/ Water	Atom	Distance (Å)	Sugar	Atom	Protein/ Water	Atom	Distance (Å)
ΔGlcUA	O2	Gln405	NE2	2.9	GalNAc	O3	Arg393	NH2	2.9
	O3	Tyr409	OH	2.7		O6	Lys210	NZ	2.9
	O3	Glu410	OE2	2.7		O7	His36	NE2	2.8
	O6A	Ser287	N	3.0		O7	Arg393	NH2	3.1
	O2	water80		2.7		N2	Tyr146	OH	2.9
	O6A	water52		2.7		O1	water72		2.6
	O6B	water143		2.7		O4	water143		2.7
						O6	water55		2.7
						O6	water621		2.6
						O7	water80		3.0
						O7	water1090		3.0

van der Waals (C-C distance <4.5 Å)

Sugar	Atom	Protein/ Water	Atom	Distance (Å)	Sugar	Atom	Protein/ Water	Atom	Distance (Å)
ΔGlcUA	C1	Trp284	CD2	4.1	GalNAc	C1	His36	CE1	4.3
	C1	Trp284	CE2	4.3		C1	Leu326	CD2	4.2
	C1	Trp284	CE3	3.9		C2	His36	CE1	4.0
	C1	Trp284	CH2	4.1		C3	Trp284	CE2	4.0
	C1	Trp284	CZ2	4.3		C3	Trp284	CH2	4.3
	C1	Trp284	CZ3	3.9		C3	Trp284	CZ2	3.9
	C3	Trp284	CE3	4.3		C4	Trp284	CD1	4.3
	C3	Trp284	CZ3	4.1		C4	Trp284	CE2	4.0
	C3	Arg322	CZ	4.4		C4	Trp284	CZ2	4.3
	C3	Glu410	CD2	4.1		C5	Trp284	CD1	4.3
	C4	Trp284	CE3	3.8		C5	Trp284	CE2	4.1
	C4	Trp284	CZ3	4.2		C5	Trp284	CZ2	4.4
	C4	Leu389	CD2	4.3		C6	Leu37	CD2	4.2
	C4	Glu410	CD	3.9		C6	Arg204	CZ	4.2
	C5	Trp284	CB	4.1		C6	Trp284	CD1	4.2
	C5	Trp284	CD2	3.9		C7	His36	CE1	4.0
	C5	Trp284	CE3	3.6		C7	Tyr146	CE1	4.3
	C5	Trp284	CG	4.2		C7	Tyr146	CZ	4.4
	C5	Trp284	CZ3	4.2		C7	Leu326	CD2	4.2
	C5	Leu389	CD2	3.7		C8	Tyr146	CE1	3.7
	C6	Trp284	CB	3.4		C8	Tyr146	CZ	3.8
	C6	Trp284	CD2	4.1		C8	Leu326	CD2	4.0
	C6	Trp284	CE3	4.0		C8	Arg400	CG	4.1
	C6	Trp284	CG	3.9					
	C6	Ser287	CB	3.7					
	C6	Leu389	CD2	3.8					
	C6	Trp413	CH2	4.4					

Table 3-4. Interactions between Smon0123 (N-18/C-5) and CΔ4S

Hydrogen bonds (<3.3 Å)

Sugar	Atom	Protein/ Water	Atom	Distance (Å)	Sugar	Atom	Protein/ Water	Atom	Distance (Å)
ΔGlcUA	O2	Gln405	NE2	2.9	GalNAc	O1S	Arg393	NE	2.7
	O3	Tyr409	OH	2.9		O1S	Arg393	NH2	3.0
	O3	Glu410	OE2	2.7		O2S	Arg204	NH1	3.1
	O6A	Ser287	N	3.0		O2S	Arg204	NH2	2.8
	O2	water4		2.7		O3S	Arg204	NH1	3.2
	O6A	water6		2.8		O3	Arg393	NH2	2.9
						O6	Lys210	NZ	2.8
						O7	His36	NE2	2.9
						O7	Arg393	NH2	3.1
						N	Tyr146	OH	2.9
						O1S	water56		2.8
						O6	water301		2.7
						O6	water324		2.6
						O7	water4		2.9
						O7	water543		3.0

van der Waals (C-C distance <4.5 Å)

Sugar	Atom	Protein/ Water	Atom	Distance (Å)	Sugar	Atom	Protein/ Water	Atom	Distance (Å)
ΔGlcUA	C1	Trp284	CD2	4.2	GalNAc4S	C1	Leu326	CD2	4.2
	C1	Trp284	CE2	4.4		C2	His36	CE1	4.4
	C1	Trp284	CE3	4.0		C3	Trp284	CE2	4.1
	C1	Trp284	CH2	4.1		C3	Trp284	CH2	4.4
	C1	Trp284	CZ2	4.4		C3	Trp284	CZ2	4.0
	C1	Trp284	CZ3	3.9		C4	Trp284	CD1	4.4
	C3	Trp284	CE3	4.2		C4	Trp284	CE2	4.1
	C3	Trp284	CZ3	4.1		C4	Trp284	CZ2	4.4
	C3	Arg322	CZ	4.4		C5	Trp284	CD1	4.2
	C3	Glu410	CD	4.1		C5	Trp284	CE2	4.0
	C4	Trp284	CE3	3.9		C5	Trp284	CZ2	4.3
	C4	Trp284	CZ3	4.2		C6	Leu37	CD2	4.2
	C4	Leu389	CD2	4.3		C6	Arg204	CZ	4.3
	C4	Glu410	CD	3.9		C6	Trp284	CD1	4.2
	C5	Trp284	CB	4.2		C7	His36	CE1	4.0
	C5	Trp284	CD2	3.9		C7	Tyr146	CE1	4.3
	C5	Trp284	CE3	3.6		C7	Tyr146	CZ	4.3
	C5	Trp284	CG	4.3		C7	Leu326	CD2	4.3
	C5	Trp284	CZ3	4.2		C8	Tyr146	CE1	3.6
	C5	Leu389	CD2	3.7		C8	Tyr146	CZ	3.6
	C6	Trp284	CB	3.4		C8	Leu326	CD2	4.2
	C6	Trp284	CD2	4.0		C8	Arg400	CG	4.2
	C6	Trp284	CE3	3.9					
	C6	Trp284	CG	3.9					
	C6	Ser287	CB	3.7					
	C6	Leu389	CD2	3.7					

Table 3-5. Interactions between Smon0123 (N-18/C-5) and CΔ6S

Hydrogen bonds (<3.3 Å)

Sugar	Atom	Protein/ Water	Atom	Distance (Å)	Sugar	Atom	Protein/ Water	Atom	Distance (Å)
ΔGlcA	O2	Gln405	NE2	3.0	GalNAc6S	O3	Arg393	NH2	3.0
	O3	Glu410	OE2	2.7		O3S	Arg204	O	3.2
	O3	Tyr409	OH	2.7		O7	His36	NE2	2.8
	O6A	Ser287	N	2.9		N	Tyr146	OH	2.9
	O2	water770		2.7		O1S	water766		3.2
	O6A	water757		2.8		O2S	water795		2.5
	O6B	water767		2.6		O4	water767		2.7
						O7	water770		3.0

van der Waals (C-C distance <4.5 Å)

Sugar	Atom	Protein/ Water	Atom	Distance (Å)	Sugar	Atom	Protein/ Water	Atom	Distance (Å)
ΔGlcUA	C1	Trp284	CD2	4.1	GalNAc6S	C1	His36	CE1	4.3
	C1	Trp284	CE2	4.3		C1	Leu37	CD2	4.4
	C1	Trp284	CE3	3.9		C1	Leu326	CD2	4.1
	C1	Trp284	CH2	4.1		C2	His36	CE1	4.4
	C1	Trp284	CZ2	4.3		C3	Trp284	CE2	4.0
	C1	Trp284	CZ3	3.9		C3	Trp284	CH2	4.3
	C1	Leu389	CD2	4.2		C3	Trp284	CZ2	3.9
	C2	Leu389	CD2	4.1		C4	Trp284	CD1	4.1
	C3	Trp284	CE3	4.3		C4	Trp284	CD2	4.3
	C3	Trp284	CZ3	4.1		C4	Trp284	CE2	3.8
	C3	Glu410	CD	4.1		C4	Trp284	CZ2	4.2
	C4	Trp284	CE3	3.8		C5	Trp284	CD1	4.1
	C4	Trp284	CZ3	4.1		C5	Trp284	CE2	3.9
	C4	Leu389	CD2	4.1		C5	Trp284	CZ2	4.3
	C4	Glu410	CD	3.9		C6	Arg204	CZ	4.3
	C5	Trp284	CB	4.1		C6	Trp284	CD1	4.0
	C5	Trp284	CD2	3.9		C7	His36	CE1	3.9
	C5	Trp284	CE3	3.6		C7	Tyr146	CE1	4.3
	C5	Trp284	CG	4.2		C7	Tyr146	CZ	4.3
	C5	Trp284	CZ3	4.3		C7	Leu326	CD2	4.2
	C5	Leu389	CD2	3.5		C8	Tyr146	CE1	3.7
	C6	Trp284	CB	3.3		C8	Tyr146	CZ	3.8
	C6	Trp284	CD2	4.1		C8	Leu326	CD2	4.0
	C6	Trp284	CE3	4.0		C8	Arg400	CB	4.3
	C6	Trp284	CG	3.9		C8	Arg400	CG	3.9
	C6	Ser287	CA	4.4					
	C6	Ser287	CB	3.6					
	C6	Leu389	CD2	3.7					

Table 3-6. Interactions between Smon0123 (N-18/C-5) and CΔ4S6S

Hydrogen bonds (<3.3 Å)

Sugar	Atom	Protein/ Water	Atom	Distance (Å)	Sugar	Atom	Protein/ Water	Atom	Distance (Å)
ΔGlcUA	O2	Gln405	NE2	2.9	GalNAc4S6S	O2S	Lys210	NZ	2.8
	O3	Tyr409	OH	2.6		O2S	Trp284	NE1	3.2
	O3	Glu410	OE2	2.8		O3	Arg393	NH2	2.8
	O6A	Ser287	OG	3.1		O4S	Arg393	NE	2.7
	O6A	Ser287	N	2.9		O6S	Arg204	NH1	3.0
	O2	water5		2.7		O6S	Arg204	NH2	2.9
	O6A	water706		2.8		O7	His36	NE2	2.9
	O6B	water24		2.9		O7	Arg393	NH2	3.1
						N	Tyr146	OH	2.9
						O3S	water113		3.0
						O6S	water24		2.7
						O7	water5		3.0

van der Waals (C-C distance <4.5 Å)

Sugar	Atom	Protein/ Water	Atom	Distance (Å)	Sugar	Atom	Protein/ Water	Atom	Distance (Å)
ΔGlcUA	C1	Trp284	CD2	4.2	GalNAc4S6S	C1	Leu326	CD2	4.2
	C1	Trp284	CE2	4.4		C3	Trp284	CE2	4.1
	C1	Trp284	CE3	4.1		C3	Trp284	CH2	4.2
	C1	Trp284	CH2	4.1		C3	Trp284	CZ2	3.8
	C1	Trp284	CZ2	4.4		C4	Trp284	CE2	4.0
	C1	Trp284	CZ3	4.0		C4	Trp284	CZ2	4.3
	C1	Leu389	CD2	4.0		C5	Trp284	CE2	4.1
	C2	Leu389	CD2	4.1		C5	Trp284	CZ2	4.3
	C3	Trp284	CE3	4.3		C7	His36	CE1	4.0
	C3	Trp284	CZ3	4.1		C7	Tyr146	CE1	4.4
	C3	Glu410	CD	4.1		C7	Tyr146	CZ	4.3
	C4	Trp284	CE3	3.9		C7	Leu326	CD2	3.9
	C4	Trp284	CZ3	4.3		C8	Tyr146	CE1	3.7
	C4	Leu389	CD2	3.9		C8	Tyr146	CZ	3.6
	C4	Glu410	CD	4.0		C8	Leu326	CD2	3.8
	C5	Trp284	CB	4.3					
	C5	Trp284	CD2	4.0					
	C5	Trp284	CE3	3.8					
	C5	Trp284	CG	4.3					
	C5	Trp284	CZ3	4.4					
	C5	Leu389	CD2	3.2					
	C6	Trp284	CB	3.5					
	C6	Trp284	CD2	4.1					
	C6	Trp284	CE3	4.1					
	C6	Trp284	CG	3.9					
	C6	Ser287	CA	4.3					
	C6	Ser287	CB	3.5					
	C6	Leu389	CD2	3.5					
	C6	Trp413	CH2	4.3					

CΔ4S6S-bound Smon0123 formed hydrogen bonds between Gly385 (N2 subdomain) and Asn294 (C1 subdomain) and between Gln405 (N2 subdomain) and Arg322 (C1 subdomain) in terms of ii), structural features of i) and iii) were commonly observed in all substrate-bound Smon0123. Thus, substrate-bound Smon0123 provided additional hydrogen bonds between N1 and C2 subdomains. However, Smon0123/CΔ4S6S formed specific hydrogen bonds between N2 and C2 subdomains, which were not observed in the other substrate (CΔ0S, CΔ4S, and CΔ6S)-bound Smon0123. Substrate binding subsequently induced conformational changes between interdomain interactions, resulting in a more rigid structure than substrate-free Smon0123.

Alternative Substrate-Bound Conformation of Smon0123

To investigate the magnitude of the hinge-bending motion, N domains of substrate-free and -bound Smon0123 were superimposed, and rotation and translation of C domains were calculated from centers of gravity using the FIT program (Fig. 3-9A). The structures of non- or mono-sulfated unsaturated chondroitin disaccharide (CΔ0S, CΔ4S, or CΔ6S)-bound Smon0123 was found to assume 47°-closed conformations compared with substrate-free Smon0123. On the other hand, the magnitude of the hinge-bending motion of the CΔ4S6S-bound Smon0123 structure was determined to be 39°.

Four substrate-bound Smon0123 forms (CΔ0S, CΔ4S, CΔ6S, and CΔ4S6S) were compared by superimposing their substrate-binding sites. Hence, some residues such as Arg204, Lys210, Trp284, and Ser287 in Smon0123/CΔ4S6S were located in different positions from those in other substrate-bound Smon0123 (Fig. 3-9B and C). Arg204 formed hydrogen bonds with each sulfate group of CΔ4S and CΔ6S, and one of the two sulfate groups (at the C-4 position) of CΔ4S6S. Lys210 made hydrogen bonds with hydroxyl groups at the C-6 position of CΔ0S and CΔ4S but not with the sulfate group of CΔ6S, whereas Lys210 formed a hydrogen bond with the sulfate group at the C-6 position of CΔ4S6S. The distance between the side chain of Lys210 in CΔ4S6S-bound Smon0123 and that in the other substrate-bound Smon0123 was approximately 6.9 Å. Trp284 formed a hydrogen bond only with the sulfate group at the C-4 position of CΔ4S6S, although all substrates (CΔ0S, CΔ4S, CΔ6S, and CΔ4S6S) were bound to Trp284 by van der Waals contacts. Ser287 formed hydrogen bonds with hydroxyl groups at the C-6 position of ΔGlcUA in all substrates. All these amino acid residues (Arg204, Lys210, Trp284, and Ser287) belonged to the C1 subdomain, whereas the other amino acid residues located in the substrate-binding site belonged to the N1 or N2 subdomains. Therefore, two sulfate groups in CΔ4S6S shifted the arrangements of

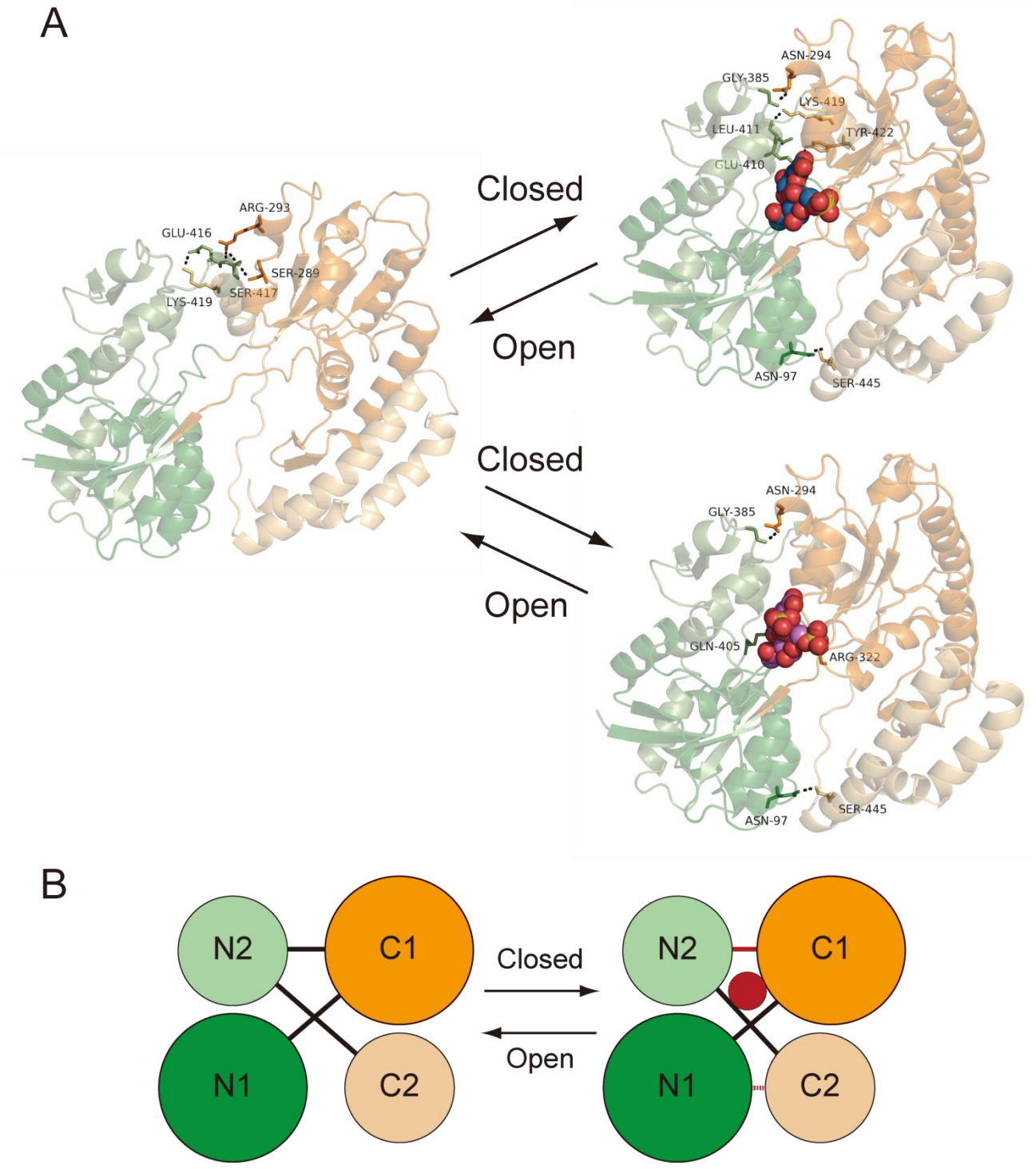

Figure 3-8. Interdomain interactions by substrate binding. Interdomain differences between substrate-free (left) and substrate-bound (right) Smon0123. Green, N1 subdomain; light green, N2 subdomain; orange, C1 subdomain; and light orange, C2 subdomain. (A) Upper, CΔ6S-bound Smon0123; lower, CΔ4S6S-bound Smon0123. (B) Substrate binding (red circle) induces the changes of hydrogen bonds between the subdomains. In substrate-bound Smon0123, hydrogen bonds were formed between N1 and C2 subdomains (red broken line), which disappeared and were alternatively formed between N2 and C1 subdomains (red line) compared with substrate-free Smon0123.

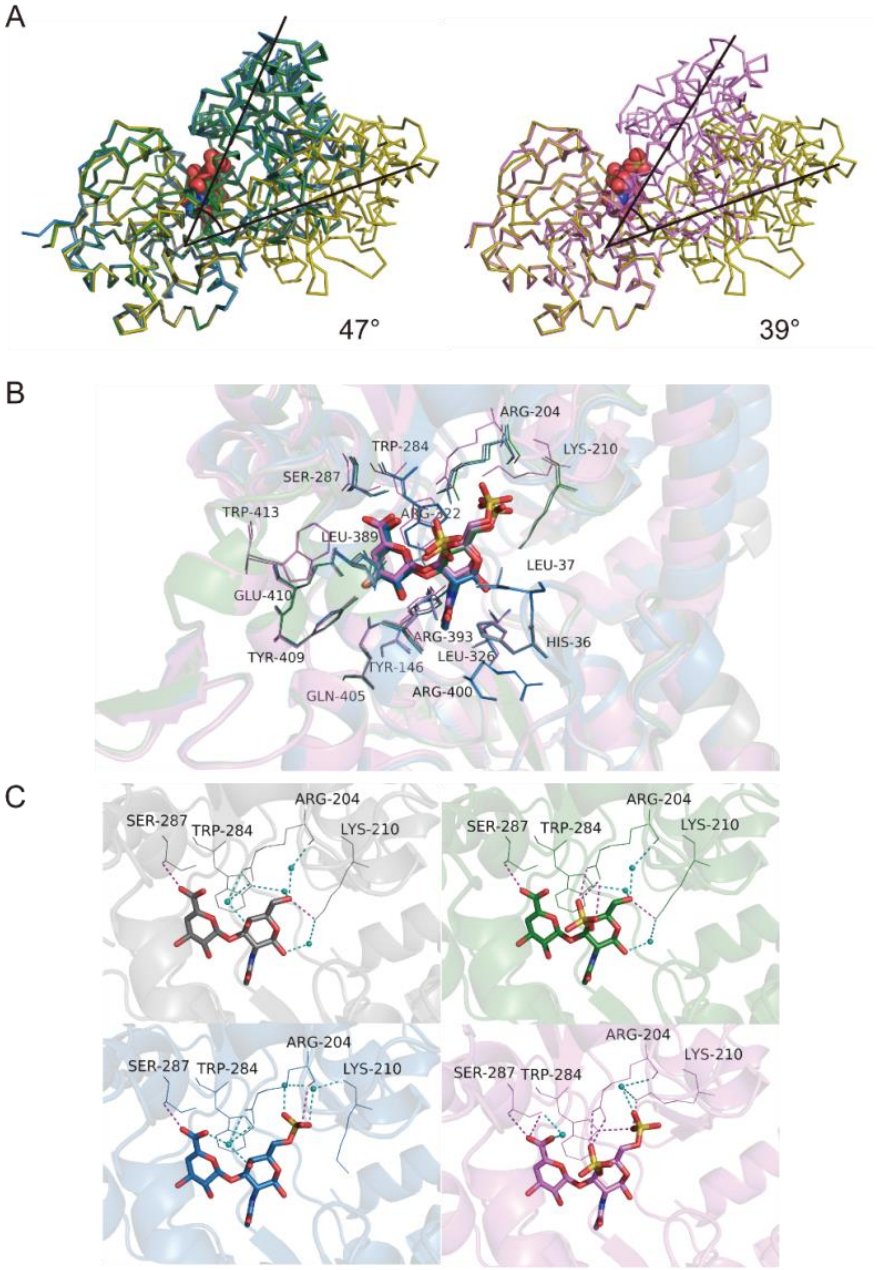

Figure 3-9. Hinge-bending motion of substrate-free and substrate-bound Smon0123. (A) N domains of substrate-free and -bound Smon0123 were superimposed. Gray, CΔ0S-bound; green, CΔ4S-bound; blue, CΔ6S-bound; pink, CΔ4S6S-bound; and olive, substrate-free Smon0123. Ribbon and ball models show the main chain of Smon0123 and disaccharides, respectively. Although the domains of CΔ0S-, CΔ4S-, and CΔ6S-bound Smon0123 were 47° more closed than those of substrate-free Smon0123 (left), the hinge-bending motion of CΔ4S6S-bound Smon0123 was 39° (right). (B) Smon0123 amino acid residues directly formed hydrogen bonds and van der Waals contacts with CΔ0S (gray), CΔ4S (green), CΔ6S (blue), and CΔ4S6S (pink). (C) Some residues of CΔ4S6S-bound Smon0123 (pink) located in a different position from those in the other substrate-bound Smon0123 (gray, CΔ0S; green, CΔ4S; and blue, CΔ6S). The stick models show unsaturated chondroitin disaccharides, and the line models show Arg204, Lys210, Trp284, and Ser287 residues. Small cyan balls show water molecules (oxygen atoms). Magenta and cyan dashed lines show direct and indirect hydrogen bonds, respectively.

amino acid residues in the C1 subdomain, resulting in conformational changes in Smon0123/CΔ4S6S owing to the movement of the C domain. Moreover, Smon0123 showed lower affinity with CΔ4S6S than the other chondroitin disaccharides (CΔ0S, CΔ4S, and CΔ6S), suggesting the influence of the interactions among the four subdomains on the affinity level with substrates.

Expression and Purification of Membrane-Bound ABC Transporter

Because Smon0123 was identified as an unsaturated GAG disaccharide-binding protein, the cooperative function of Smon0123 and ABC transporter, interacting with each other at the ratio of one to one, should be focused. However, it is difficult to analyze a membrane-bound protein with hetero-subunits. The *S. moniliformis* ABC transporter is considered to consist of tetramer subunits of two membrane-spanning subunits (Smon0121-Smon0122) and ATP-binding subunits (Smon0120-Smon0120) by primary structure-based (homology and topology) analysis. The recombinant ABC transporter (Smon0121-Smon0122/Smon0120-Smon0120) was successfully expressed in *E. coli* cells and purified from the cell membrane to homogeneity by the suitable construction of the expression system of protein subunits and their solubilization with detergents.

Three genes (*smon0120*, *smon0121*, and *smon0122*) coding for Smon0120, Smon0121, and Smon0122, respectively, locate sequentially in that order in the *S. moniliformis* genome and form the operon structure (Fig. 3-2). Thus, this operon (*smon0120-0121-0122*) was inserted into an *E. coli* expression vector with a slight modification of 10 histidine residues added at the C-terminus of Smon0122. *E. coli* cell membranes expressing the ABC transporter were obtained from the cell extract by ultracentrifugation and were solubilized with DDM. The transporter was purified by a metal affinity chromatography (Ni-NTA) and gel filtration chromatography (HiLoad 16/60 Superdex 200 pg). The SDS-PAGE profile indicated that the purified sample contained three proteins corresponding to the transmembrane domain (Smon0121-Smon0122) and ATPase domain (Smon0120) (Fig. 3-10B). The protein corresponding to Smon0122 was also detected by immunoblotting using anti-histidine tag antibodies (Fig. 3-10C). The ABC transporter was probably eluted as a tetramer (theoretical molecular mass of approximately 150 kDa) in size on gel filtration (Fig. 3-10A, bold arrow), although the eluted protein was thought to have molecular mass of slightly over 158 kDa based on the elution volume. This difference in molecular mass was possibly due to the presence of a detergent in the eluted buffer. These results clearly demonstrate the tetramer formation of the purified ABC transporter [Smon0121-Smon0122(10xHis)/Smon0120-Smon0120].

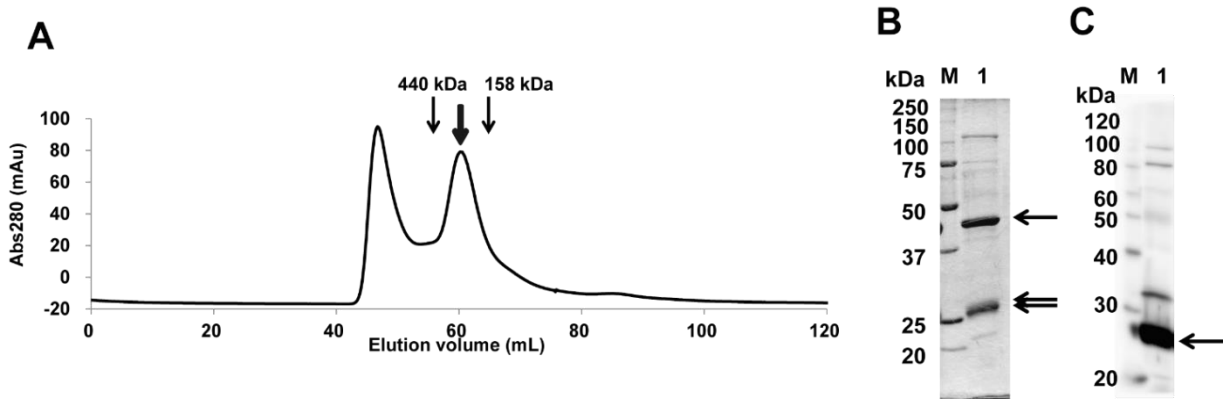

Figure 3-10. Expression and characterization of binding protein-dependent ABC transporter. (A) Elution profile of Smon0121-Smon0122(10xHis)/Smon0120-Smon0120 via gel filtration chromatography. Left and right-sided peaks show an aggregate and a tetramer, respectively. Volumes required for elution of the standard ferritin (440 kDa) and aldolase (158 kDa) are indicated by black arrows. (B) SDS-PAGE followed by CBB staining. Lane M, protein standards with molecular masses of 250, 150, 100, 75, 50, 37, 25, and 20 kDa; lane 1, purified Smon0121-Smon0122(10xHis)/Smon0120-Smon0120. (C) Immunoblotting using anti-histidine tag antibodies. Lane M, protein standards with molecular masses of 120, 100, 80, 60, 50, 40, 30, and 20 kDa; lane 1, purified Smon0121-Smon0122(10xHis)/Smon0120-Smon0120.

Enhancement of ATPase Activity of the ABC Transporter by Smon0123 and Unsaturated GAG Disaccharides

Because ABC transporters generate the energy of ATP hydrolysis to transport substrates (3), the ATPase activity of the purified Smon0121-Smon0122(10xHis)/Smon0120-Smon0120 was measured to investigate the import of unsaturated GAG disaccharides by the ABC transporter. Although purified Smon0121-Smon0122(10xHis)/Smon0120-Smon0120 in the soluble form with detergents exhibited ATPase activity, there was no significant difference in the activity between the presence and absence of Smon0123 and/or unsaturated GAG disaccharides. Thus, the assay was performed using a proteoliposome (27).

The purified Smon0121-Smon0122(10xHis)/Smon0120-Smon0120 was reconstructed in liposomes constituted by phospholipids. Various disaccharides were added to the proteoliposome in the presence of Smon0123, and the phosphate ion liberated through ATP hydrolysis was measured by the molybdenum blue method (19) (Fig. 3-11). The ATPase activity in the presence of non-GAG disaccharides as the negative control such as cellobiose and unsaturated alginate disaccharide (d2M) except for *N*,*N*'-diacetylchitobiose was comparable with that in the absence of disaccharides (PLS). The enhancement of the ATPase activity in the presence of *N*,*N*'-diacetylchitobiose was probably due to the similarity in component between GAG disaccharides and *N*,*N*'-diacetylchitobiose. Unsaturated hyaluronan and chondroitin disaccharides (ΔHA, CΔ0S, CΔ4S, CΔ6S, and CΔ4S6S)

significantly enhanced the ATPase activity of the proteoliposome, while the enzyme activity in the presence of unsaturated heparin disaccharides (HΔ0S and HΔ6S) was comparable with that in PLS. The ATPase activity in the presence of CΔ4S6S was lowest among the unsaturated chondroitin disaccharides, suggesting that CΔ4S6S bound to Smon0123 in the 39°-closed conformation was possibly unpreferable for ABC transporter in comparison with other GAG disaccharides bound to Smon0123 in the 47°-closed conformation.

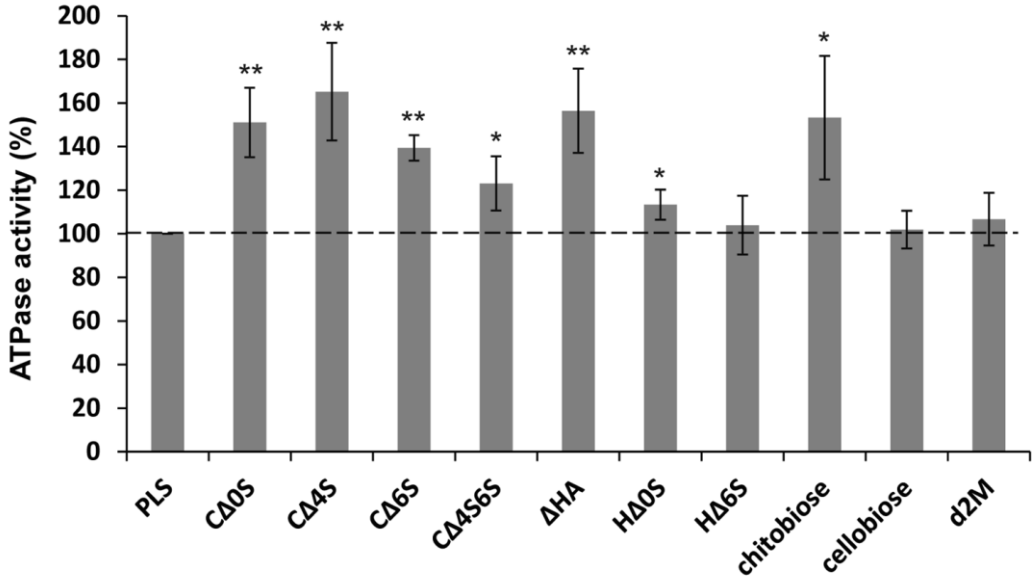

Figure 3-11. ATPase activity of the ABC transporter. ATPase activity of the Smon0121-Smon0122(10xHis)/Smon0120-Smon0120 in liposomes in the presence or absence of various disaccharides. PLS, proteoliposome without disaccharides; chitobiose, *N*,*N*'-diacetylchitobiose; d2M, unsaturated alginate disaccharide. The ATPase activity in PLS was taken as 100 %. Each data represents the average of triplicate individual experiments (means ± standard errors of the means).

Discussion

For the first time, the solute-binding protein-dependent ABC transporter responsible for the import system of sulfated GAGs was found in bacteria and characterized through molecular and structural biology. While PTS phosphorylates substrates at the C-6 position during transport, the ABC transporter imports substrates without any substrate modification. The *S. moniliformis* ABC transporter was demonstrated to be active on various unsaturated GAG disaccharides, particularly unsaturated sulfate group-free chondroitin and hyaluronan disaccharides and uniquely (relative to PTS GAG disaccharide import) unsaturated chondroitin disaccharide with a sulfate group at the C-6 position of GalNAc (CΔ6S), which is an unsuitable substrate for PTS.

Based on the above-mentioned results and streptococcal GAG assimilation system (10), the corresponding *Streptobacillus* model for the degradation and import of GAG was postulated in Fig. 3-12, right. Because PL family 8 hyaluronate lyase is active on hyaluronan and chondroitin sulfate (28), extracellular GAGs such as hyaluronan and chondroitin sulfate are depolymerized to unsaturated disaccharides by hyaluronate lyase(s) (Smon0117 and/or Smon0125). Similarly, heparinase (Smon0124) probably acts on extracellular heparin and heparan sulfate. The resultant unsaturated disaccharides are imported to the periplasm through the outer membrane by an unknown channel/transporter. A periplasmic solute-binding protein (Smon0123) captures unsaturated GAG disaccharides with the 1,3-glycoside bond and delivers substrates to an ABC transporter localized in the cytoplasmic membrane. The ABC transporter consists of four subunits (Smon0121-Smon0122/Smon0120-Smon0120) and incorporates unsaturated disaccharides into the cytoplasm with an energy derived through ATP hydrolysis. Since the localization prediction tool *PSORT-B* (29) suggests that sulfatase (Smon0126) and UGL (Smon0127) are localized in the cytoplasm, unsaturated disaccharides are degraded to constituent monosaccharides in the cytoplasm by GH 88 hydrolase UGL (Smon0127) before and/or after desulfation by sulfatase (Smon0126). In fact, Smon0127 UGL was found to be expressed in the bacterial cells. No sulfatase activity toward CΔ4S was detected in the extracellular fraction (Fig. 3-5A). The Smon0127 showed a preference for non-sulfated GAG disaccharides, although sulfated GAG disaccharides were also degraded by the enzyme. The substrate specificity of Smon0127 suggests that the sulfatase reaction probably occurs before degradation to constituent monosaccharides by UGL.

Smon0123 was demonstrated to bind to unsaturated hyaluronan and chondroitin disaccharides by DSF and fluorescent spectrum analysis (Fig. 3-6). The substrate specificity of Smon0123 coincided with that of Smon0121-Smon0122(10xHis)/Smon0120-Smon0120 for ATPase activity (Fig. 3-11), indicating that the ABC transporter interacts with substrate-bound Smon0123 (closed form), but not the substrate-free form, and triggers ATP hydrolysis. Distinct from substrate-free Smon0123 in the open conformation, the binding protein in complex with the substrate adopts the closed conformation by accommodating the substrate at the cleft between the N- and C-domains (Fig. 3-7). Therefore, the closed conformation of substrate-bound Smon0123 is considered to be important for association with the ABC transporter.

Structure determination of Smon0123 with CΔ6S is particularly important because this result directly demonstrates that CΔ6S, unsuitable for PTS, becomes a substrate for the *S. moniliformis* ABC transporter. The binding mode of Smon0123 to unsaturated chondroitin disaccharides is

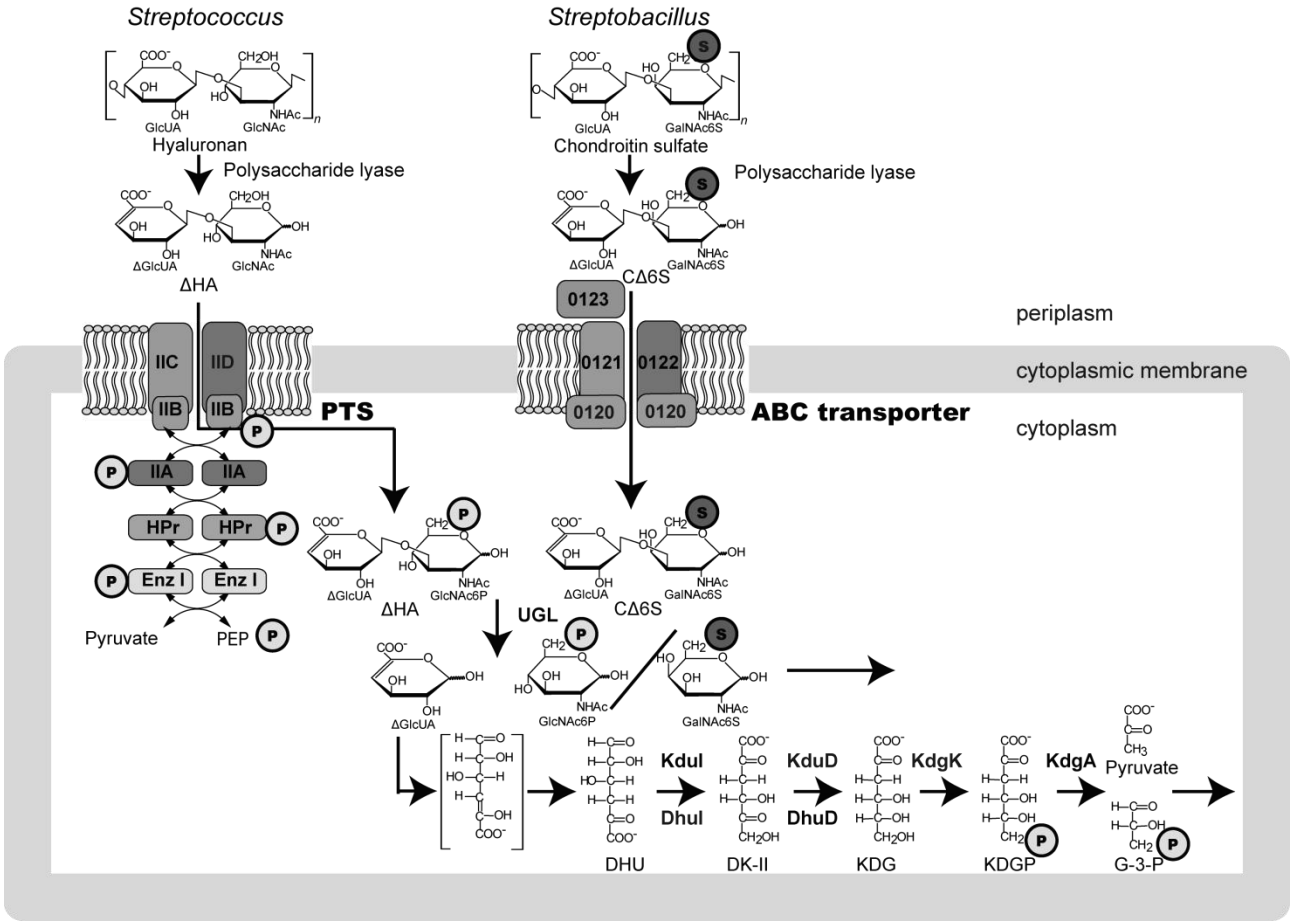

Figure 3-12. Bacterial system for degradation and import of GAGs. GAGs such as hyaluronan and chondroitin sulfate are depolymerized to unsaturated disaccharides by extracellular or cell-surface polysaccharide lyases. The resultant unsaturated disaccharides are incorporated to cytoplasm by PTS or periplasmic binding protein-dependent ABC transporter. In the case of PTS, substrates (unsaturated disaccharides) are phosphorylated across the cytoplasmic membrane. Unsaturated disaccharides are degraded to constituent monosaccharides (unsaturated uronate and amino sugar) by UGL, and the resultant unsaturated uronate is metabolized to pyruvate and glyceraldehyde-3-phosphate (G-3-P) by subsequent reactions of isomerase, reductase, kinase and aldolase. PEP, phosphoenolpyruvate; P enclosed in a circle, phosphate group; S enclosed in a circle, sulfate group.

discussed as follows. The cleft of Smon0123 seems to have spatial allowance. In the interaction between Smon0123 and CΔ0S, numerous water molecules are located in the space where a sulfate group of CΔ4S or CΔ6S is accommodated. The sulfate group of each substrate is situated close to the binding site of Smon0123 and directly forms hydrogen bonds with several residues of Smon0123. The C-C contacts of Smon0123 with CΔ6S also increase compared with those with CΔ0S. In addition, the pyranose ring of amino sugar in unsaturated GAG disaccharide with 1,4-glycoside bond would be in reverse to that in unsaturated chondroitin disaccharide, suggesting that the low affinity of Smon0123 with unsaturated GAG disaccharides with 1,4-glycoside bond is

due to this structural difference in arrangement of the pyranose ring.

Judging from the substrate specificity of Smon0123 (binding protein) and Smon0127 (UGL), the degradation of hyaluronan and chondroitin sulfate by *S. moniliformis* is reasonable (Fig. 3-3). Heparin is lethal for this bacterium, although putative heparinase (Smon0124) is encoded in the GAG genetic cluster (Fig. 3-2). There is a possibility that heparin oligosaccharide produced from heparin by putative heparinase inhibits bacterial growth. This result suggests that heparin is extremely scarce at the colonization site of *S. moniliformis*, contributing to the compositional analysis of GAGs in extracellular matrices of animal cells. There is a possibility that heparin is rich in the oral cavity in humans but scarce in rodents. Heparin is expected to become a potential anti-*Streptobacillus* agent.

S. moniliformis is normally indigenous to rodent oral cavity and belongs to a phylum of fusobacteria. Fusobacteria such as *Fusobacterium* and *Leptotrichia* usually inhabit the oral cavity and gastrointestinal tract of animals including humans (30). Non-sulfated hyaluronan as well as sulfated GAGs such as chondroitin sulfate are abundant in animal oral cavities (31). GAGs provide structures of tissues with a strong network due to the high water absorption. Gingiva in the oral mucosa is known to contain particularly rich sulfated GAGs due to the high pressure of mastication (32). Besides, dermatan sulfate and chondroitin sulfate are rich in connective tissues of the oral mucosa and connective tissue papilla of the anterior and posterior palate in rodents (31). Therefore, the degradation and import systems of sulfated GAGs in *S. moniliformis* are feasible for its colonization in rodent oral cavities, abundant in sulfated GAGs.

Homologous genes with *S. moniliformis* ABC transporter genes are found in the genome of some fusobacteria. *Fusobacterium mortiferum* (NCBI BioProject ID, 32421) and *Leptotrichia goodfellowii* (NCBI BioProject ID, 43669) form the GAG genetic cluster including ABC transporter genes in bacterial genomes, indicating that the GAG import system is common to these fusobacteria. Some fusobacteria are pathogenic and cause infection in some organs and tissues such as the lung, head neck, cranium, and meninx (33). This fusobacterial system for the degradation and import of GAG may be involved in colonization and/or infection to host cells, and inhibitors for the bacterial system are expected to develop novel therapy agents.

Solute-binding proteins adopt open and closed conformations in equilibrium even in the absence of substrates (34). The cleft is opened up to the solvent to allow substrate to freely bind and dissociate, causing flexibility of the structure (35). Some studies have reported that the crystal structures of substrate-free binding proteins such as leucine-binding protein (34), allose-binding

protein (35), galactose-binding protein (36), and ribose-binding protein (37) form a range of open conformation. However, once the protein recognizes the substrates and closes its domains, the reopening of the protein should be severely restricted because the substrate-bound protein needs to form a complex with the ABC transporter and transfer the substrate. The substrate first binds to a domain of the protein, followed by contact with another domain owing to thermal fluctuations and forms additional contacts to stabilize the closed conformation (38). Therefore, substrate-bound conformations show much less variations (34). The glucose-binding protein of *Pseudomonas putida* forms both glucose and galactose-bound structures, and these two complex structures adopt the closed conformation by the hinge-bending motion, although the magnitude of the hinge-bending motions between the two structures are identical (39). Furthermore, AlgQ1 and AlgQ2, which are homologous to Smon0123, exhibit no structural changes depending on various oligoalginates with different constituent sugars and/or polymerization degrees (25, 40). Conversely, the structures of some solute-binding proteins assumed a different hinge-bending motion even in the presence of same substrates, probably because of the constraints placed on the protein by the crystal-packing interactions (41). The possibility that the different conformational change between CΔ4S6S-bound Smon0123 and other substrate-bound Smon0123 is owing to crystallization conditions is low because Smon0123/CΔ4S6S did not form crystals under the crystallization conditions of Smon0123/CΔ0S, Smon0123/CΔ4S, and Smon0123/CΔ6S, and vice versa. Furthermore, to clarify this assumption, Smon0123 was again crystallized in the presence of CΔ4S6S with different crystallization conditions for structure determination. The magnitude of the hinge-bending motion in the crystal structure was unexpectedly determined to be 47°; however, CΔ4S was bound to Smon0123 instead of CΔ4S6S, which was used as a ligand. This is possibly because of the release of the sulfate group at the C-6 position from CΔ4S6S during crystallization or the presence of contaminated CΔ4S in CΔ4S6S. This phenomenon also caused in crystallization of Smon0123/CΔ6S. Although Smon0123 has been suspected to remove sulfate groups of the substrates, no sulfatase activity of Smon0123 was detected by TLC (Fig. 3-5).

The alginate ABC transporter in *Sphingomonas* sp. A1 comprises four subunits of the transmembrane domain (AlgM1-AlgM2) and ATP-binding domain (AlgS-AlgS). The complex structure of the alginate ABC transporter (AlgM1-AlgM2/AlgS-AlgS) with the alginate-binding protein AlgQ2 indicates the interaction mode between the binding protein and the ABC transporter (27). In particular, the helix 5c of AlgM2 is crucial for the interaction with AlgQ2. Each subunit of the alginate ABC transporter shows >ca. 40% sequence identity with that of the *Streptobacillus* one

(AlgM1 vs. Smon0121, 49%; AlgM2 vs. Smon0122, 45%; AlgS vs. Smon0120, 49%; and AlgQ2 vs. Smon0123, 39%). To predict the structure of the *Streptobacillus* ABC transporter, homology modeling was performed using the SWISS-MODEL program (42) (Fig. 3-13A and B). Each subunit (Smon0120, Smon0121, and Smon0122) was modeled and merged to the alginate ABC transporter, resulting in a very similar structure. The crystal structures of substrate-bound Smon0123 and AlgQ2 formed complexes with AlgM1-AlgM2/AlgS-AlgS, which were also very well superimposed.

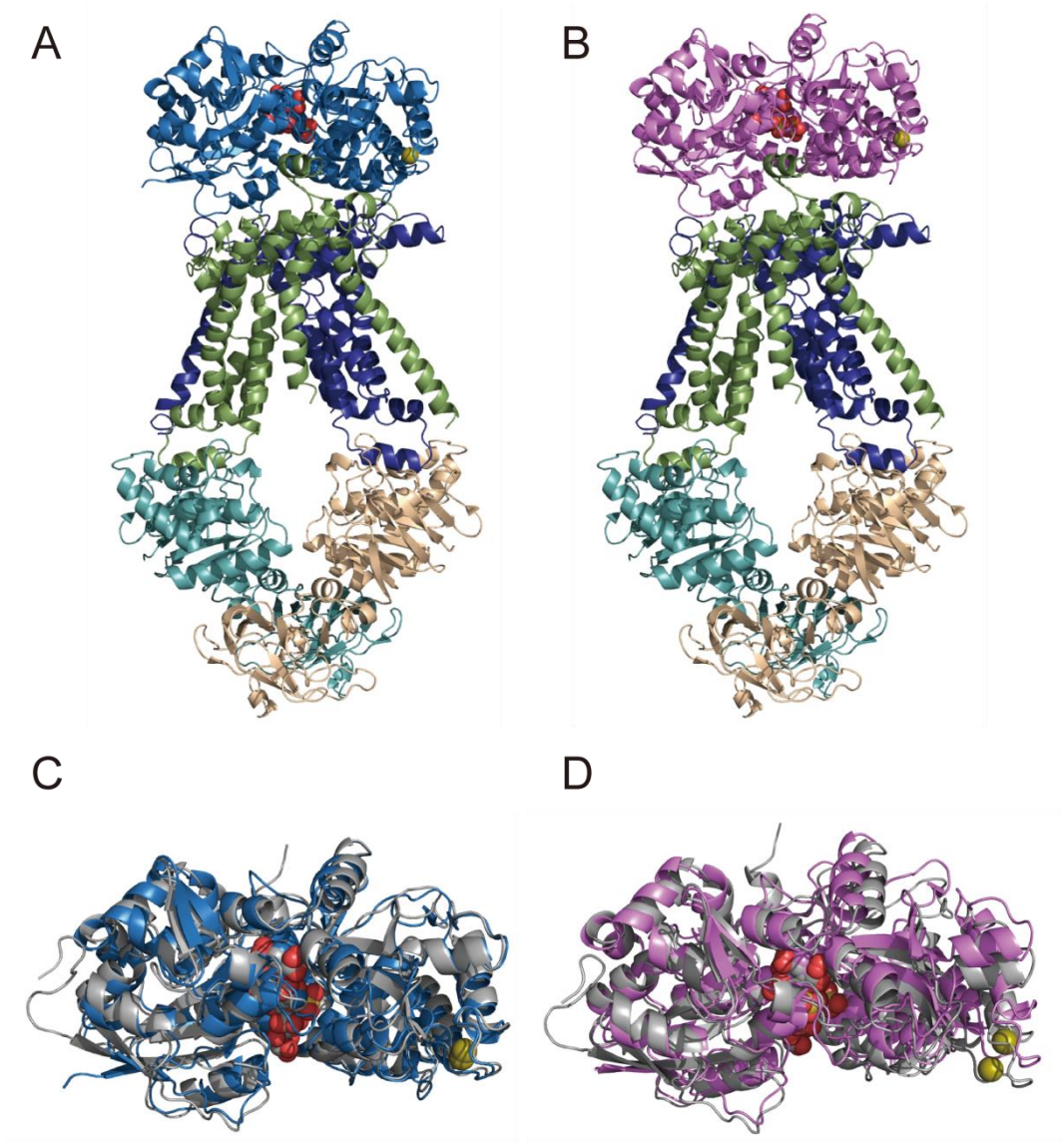

Figure 3-13. Interaction between Smon0123 and Smon0121-Smon0122/Smon0120-Smon0120. Structure modeling of the complex of CΔ6S-bound Smon0123 (A) or CΔ4S6S-bound Smon0123 (B) and Smon0121-Smon0122/Smon0120-Smon0120. Dark blue, Smon0121; light green, Smon0122; cyan and light orange, Smon0120; blue, Smon0123/CΔ6S; and pink, Smon0123/CΔ4S6S. The olive ball shows calcium ion. (B) The superimposition of CΔ6S-bound Smon0123 (C) or CΔ4S6S-bound Smon0123 (D) on AlgQ2 (gray).

Smon0123 probably interacts with the ABC transporter by binding to the helix 5c, also conserved in Smon0122. Dali server (43) was used to clarify whether Smon0123/CΔ6S or Smon0123/CΔ4S6S is similar to substrate-bound AlgQ2 in the complex form (AlgQ2/AlgM1-AlgM2/AlgS-AlgS). The substrate-bound AlgQ2 showed a higher *Z*-score with Smon0123/CΔ6S (Fig. 3-13C) than with Smon0123/CΔ4S6S (Fig. 3-13D), indicating that CΔ0S, CΔ4S, and CΔ6S-bound Smon0123 forms (47°-closed structures) are more suitable than CΔ4S6S-bound ones (39°-closed structures) to interact with the ABC transporter (Smon0121-Smon0122/Smon0120-Smon0120). Substrate-bound AlgQ2 in the closed conformation has recently been revealed to induce ATP hydrolysis by interacting with inward-facing AlgM1-AlgM2/AlgS-AlgS (44). In the case of the CΔ4S6S-bound 39°-closed form, proper docking between the binding protein and ABC transporter and the following ATP hydrolysis and substrate import are considered to be somewhat difficult. Considering the enzymatic properties of Smon0127, the ABC transporter is possibly unable to incorporate CΔ4S6S to save energy generated via ATP hydrolysis. In fact, the enhancement of its ATPase activity in the presence of CΔ4S6S was lower than that of CΔ0S and CΔ4S (Fig. 3-11), suggesting that CΔ4S6S-bound Smon0123 in the 39°-closed conformation is unpreferable for docking with the ABC transporter compared to that in the 47°-closed conformation. Therefore, Smon0123 is suggested to select preferable substrates by two steps, based on whether to bind and how to bind. Alternative substrate-bound conformation probably prevents the import of the unfavorable substrate CΔ4S6S.

In this CHAPTER, the bacterial import system of sulfated and non-sulfated GAGs was identified as the solute-binding protein-dependent ABC transporter and clarified to be functionally expressed in pathogenic *S. moniliformis* through molecular and structural biology. The solute-binding protein Smon0123 adopted two 39°- and 47°-closed conformations depending on the sulfate group(s) in the substrate by the hinge-bending motion. The two sulfate groups in CΔ4S6S shifted the arrangements of the substrate-binding residues in the C1 subdomain, followed by a dynamic conformational change.

References

1. Elliott, S. P. (2007) Rat bite fever and *Streptobacillus moniliformis*. *Clin. Microbiol. Rev.* **20**, 13-22
2. Graves, M. H., and Janda, J. M. (2001) Rat-bite fever (*Streptobacillus moniliformis*): a potential emerging disease. *Int. J. Infect. Dis.* **5**, 151-154

3. Davidson, A. L., and Chen, J. (2004) ATP-binding cassette transporters in bacteria. *Annu. Rev. Biochem.* **73**, 241-268
4. Locher, K. P., Lee, A. T., and Rees, D. C. (2002) The *E. coli* BtuCD structure: a framework for ABC transporter architecture and mechanism. *Science* **296**, 1091-1098
5. Tam, R., and Saier, M. (1993) Structural, functional, and evolutionary relationships among extracellular solute-binding receptors of bacteria. *Microbiol. Rev.* **57**, 320-346
6. Wang, S., Ogata, M., Horita, S., Ohtsuka, J., Nagata, K., and Tanokura, M. (2014) A novel mode of ferric ion coordination by the periplasmic ferric ion-binding subunit FbpA of an ABC-type iron transporter from *Thermus thermophilus* HB8. *Acta Crystallogr. Sect. D: Cryst. Struct. Commun.* **70**, 196-202
7. Chen, J., Sharma, S., Quiocho, F. A., and Davidson, A. L. (2001) Trapping the transition state of an ATP-binding cassette transporter: evidence for a concerted mechanism of maltose transport. *Proc. Natl. Acad. Sci. U. S. A.* **98**, 1525-1530
8. Sambrook, J., Fritsch, E. F., and Maniatis, T. (1989) *Molecular cloning: a laboratory manual*, Cold spring harbor laboratory press
9. Smith, R. F., and Willett, N. P. (1968) Rapid plate method for screening hyaluronidase and chondroitin sulfatase-producing microorganisms. *Appl. Microbiol.* **16**, 1434-1436
10. Maruyama, Y., Nakamichi, Y., Itoh, T., Mikami, B., Hashimoto, W., and Murata, K. (2009) Substrate specificity of streptococcal unsaturated glucuronyl hydrolases for sulfated glycosaminoglycan. *J. Biol. Chem.* **284**, 18059-18069
11. Nakamichi, Y., Mikami, B., Murata, K., and Hashimoto, W. (2014) Crystal structure of a bacterial unsaturated glucuronyl hydrolase with specificity for heparin. *J. Biol. Chem.* **289**, 4787-4797
12. Niesen, F. H., Berglund, H., and Vedadi, M. (2007) The use of differential scanning fluorimetry to detect ligand interactions that promote protein stability. *Nature Protoc.* **2**, 2212-2221
13. Ohnishi, M., Yamashita, T., and Hiromi, K. (1977) Static and kinetic studies by fluorometry on the interaction between gluconolactone and glucoamylase from *Rh. niveus*. *J. Biochem.* **81**, 99-105
14. Otwinowski, Z., and Minor, W. (1997) Processing of X-ray diffraction data collected in oscillation mode. *Meth. Enzymol.* **276**, 307-326
15. Vagin, A., and Teplyakov, A. (1997) MOLREP: an automated program for molecular

replacement. *J. App. Crystallog.* **30**, 1022-1025

16. Adams, P. D., Afonine, P. V., Bunkoczi, G., Chen, V. B., Davis, I. W., Echols, N., Headd, J. J., Hung, L.-W., Kapral, G. J., and Grosse-Kunstleve, R. W. (2010) PHENIX: a comprehensive Python-based system for macromolecular structure solution. *Acta Crystallogr. Sect. D: Cryst. Struct. Commun.* **66**, 213-221
17. Emsley, P., Lohkamp, B., Scott, W. G., and Cowtan, K. (2010) Features and development of Coot. *Acta Crystallogr. Sect. D: Cryst. Struct. Commun.* **66**, 486-501
18. DeLano, W. L. (2002) The PyMOL molecular graphics system.
19. Chifflet, S., Torriglia, A., Chiesa, R., and Tolosa, S. (1988) A method for the determination of inorganic phosphate in the presence of labile organic phosphate and high concentrations of protein: application to lens ATPases. *Anal. Biochem.* **168**, 1-4
20. Gerstein, M., Anderson, B. F., Norris, G. E., Baker, E. N., Lesk, A. M., and Chothia, C. (1993) Domain closure in lactoferrin: two hinges produce a see-saw motion between alternative close-packed interfaces. *J. Mol. Biol.* **234**, 357-372
21. Mizutani, K., Mikami, B., and Hirose, M. (2001) Domain closure mechanism in transferrins: new viewpoints about the hinge structure and motion as deduced from high resolution crystal structures of ovotransferrin N-lobe. *J. Mol. Biol.* **309**, 937-947
22. Nolan, M., Gronow, S., Lapidus, A., Ivanova, N., Copeland, A., Lucas, S., Del Rio, T. G., Chen, F., Tice, H., Pitluck, S., Cheng, J.-F., Sims, D., Meincke, L., Bruce, D., Goodwin, L., Brettin, T., Han, C., Detter, J. C., Ovchinikova, G., Pati, A., Mavromatis, K., Mikhailova, N., Chen, A., Palaniappan, K., Land, M., Hauser, L., Chang, Y.-J., Jeffries, C. D., Rohde, M., Sproer, C., Goker, M., Bristow, J., Eisen, J. A., Markowitz, V., Hugenholtz, P., Kyrpides, N. C., Klenk, H.-P., and Chain, P. (2009) Complete genome sequence of *Streptobacillus moniliformis* type strain (9901 T). *Stand. Genomic Sci.* **1**, 300-307
23. Juncker, A. S., Willenbrock, H., Von Heijne, G., Brunak, S., Nielsen, H., and Krogh, A. (2003) Prediction of lipoprotein signal peptides in Gram-negative bacteria. *Protein Sci.* **12**, 1652-1662
24. Nakamichi, Y., Maruyama, Y., Mikami, B., Hashimoto, W., and Murata, K. (2011) Structural determinants in streptococcal unsaturated glucuronyl hydrolase for recognition of glycosaminoglycan sulfate groups. *J. Biol. Chem.* **286**, 6262-6271
25. Nishitani, Y., Maruyama, Y., Itoh, T., Mikami, B., Hashimoto, W., and Murata, K. (2012) Recognition of heteropolysaccharide alginate by periplasmic solute-binding proteins of a

bacterial ABC transporter. *Biochemistry* **51**, 3622-3633

26. Dwyer, M. A., and Hellinga, H. W. (2004) Periplasmic binding proteins: a versatile superfamily for protein engineering. *Curr. Opin. Struct. Biol.* **14**, 495-504
27. Maruyama, Y., Itoh, T., Kaneko, A., Nishitani, Y., Mikami, B., Hashimoto, W., and Murata, K. (2015) Structure of a bacterial ABC transporter involved in the import of an acidic polysaccharide alginate. *Structure* **23**, 1643-1654
28. Garron, M.-L., and Cygler, M. (2010) Structural and mechanistic classification of uronic acid-containing polysaccharide lyases. *Glycobiology* **20**, 1547-1573
29. Gardy, J. L., Spencer, C., Wang, K., Ester, M., Tusnady, G. E., Simon, I. n., Hua, S., Lambert, C., Nakai, K., and Brinkman, F. S. (2003) PSORT-B: Improving protein subcellular localization prediction for Gram-negative bacteria. *Nucleic Acids Res.* **31**, 3613-3617
30. Dewhirst, F. E., Chen, T., Izard, J., Paster, B. J., Tanner, A. C., Yu, W.-H., Lakshmanan, A., and Wade, W. G. (2010) The human oral microbiome. *J. Bacteriol.* **192**, 5002-5017
31. Pedlar, J. (1984) Biochemistry of glycosaminoglycans in the skin and oral mucosa of the rat. *Arch. Oral Biol.* **29**, 591-597
32. Pedlar, J. (1979) Histochemistry of glycosaminoglycans in the skin and oral mucosa of the rat. *Arch. Oral Biol.* **24**, 777-786
33. Brook, I. (1994) Fusobacterial infections in children. *J. Infect.* **28**, 155-165
34. Magnusson, U., Salopek-Sondi, B., Luck, L. A., and Mowbray, S. L. (2004) X-ray structures of the leucine-binding protein illustrate conformational changes and the basis of ligand specificity. *J. Biol. Chem.* **279**, 8747-8752
35. Magnusson, U., Chaudhuri, B. N., Ko, J., Park, C., Jones, T. A., and Mowbray, S. L. (2002) Hinge-bending motion of D-allose-binding protein from *Escherichia coli*: three open conformations. *J. Biol. Chem.* **277**, 14077-14084
36. Careaga, C. L., Sutherland, J., Sabeti, J., and Falke, J. J. (1995) Large amplitude twisting motions of an interdomain hinge: a disulfide trapping study of the galactose-glucose binding protein. *Biochemistry* **34**, 3048-3055
37. Bjorkman, A. J., and Mowbray, S. L. (1998) Multiple open forms of ribose-binding protein trace the path of its conformational change. *J. Mol. Biol.* **279**, 651-664
38. Gerstein, M., Lesk, A. M., and Chothia, C. (1994) Structural mechanisms for domain movements in proteins. *Biochemistry* **33**, 6739-6749

39. Pandey, S., Modak, A., Phale, P. S., and Bhaumik, P. (2016) High resolution structures of periplasmic glucose-binding protein of *Pseudomonas putida* CSV86 reveal structural basis of its substrate specificity. *J. Biol. Chem.* **291**, 7844-7857
40. Momma, K., Mishima, Y., Hashimoto, W., Mikami, B., and Murata, K. (2005) Direct evidence for *Sphingomonas* sp. A1 periplasmic proteins as macromolecule-binding proteins associated with the ABC transporter: molecular insights into alginate transport in the periplasm. *Biochemistry* **44**, 5053-5064
41. Borrok, M. J., Kiessling, L. L., and Forest, K. T. (2007) Conformational changes of glucose/galactose-binding protein illuminated by open, unliganded, and ultra-high-resolution ligand-bound structures. *Protein Sci.* **16**, 1032-1041
42. Guex, N., and Peitsch, M. C. (1997) SWISS-MODEL and the Swiss-Pdb Viewer: an environment for comparative protein modeling. *Electrophoresis* **18**, 2714-2723
43. Holm, L., and Rosenstrom, P. (2010) Dali server: conservation mapping in 3D. *Nucleic Acids Res.* **38**, W545-W549
44. Kaneko, A., Uenishi, K., Maruyama, Y., Mizuno, N., Baba, S., Kumasaka, T., Mikami, B., Murata, K., and Hashimoto, W. (2017) A solute-binding protein in the closed conformation induces ATP hydrolysis in a bacterial ATP-binding cassette transporter involved in the import of alginate. *J. Biol. Chem.* **292**, 15681-15690

CONCLUSION

1. Non-sulfated unsaturated hyaluronan disaccharide produced from animal extracellular hyaluronan by streptococcal cell surface hyaluronate lyase was incorporated into the bacterial cytoplasm by a sugar import PTS through transfer of a phosphate group from phosphoenolpyruvate to the sugar substrate at the C-6 position. The crystal structure of streptococcal EIIA, one of the PTS components, was determined to contain a Rossman-fold. Docking of EIIA with EIIB by modeling provided structural insights into the phosphate transfer mechanism. Streptococcal UGL degradation of unsaturated GAG disaccharides was inhibited by glycine. Unsaturated uronates produced from unsaturated GAG disaccharides by UGL were metabolized to KDG by successive reactions of the isomerase DhuI and the NADH-dependent reductase DhuD.

2. After consumption of favorable food-derived nutrition factors, human intestinal microbiota were found to degrade and utilize host extracellular GAGs such as chondroitin sulfate C and heparin. A probiotic *Lactobacillus* found in human gut microbiota also degraded heparin, and genes coding for PTS, together with heparin-degrading/metabolizing enzymes, were assembled in a cluster in the bacterial genome. The attachment of the *Lactobacillus* cells to human intestinal cells was significantly inhibited by heparin. *S. agalactiae* cells resident in human intestine and vagina were also appeared to adhere to these host epithelial cells through GAGs.

3. A novel solute-binding protein-dependent ABC transporter was identified in *Streptobacillus* as an importer of both sulfated and non-sulfated GAG disaccharides. Disaccharides with a sulfate group at the C-6 position, which were unsuitable for uptake by a PTS, enhanced ATPase activity of the ABC transporter as a substrate. Crystal structures of the binding protein in complex with various disaccharides revealed its flexible binding mode to sulfated and non-sulfated substrates, and two 39°- and 47°-closed conformations depending on the sulfate group(s) in the substrate by the hinge-bending motion.

This study identified two different bacterial transport systems for the import of fragmented GAGs, *Streptococcus* PTS and *Streptobacillus* ABC transporter using molecular biology, and structural determinants for partial phosphorylation in PTS and sulfate recognition in ABC transporter system were characterized by X-ray crystallography.

ACKNOWLEDGEMENTS

The author would like to express her deepest appreciation to Dr. Wataru Hashimoto, Professor of Graduate School of Agriculture, Kyoto University, for his elaborated guidance, meaningful suggestion, and considerable encouragement that make her research great achievement.

The author is deeply grateful to Dr. Shigeyuki Kawai, Assistant Professor of Graduate School of Agriculture, Kyoto University (currently Professor of Research Institute for Bioresources and Biotechnology, Ishikawa Prefectural University), for his constructive advice and warm guidance.

The author deeply acknowledges Dr. Bunzo Mikami, Professor of Graduate School of Agriculture, Kyoto University, for his thoughtful instruction about X-ray crystallography.

The author would like to express her gratitude to Dr. Kousaku Murata, Emeritus Professor of Graduate School of Agriculture, Kyoto University (currently Professor of Faculty of Science and Engineering, Setsunan University), for his warm encouragement and suggestion.

The author owes gratitude to Dr. Yukie Maruyama, Assistant Professor of Faculty of Science and Engineering, Setsunan University, for her polite guidance especially in X-ray diffraction measurement.

The author is indebted to Dr. Yusuke Nakamichi, Doctoral Student of Graduate School of Agriculture, Kyoto University (currently Post-Doctoral Fellow of National Institute of Advanced Industrial Science and Technology), and Dr. Ryuichi Takase, Doctoral Student of Graduate School of Agriculture, Kyoto University (currently Post-Doctoral Fellow of Thomas Jefferson University), for their kind technical guidance and meaningful discussion.

The author would like to acknowledge the members of the Laboratory of Basic and Applied Molecular Biotechnology, Division of Food Science and Biotechnology, Graduate School of Agriculture, Kyoto University, for their assistance.

Finally, the author would like to express special thanks to her family for their best sympathetic support.

Sayoko OIKI

LIST OF PUBLICATIONS

Original papers

1. **Sayoko Oiki, Yusuke Nakamichi, Yukie Maruyama, Bunzo Mikami, Kousaku Murata, and Wataru Hashimoto.** Streptococcal phosphotransferase system incorporates unsaturated hyaluronan disaccharides from host extracellular matrices.
   In preparation.
2. **Keigo Kawai, Reiko Kamochi, Sayoko Oiki, Kousaku Murata, and Wataru Hashimoto.** Probiotics in human gut microbiota can degrade host glycosaminoglycans.
   ***Sci. Rep.*, 8(1),** Article number: 10674 (2018).
3. **Sayoko Oiki, Reiko Kamochi, Bunzo Mikami, Kousaku Murata, and Wataru Hashimoto.** Alternative substrate-bound conformation of bacterial solute-binding protein involved in the import of mammalian host glycosaminoglycans.
   ***Sci. Rep.*, 7(1),** Article number: 17005 (2017).
4. **Sayoko Oiki, Bunzo Mikami, Yukie Maruyama, Kousaku Murata, and Wataru Hashimoto.** A bacterial ABC transporter enables import of mammalian host glycosaminoglycans.
   ***Sci. Rep.*, 7(1),** Article number: 1069 (2017).
5. **Yusuke Nakamichi, Sayoko Oiki, Bunzo Mikami, Kousaku Murata, and Wataru Hashimoto.** Conformational change in the active site of Streptococcal unsaturated glucuronyl hydrolase through site-directed mutagenesis at Asp-115.
   ***Protein J.*, 35(4),** 300-309 (2016).
6. **Yukie Maruyama, Sayoko Oiki, Ryuichi Takase, Bunzo Mikami, Kousaku Murata, and Wataru Hashimoto.** Metabolic fate of unsaturated glucuronic/iduronic acids from glycosaminoglycans: Molecular identification and structure determination of streptococcal isomerase and dehydrogenase.
   ***J. Biol. Chem.*, 290(10),** 6281-6292 (2015).

Review article

1. **老木紗予子，中道優介，丸山如江，村田幸作，橋本　渉.** 病原細菌による宿主細胞外グリコサミノグリカンの断片化・輸送・分解・代謝に関わる分子機構.
   ***生化学*, 89(6),** 866-871 (2017).

Related paper

1. **Ryuichi Takase, Yukie Maruyama, Sayoko Oiki, Bunzo Mikami, Kousaku Murata, and Wataru Hashimoto.** Structural determinants in bacterial 2-keto-3-deoxy-D-gluconate dehydrogenase KduD for dual-coenzyme specificity.
   ***Proteins*, 84(7),** 934-947 (2016).